12-2017

Electrophysiological, Behavioral, and Histological Assessment of the Thalamocortical Network as a Stimulation Target for Central Auditory Neuroprostheses

Ryan Scott Verner
Purdue University

ELECTROPHYSIOLOGICAL, BEHAVIORAL, AND HISTOLOGICAL ASSESSMENT OF THE THALAMOCORTICAL NETWORK AS A STIMULATION TARGET FOR CENTRAL AUDITORY NEUROPROSTHESES

by

Ryan Scott Verner

A Dissertation

Submitted to the Faculty of Purdue University

In Partial Fulfillment of the Requirements for the degree of

Doctor of Philosophy in Biomedical Engineering

Weldon School of Biomedical Engineering

West Lafayette, Indiana

December 2017

THE PURDUE UNIVERSITY GRADUATE SCHOOL
STATEMENT OF COMMITTEE APPROVAL

Dr. Edward Bartlett, Chair

Department of Biological Sciences, Purdue University

Weldon School of Biomedical Engineering, Purdue University

Dr. Pedro Irazoqui

Weldon School of Biomedical Engineering, Purdue University

Department of Electrical and Computer Engineering, Purdue University

Dr. Michael Heinz

Department of Speech Language and Hearing Sciences, Purdue University

Weldon School of Biomedical Engineering, Purdue University

Dr. Kevin Otto

Department of Biomedical Engineering, University of Florida

Dr. Sliman Bensmaia

Department of Organismal Biology and Anatomy, University of Chicago

Approved by:

Dr. George Wodicka

Head of the Weldon School of Biomedical Engineering

This dissertation is dedicated to all my educators, advisors, family, and friends. Without their hard work and guidance, I would not have achieved such a tremendous goal.

ACKNOWLEDGMENTS

Throughout my graduate career, I've had the extreme luck of meeting phenomenal scientists and engineers. My advisors were understanding of my needs and gave me the space to achieve my personal and professional goals. My colleagues were enthusiastic about their work, and always available to teach me new skills or tackle a new collaborative project. My students were receptive to training and worked hard to make an impact on my projects.

However, I feel most grateful to my wife, whose determination on her own project was so inspirational that it drove me to work harder. Thanks Kari. I can't wait to handle our next challenge alongside you.

TABLE OF CONTENTS

LIST OF TABLES

LIST OF FIGURES

LIST OF ABBREVIATIONS

A1 – Primary Auditory Cortex

A2 – Secondary Auditory Cortex

MGB – Medial Geniculate Body

MGV – Ventral Division of the Medial Geniculate Body

MGM – Medial Division of the Medial Geniculate Body

MGD – Dorsal Division of the Medial Geniculate Body

ICMS – Intracortical Microstimulation

ITMS – Intrathalamic Microstimulation

SH – Subhypnotic

JH – Just Hypnotic

W – Wake

R – Recovery

ABSTRACT

Author: Verner, Ryan S. PhD
Institution: Purdue University
Degree Received: December 2017
Title: Electrophysiological, Behavioral, and Histological Assessment of the Thalamocortical Network as a Stimulation Target for Central Auditory Neuroprostheses
Major Professor: Edward Bartlett, PhD

Brain-machine interfaces aim to restore natural sensation or locomotion to individuals who have lost such ability. While the field of neuroprostheses has developed some flagship technologies which have enjoyed great clinical success, such as the cochlear implant, it is generally understood that no single device will be ideal for all patients. For example, the cochlear implant is unable to help patients suffering from neurofibromatosis type 2, which is commonly characterized by bilateral vestibular schwannomas for which surgical removal requires transection of the auditory nerve. In an effort to develop stimulatory neuroprostheses which can help the maximum number of patients, research groups have developed central sensory neuroprostheses. However, moving through ascending sensory processing centers introduces more uniqueness of neuronal feature selectivity and greater coding complexity, and chronic implantation of devices becomes less efficacious as the brain's glial cells respond to implanted devices. In this work, we propose a neuroprosthetic targeting auditory thalamus, specifically the ventral division of the medial geniculate body (MGV). Thalamus represents an information bottleneck through which many sensory systems send information. Primary (MGV) and non-primary (MGD, MGM) subdivisions provide parallel auditory inputs to cortex and receive feedback excitation and inhibition from cortex and thalamic reticular nucleus (TRN), respectively. We characterize the potential of the thalamocortical circuit as a neuroprosthetic target through electrophysiological, behavioral, and histological methods.

1. INTRODUCTION

1.1 Anatomy and Physiology of the Thalamocortical System

1.1.1 Auditory thalamus: structure and function

The ventral division of the MGB (MGV) is part of the lemniscal auditory pathway. MGV is tonotopically organized with lower pitches on the dorsolateral edge and higher pitches on the ventromedial edge, bordering the dorsal and medial subdivisions (Kimura A et al. 2005). The MGV is also known to be rate sensitive in the rostrocaudal plane (Rouiller EM et al. 1989), and this rostrocaudal organization plays a role in thalamocortical signaling of temporal information to A1 (Read HL et al. 2011). MGV consists primarily of tufted neurons with 6 to 8 dendrites, each with approximately 40 branching points (MOREST DK 1964; Clerici WJ et al. 1990). MGV is highly interconnected with the pre-thalamic centers, specifically IC, and with cortical structures. Recently, a smaller pathway from the cochlear nucleus has been shown to interface directly with the MGV, carrying with it some tracts from Nucleus X of the vestibular system, which is believed to allow for the integration of pinna location and head orientation in the lemniscal pathway (Malmierca MS et al. 2002). MGV also sends excitatory signals to the thalamic reticular nucleus (TRN) (Conley M et al. 1991; Crabtree JW 1998), which is a GABAeric center believed to be associated with temporal feedback. Retrograde and anterograde tracer studies revealed significant corticothalamic and thalamocortical connections associated with MGV (Clerici WJ and JR Coleman 1990; Bartlett EL et al. 2000), though corticothalamic axon terminals were typically very small in the region (Bartlett EL *et al.* 2000). The ventral thalamocortical pathways innervate tonotopic regions of A1 (Fig. 1.1).

Thalamus was traditionally thought of as a relay center for ascending sensory information, however, recent work has revealed the auditory thalamus plays a significant role in auditory processing. Tonotopically organized neurons are tuned for narrow bandwidths and are optimal for spectral processing (Bartlett EL and X Wang 2011). Neurons in MGD are not tonotopically organized, but they do exhibit exceptional temporal synchrony and are optimized for the processing of temporally modulated signals (Bartlett EL and X Wang 2011). MGD neurons have broad tuning properties, though some neurons in the posterior MGD are completely ignorant of tone or noise, responding only to specific stimulus features such as modulation rates

(Bartlett EL and X Wang 2011). This segregation of analysis between two regions allows for more specialization in later cortical processing, as MGV connects to A1 and MGD connects to A2, although the highly specialized neurons in posterior MGD connect only to belt regions of auditory cortex (Bartlett EL and X Wang 2011).

The processing of temporal information in the ascending auditory system tends to shift from a temporal code in the early nuclei, to a rate code in later nuclei. In auditory thalamus, both coding schemes exist (Bartlett EL and X Wang 2007). This allows the MGB to accurately code a range of temporally modulated signals outside of its synchronization limit. Neurons in MGD are typically burst-mode neurons, with a 77% prevalence, compared to a 17% prevalence in MGV (He J and B Hu 2002). Bursting neurons have been shown to have increased first spike latency (He J and B Hu 2002), but this latency doesn't seem to affect their phase locking capacity. Early electrophysiological work in MGB revealed thalamic cells to be more reliable at temporal coding than cortical cells (Creutzfeldt O et al. 1980), and later work attempted to parse these synchronized cells into special categories using their responses to click train stimuli (Rouiller E et al. 1981). Rouiller and colleagues identified "lockers", which are highly synchronized temporal coding neurons; "groupers", which are loosely synchronized to lower click rates; and "special responders", which prefer to focus on features of the stimulus presentation (Rouiller E *et al.* 1981). Much more recently, these same cells were reclassified to reveal neurons which responded to the fastest click rates with a rate code, as opposed to a temporal code (Bartlett EL and X Wang 2007). Regardless of the classification scheme, it is widely accepted that neurons in the MGB are more receptive to temporal information than those in cortex. In a study of ascending best temporal modulation frequencies (bTMFs) for amplitude modulated tones in squirrel monkeys, bTMF median ranges decreased from 32-64 Hz in IC (Müller-Preuss P 1986), 4-32 Hz in MGB (Preuss A and P Müller-Preuss 1990), and 4-16 Hz in cortex (Fastl H et al. 1986; Gaese B and J Ostwald 1995). This finding suggests that temporal information of the stimulus is either extracted prior to cortical processing or that the temporal information is transformed from temporal coding to rate coding as the signal approaches cortex.

In addition to the transformation of temporal information, the MGB must also code amplitude cues. Stimulus amplitude can change based on stimulus' location in space or intensity. Cells in MGB encode stimulus intensity with either a monotonic or non-monotonic rate code (Aitkin LM and SM Prain 1974). Depending on a neuron's connectivity within MGB, it may

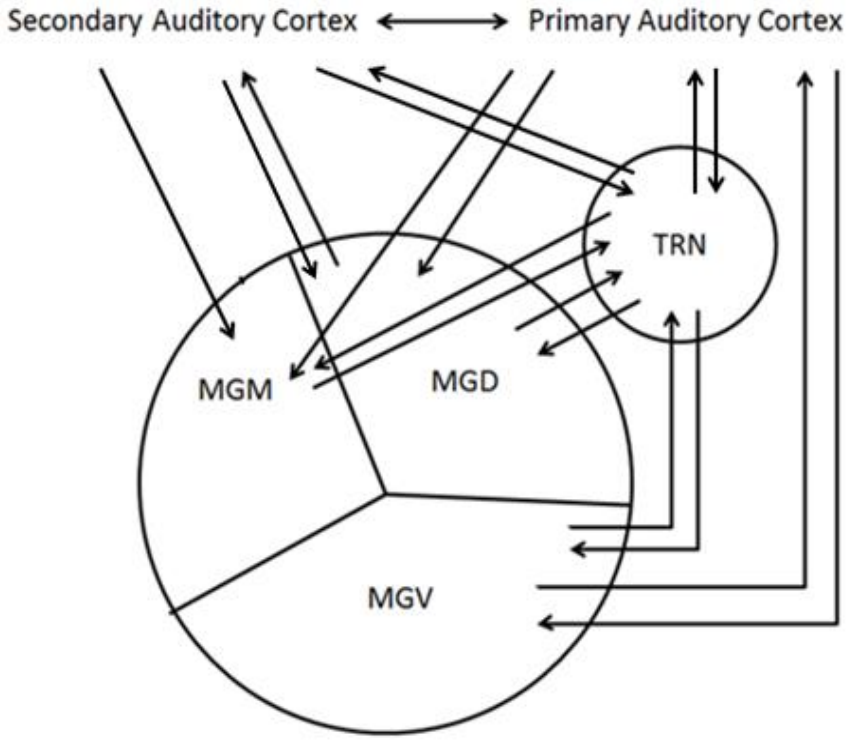

Figure 1.1: Information flow in the medial geniculate body.

exhibit strong tonic activity, strong phasic activity followed by inhibition, or be completely inhibited in the presence of a stimulus of any suprathreshold amplitude (Yu YQ et al. 2004).

Adaptation to specific stimuli or tasks is of critical importance to behavior, and at least a portion of this adaptation is known to occur in the MGB. The adaptation properties of MGV were originally described in response to remapping of receptive fields from their physiologic characteristic frequency to a task-related frequency for approximately 1 hour (Edeline JM and NM Weinberger 1991). Later work on adaptation focused on adaptation to stimuli. In 2004, the MGB was shown to exhibit no such adaptation (Ulanovsky N et al. 2004), but a response by Anderson et al. in 2009 revealed SSA in MGM and MGV (Anderson LA et al. 2009). Anderson and colleagues believed their results and posited that no such adaptation occurred in MGD, but it is more likely that the use of ketamine affected their results. To more accurately assess the presence of SSA in MGD, one study utilized urethane anesthesia so as not to suppress non-lemniscal cells, emphasizing the importance of anesthetic choice. This study reported SSA in all regions of MGB, with a heavy preference to MGM (Antunes FM et al. 2010). This finding agrees with the strong corticothalamic input received by MGM and the region's connectivity to TRN, which could be used to influence other geniculate and cortical centers with inhibitory activity.

1.1.2 Thalamocortical transformation

Thalamocortical signaling is not just a simple, one way transmission between thalamus and cortex. Ascending auditory input to cortex is transformed via transmission, much like thalamus or cortex parses input features into specific coding strategies. In fact, information theory approaches have shown that information coded by each unit decreases as signals ascend through the auditory system (Chechik G et al. 2006), however, this may be confounded by the fact that the auditory system uses sub-optimal codes(Carney LH et al. 2014). This finding would seem counterintuitive, as higher level information processing tends to occur in cortex, so a reduction in information per unit between thalamus and cortex would hinder processing. However, the number of units in cortex greatly exceeds the number of units in the MGB, therefore counteracting the loss of information per unit by instituting a population code.

Considering temporal information is coded along the rostrocaudal plane of MGV and spectral information is coded in the lateromedial direction, individual neurons might code for

differing amounts of spectral or temporal information, requiring a mechanism to parse or combine these features in cortex(Read HL *et al.* 2011). The transfer of information between a smaller number of thalamic cells and a large number of cortical cells gives rise to various types of functional convergence, described as inheritance, ensemble, or construction convergence by Lee Miller and colleagues(Miller LM, MA Escabí, HL Read, et al. 2001). Inheritance convergence uses thalamic neurons which code for identical stimulus features to represent that same set of features in cortex and is the classical, pure-transmission understanding of thalamocortical transmission (Fig. 1.2). Construction convergence pathways consist of neurons that code many different features to drive a cortical representation of all features, combined. Ensemble convergence is demonstrated when a cortical neuron codes for a single stimulus feature, but uses information from thalamic cells which might also code for other features. Functionally connected neurons, confirmed by high levels of synchrony, tend to be more selective for similar spectrotemporal stimulus features, providing evidence for functional convergence(Miller LM, MA Escabí and CE Schreiner 2001). Functional convergence doesn't only occur in thalamocortical transmission, though. Construction convergence is present in Layer 5 of A1 as neurons integrate responses from many distinct feature detectors in Layers 2 and 3. Ensemble convergence can also be seen in the "special responder" neurons of MGB, which integrate various IC inputs to respond to a single feature for which all inputs partially coded.

Feedback is another key component of thalamocortical transformation. Early work in assessing communication between thalamus and cortex utilized cortical cooling to attenuate corticothalamic signaling (Villa AE and M Abeles 1990; Villa AE et al. 1991). Corticothalamic signaling was shown to alter the best frequency and best bandwidth properties of neurons in MGV(Villa AE *et al.* 1991) through inhibitory connections. Later, studies of fine-frequency tuning show that animals which use vocalizations for higher level function, such as marmosets, humans, and bats, have highly precise frequency tuning (Bartlett EL et al. 2011). During sustained tones, frequency tuning becomes even more refined as inhibitory sidebands suppress frequencies other than the stimulus tone for up to 100ms after the stimulus has abated (Sadagopan S and X Wang 2010). This frequency tuning confirms the existence of a feedback circuit which refines frequency information during stimulus presentation. Because feedback from A1 typically results in the development of inhibitory spectrotemporal sidebands to tune

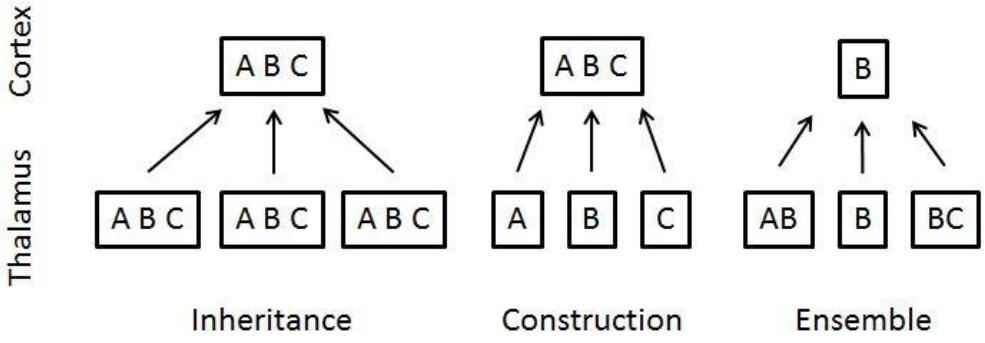

Figure 1.2: Functional convergence in the thalamocortical circuit.

ascending signals, SSA and task-related adaptation would be expected to change with age. Surprisingly, this is not the case (Richardson BD et al. 2013). SSA represents a feedback loop, so it is possible that constant feedback forces the circuit into the optimal inhibitory state, regardless of the level of baseline inhibitory activity. One would expect the aged central auditory pathway to exhibit slower adaptation in this case, but instead, aged animals adapted to stimuli with a nearly identical time course as young rats (Richardson BD *et al.* 2013). This could indicate that the mechanism of ascending adaptation in MGB is at least partially an excitatory process, which could be explored with a detailed study of corticothalamic axon terminals in MGV or the feedback circuit between TRN and MGV.

1.1.3 Primary auditory cortex: structure and function

Consistent with other processing stations of the auditory pathway, primary auditory cortex exhibits a tonotopic structure which is roughly organized in the rostrocaudal plane (Sally S and J Kelly 1988). Though neurons tuned to lower frequencies tend to reside in the caudal region of A1(Sally S and J Kelly 1988), recent work with *in vivo* 2-photon calcium imaging has revealed that the overarching tonotopic structure is not present on scales smaller than 100 microns (Bandyopadhyay S et al. 2010). In fact, neighboring neurons are chaotically tuned for frequency, bandwidth, and amplitude. Some work has similarly attempted to map A1 in terms of temporal processing capacity, revealing weak temporal coding in the dorsal regions of rat A1 (Kilgard M and M Merzenich 1999), which surprisingly contains a high number neurons tuned to rodent vocalization frequencies. Most importantly, this large-scale organization of A1 implicates the presence of similar columnar organization that is seen in the primary visual cortex (Dräger UC 1975) and somatosensory cortex (Petersen RS and ME Diamond 2000).

Each column of cortex is arranged in 6 layers which are defined by cell sizes, shapes, and connectivity. Thalamocortical input feeds in to layer 4, which is roughly defined as a region of non-pyramidal cells lying between pyramidal cell layers 2/3 and 5 (Winer JA 1984). Layer 4 consists of small, medium, and large tufted cells, increasing in size with depth in cortex(Winer JA 1984). The region also contains a few large multipolar cells, double bouquet cells, and perhaps spiny stellate cells (Winer JA 1984), though there is still discussion about the presence of spiny stellate cells in cat A1 (Smith PH and LC Populin 2001). All cells in layer 4 favor a columnar dendritic structure (Winer JA 1984), reinforcing the large-scale columnar organization

of A1. Layer 4 has heavy connections to layer 2/3, a processing layer, and 5, an output layer. Layer 5 consists of pyramidal neurons which can be characterized electrophysiologically into "bursting" or "regular spiking" cells (Hefti BJ and PH Smith 2000). Bursting cells tend to be less inhibited and show significantly more dendritic branching in all layers (Hefti BJ and PH Smith 2000). It is posited by Hefti and Smith that regular spiking cells are responsible for precise inhibitory sideband activity, while bursting neurons have more broadband inhibitory effects (Hefti BJ and PH Smith 2000).

In terms of action potential properties, neurons in A1 can be segregated into fast-spiking and regular-spiking groups. Fast spiking units have better spectrotemporal feature selectivity and phase locking with lower first spike latencies and average firing rates (Atencio CA and CE Schreiner 2008). Fast spiking neurons exist preferentially in layer 4 and deep in layer 5 (Atencio CA and CE Schreiner 2008), and the proportion of fast to regular spiking neurons leads to interesting columnar properties. Layers 4 and 5, which are input and output layers to auditory centers with high temporal modulation processing capabilities, exhibit the highest temporal modulation frequency (Atencio CA and CE Schreiner 2010). Neurons in layers 5 and 6, which are both output layers providing feedback to MGB and IC, have the fastest spectral modulation frequencies and could be useful for tuning ascending frequency information (Atencio CA and CE Schreiner 2010; Bartlett EL *et al.* 2011).

Amplitude features are culled from the input stream by frequency-specific neurons which rate-code amplitude monotonically or non-monotonically. Traditionally, all amplitude coding neurons were believed to code amplitude with a monotonic rate code, with higher stimulus amplitudes corresponding to higher firing rates. Non-monotonic amplitude coding neurons have O-shaped receptive fields and had only been identified in bats until 2008 (Sadagopan S and X Wang 2008). This band pass level filter may be the primary mechanism that allows animals, including humans, to identify the presence of a specific frequency in a noisy background. These monotonic and non-monotonic neurons also play different roles in coding sinusoidally amplitude modulated (sAM) stimuli. Non-monotonic neurons tend to focus on transitions in the sound envelope, while monotonic neurons code the envelope directly with a rate code (Zhou Y and X Wang 2010).

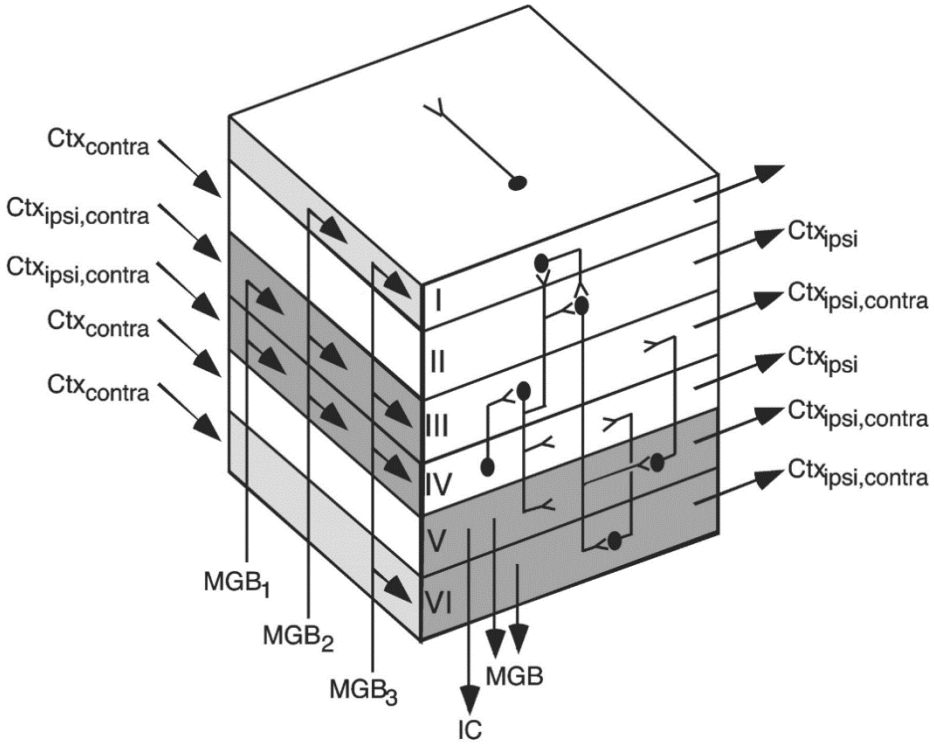

Figure 1.3: Cortical column input and output complexity.

Figure from Oxford University Press, adapted from Mitani et al. 1985, Winer 1992, and Huang and Winer 2000.

Neurons are roughly tuned to frequency within their columnar organization. However, some neurons are tuned to have broader bandwidths than others. Neurons with wide bandwidths are less common and are less effective at encoding spectral modulation than narrowly tuned cells (Atencio CA and CE Schreiner 2012). Sinusoidal frequency modulation (sFM) was revealed to have a best modulation rate of 10 Hz (Gaese B and J Ostwald 1995), but this finding was not further constrained to wideband or narrowband neurons. Some neurons rate code the directionality of sFM signals, preferred to fire during increasing or decreasing FM sweeps (Gaese B and J Ostwald 1995). Some researchers even attempted to model this preference, finding that a neuron's preference can be determined by convolving the spectrogram of an FM sweep stimulus with the neuron's spectrotemporal receptive field (STRF) response to a tone pip train stimulus (Atencio CA et al. 2007). Neurons which are not selective to a FM direction also do not seem to have a preferred modulation frequency. Confusingly, approximately ¼ of the neurons in auditory cortex do not respond to any manner of spectral cue. Previously, these neurons were believed to not have auditory functions whatsoever, however, it was recently determined that these neurons code highly specific stimulus features which are prevalent in vocalizations and speech (Sadagopan S and X Wang 2009). These neurons seem to utilize a temporal coding scheme, indicating the precise timing of a feature.

Temporal tuning refers to a neuron's ability to code the timing of stimulus presentation and is commonly measured with click train stimuli. Neurons in early auditory nuclei often code temporal information with a synchronized, or phase-locked, temporal code. In cortex, neurons only remain synchronized to very slow rates. In rats, the optimal rate for stimulus synchrony was found to be, on average, 10Hz (Gaese B and J Ostwald 1995). As stimulus presentation rate increases, a temporal synchronization boundary is reached at approximately 25 Hz (Lu T and X Wang 2000; Lu T et al. 2001), however it may be possible to artificially push neurons to an 80 Hz boundary (Koivuniemi A et al. 2011). The limit of detecting changes in temporal cues is approximately 166 Hz when using a rate code (Lu T and X Wang 2000).

1.2 Microelectrode Arrays as Neuroprostheses

Microelectrode arrays are commonly used to record single unit or local electric field activity in various regions of the brain. The primary advantage of this method is that the animal utilizes its own auditory system to transform physical stimuli into electrical impulses, so the

neural activity is similar to what an animal would experience during normal activity. Additionally, behavioral tasks can be employed for wakeful animals to study the effects of stimulus-specific and task-specific neural adaptation in sensory systems (Anderson LA *et al.* 2009; Atiani S et al. 2009; Antunes FM *et al.* 2010; Richardson BD *et al.* 2013). Comprehension of specific acoustic cues is commonly assessed behaviorally using signal detection theory (Syka J et al. 1996; Koivuniemi A *et al.* 2011). The weaknesses of these *in vivo* methods are specificity and sensitivity. It is often difficult to confidently state the location and connectivity of a neuron that is being recorded, though this problem is slowly being ameliorated through advanced histological techniques (Woolley AJ et al. 2011; Chung K et al. 2013). In chronic microelectrode studies, the neural immune response degrades the signal-to-noise ratio and recordings of single units often become lost in noise over the course of several months (Williams JC et al. 1999). This issue is also being addressed through design considerations (Skousen JL et al. 2011) and the use of special coatings (Kozai TD et al. 2012; Rao L et al. 2012). Animal mobility during wakeful recordings is also a concern, and recent work focused on wireless devices has made *in vivo* recordings more viable for highly mobile species or behavioral paradigms that require substantial movement (Eliades SJ and X Wang 2008). Despite these issues, chronic studies of the central auditory pathway using microelectrode arrays does allow for assessment of large scale changes in electrophysiological activity and the efficacy of these techniques will certainly improve with further research. In terms of prostheses as clinical tools, microelectrode arrays can be used to record neural activity and decode intended actions or to artificially stimulate neural circuits to evoke relevant percepts.

Due to their minor relevance to this work, recording prostheses will only be discussed briefly here. These prostheses primarily link the neurons of the primary motor cortex to a computer which can decode movement planning. One of the primary weaknesses of control neuroprostheses is that they lack adequate feedback to the user. In anesthetic studies, it can be demonstrated in otherwise healthy individuals that reduced somatosensory feedback diminishes control over grip force (Monzée J et al. 2003). Many groups are moving in the direction of developing bidirectional interfaces (Rouse A et al. 2011) to counter this issue, but the issue of simultaneous recording in the presence of electrical stimulation remains as a hurdle to overcome. Developing stimulation modalities for feedback in the somatosensory, auditory, and visual systems that are safe and efficacious is important for the future of these control prostheses.

1.3 Electrical Stimulation as a Clinical Tool for Restoring Sensation

In the auditory system, several key stimulus dimensions exist that clinicians and engineers can exploit to deliver functional auditory stimuli. At every level of the core central (and peripheral) auditory system, tonotopic organization allows for electrodes placed in different locations to provide perceptions of different "pitches" to the patient. "Loudness" and "bandwidth" may be somewhat synonymous in electrically stimulating implants, because while increasing the stimulus amplitude may increase the perceived amplitude by increasing firing rates or number of neurons firing (Zeng FG and RV Shannon 1994), it also increases the total volume of tissue stimulated above a perceptual threshold in the tonotopic axis as per Gauss's Law. The goal, then, is to understand the limits of pitch and amplitude discrimination in clinical neuroprostheses. Studies of acoustic discrimination of pitch and amplitude have set benchmarks for success in clinical neuroprostheses (Hack M 1971; Syka J *et al.* 1996), however, behavioral determination of the discrimination limen of these two stimulus dimensions during electrical stimulation can be muddled by the confound of "loudness" and "bandwidth". Thus far, most work on the discrimination of electrical stimulation cues has been in the field of temporal coding, specifically in the coding of individual pulses or amplitude modulated pulse trains (Romo R et al. 1998; Romo R and E Salinas 2003).

Choosing a target location for a neuroprosthetic is important to its efficacy. In every sensory system, it is favorable to interface with peripheral sensory organs or the nerves that carry their information to the brain. Thus, the most successful stimulating neuroprostheses on the market are retinal prostheses, cochlear implants, or peripheral nerve stimulators. This is primarily because the sensory organs or connecting nerves do minimal amounts of processing and all of the nerve fibers or sensory organs are responding similarly to similar inputs. Moving to the highest level of central processing introduces complications because individual neurons can have different response profiles, regardless of their proximity to each other, especially in the auditory system (Bandyopadhyay S *et al.* 2010). Generally speaking, this complexity increases at each level of the central system. Auditory brainstem implants are a clinical second choice for situations where cochlear implants would not be indicated because that target location is the first processing center of the central auditory system, however, they are known to be less effective and are more difficult to implant (Brackmann DE et al. 1993). Thus, we must aim to target a location that is sufficiently central that it is a viable option for the treatment of a large number of

patients or pathologies while also allowing the implant to effectively stimulate a perceptually relevant circuit.

1.4 Device Failure and Histological Assessment of the Device Tissue Interface

Chronically implanted electrode arrays suffer the effects of a pronounced immune response, which limits the efficacy of neuroprostheses. Fortunately, this response has become increasingly well-characterized by histological preparations. Traditional histology uses perfusion-fixed tissues and cell-specific stains or antibodies to label tissues of interest. While the field has used and still often uses frozen-fixed sections and thin slices to image small neural structures such as synapses(Bartlett EL and PH Smith 1999), more recent approaches have attempted to capture thick slices of brain tissue in order to image large, intact neural circuits in a single slice(Woolley AJ *et al.* 2011; Chung K *et al.* 2013). Thick-slice histology limits sample size by reducing the total number of slices generated from a single brain. It also reduces the resolution with which small structures can be examined deep within the slice, as light penetrating the slice will be scattered more than transmitted. However, thick-slice histology offers the ability to capture an entire electrode tract within a single slice such that the profile of the immune response can be observed in three dimensions. Additionally, the electrode itself can be captured within the slice, allowing researchers to characterize direct cellular interaction with features on the surface of the electrode.

Regardless of the method employed, the device-tissue interface has been assessed in many ways. Chronically implanted devices are known to exhibit inflammatory and neurotoxic effects, so immunohistochemistry labels such as ionized calcium-binding adapter molecule 1 (Iba1) for microglia, glial fibrillary acidity protein (GFAP) for reactive astrocytes, RIP protein antibody (RIP) for myelinated axons, and hexaribonucleotide binding protein-3 (NeuN) for neuronal nuclei, are all commonly used to assess the evolution of the inflammatory response within the brain. Previous work has revealed a proliferation and migration of local microglia toward penetrating electrodes, the formation of a multinucleated “glial sheath”, astrocytic projections attempting to encapsulate chronically implanted devices, neural atrophy around the electrode, and a reduction in myelination in deep cortical layers nearby implanted electrodes (Williams JC et al. 2007; Grill WM et al. 2009; McConnell GC et al. 2009; Woolley AJ *et al.* 2011). All of this information, collected at various time points across the profile of the complex

immune response, is currently being used by labs across the country to engineer solutions to the problem of immune rejection of chronically implanted devices.

Histological characterization of the device-tissue interface can also reveal circuit properties of local nervous tissue and reveal the physiologic effect of microstimulation. The protein c-Fos is a proto-oncogene which has upregulated expression when neurons fire action potentials. This expression begins approximately 15 minutes after prolonged neural activity and peaks approximately 1 hour after such activity (Hu E et al. 1994). Neuroscientists of many disciplines use c-Fos to identify neural targets that have been activated by natural (VanElzakker M et al. 2008), drug-induced (Graybiel AM et al. 1990; Nichols CD and E Sanders-Bush 2002), or electrical stimulation (Molander C et al. 1992). Because c-Fos is a relatively non-specific indicator of neural activity, it can be used to identify brain regions that are functionally connected to a region which has received focused stimulation and reveals that region's circuit outputs throughout the brain.

2. MUTUAL INFORMATION IN THE THALAMOCORTICAL CIRCUIT

2.1 Introduction

Despite great efforts made toward understanding the molecular and neural mechanisms of anesthetic and sedative drugs (Antkowiak B 2001; Rudolph U and B Antkowiak 2004; Franks NP 2008), a unified theory of the network changes under various levels of consciousness or unconsciousness remains elusive. Changes in neural properties in the thalamocortical network are strongly implicated as a driving force for the loss and recovery of consciousness, and this network is central to theories regarding neural correlates of consciousness (Edelman GM 2003). However, the specific roles of cortex and thalamus in changing global brain states are unclear. The role of top-down versus bottom-up processing during loss-of-consciousness is of critical importance to understanding network changes in this circuit, as understanding the origin and mechanism of loss of consciousness in thalamus and neocortex may aid in the development of new intraoperative tools to monitor loss and regain of consciousness.

Previous work studying the neural basis for loss-of-consciousness has identified that anesthetics suppress activity in thalamus, leading to suppression of ascending input into sensory cortex (Ries CR and E Puil 1999; Alkire MT et al. 2000), and laid the groundwork for the *thalamic switch hypothesis* (Alkire MT et al. 2000). However, it has been demonstrated that suppression of cortical responses can be unrelated to awareness (Kerssens C et al. 2005), and in some cases, cortical sensory responses can be dramatically enhanced rather than suppressed during unconsciousness (Imas OA et al. 2005). In fact, anesthetics tend to have minimal effects on large scale organization and responsiveness of "core" thalamic nuclei that provide the bulk of ascending input into cortex (Jones EG 1998; Saalmann YB 2014), suggesting that thalamocortical signaling remains mostly intact during unconsciousness. While this ascending information continues to activate cortex, evidence suggests that it fails to activate an anesthetized cortical network with the same efficiency as a conscious one (Boly M et al. 2012; Liu X et al. 2012). The *information integration theory of consciousness* (Tononi G 2004) captures this premise, suggesting that integration of ascending information is necessary in order for a network to achieve consciousness. According to this theory, anesthetic drugs would need to work over a wide range of neural targets to reduce the number of available network states and connectivity

between functional regions (Alkire MT et al. 2008). Thus, a closely related theory of anesthetic action, the *cognitive unbinding hypothesis* (Mashour GA 2013, 2013; Mashour GA and MT Alkire 2013), suggests that while ascending input arrives in cortical structures, corticocortical desynchrony prevents integration of information, creating lack of awareness through a disrupted perception of the environment. Both the information integration theory and cognitive unbinding hypothesis implicate changes or actions upon cortex are the primary drivers of loss-of-consciousness, suggesting that the observed thalamic suppression of ascending input is either a readout of anesthetic-induced unconsciousness, or possibly plays a complementary role. In either case, the stronger anesthetic effect on corticocortical connectivity (Massimini M et al. 2005; Ferrarelli F et al. 2010) and top-down pathways (Raz A et al. 2014) may be responsible for the modulation of cortical representation of sensory information.

We hypothesize that the thalamocortical and corticothalamic pathways will be differentially affected by anesthesia, and specifically at doses causing loss of consciousness. Information theoretic approaches in neural systems are a quick, high throughput mechanism to study information flow, and can be used with data from invasive (Nelken I et al. 1999; Nelken I et al. 2005; Chechik G *et al.* 2006) or non-invasive neural recordings (Jeong J et al. 2001; Schlögl A et al. 2002) in the operating room without the need for expensive scanning equipment or long time series. In the invasive preparation, neural spike trains can be studied as is, using the rate and temporal dynamics of a spike train to encode the stimulus. This is particularly important in the auditory thalamocortical system in which acoustic information is encoded in both spike rate and timing (Miller LM, MA Escabí, HL Read, *et al.* 2001; Miller LM, MA Escabí and CE Schreiner 2001; Miller LM et al. 2002; Bartlett EL and X Wang 2007; Wang X et al. 2008; Huetz C et al. 2009; Bartlett EL and X Wang 2011; Huetz C et al. 2011), so information theoretic approaches in this system should be designed to measure both of those response profiles.

While several studies have attempted to characterize information flow and cortical connectivity under various states of consciousness, most have used a form of peripheral, natural stimulation as a tool to activate the network. Under this experimental protocol, the stimulus passes through multiple subcortical nuclei and is already affected before reaching the thalamocortical circuit. Furthermore, feedback pathways cannot be directly assessed in the absence of feedforward pathways. Therefore in this work, we assess the information flow in the

thalamocortical and corticothalamic directions using microstimulation of each nucleus, with simultaneous recording of the neural response to stimulation in the other nucleus. Using an information theoretic approach, we characterize the reduction in network information and changes in network synchrony which further validate the role of top-down pathways during loss-of-consciousness.

2.2 Methods

Measurements were collected from 3 young adult male (age 4-6 months) Sprague-Dawley rats (Envigo, Indianapolis, IN). All procedures were approved by the Purdue Animal Care and Use Committee (PACUC 1204000631). The animals used in these studies were previously trained on an acoustic discrimination task that involved the discrimination of Gaussian noise from amplitude modulated Gaussian noise, but were naïve to the electrical stimuli used here. None of the rats had previous training related to tonal stimuli. All recordings were obtained under passive conditions and the rats were not performing any trained behaviors.

2.2.1 Surgical preparation

Aseptic animal surgeries were performed as previously described (Vetter RJ et al. 2004). Briefly, unconsciousness in rats was induced with isoflurane in air (5%) until loss of righting reflex was achieved, followed by delivery of a cocktail of ketamine (80 mg/kg) and dexmedetomidine (0.2 mg/kg) intraperitoneally to ensure a continued anesthetic depth of unconsciousness. Depth of anesthesia throughout surgery was monitored via frequent paw withdrawal reflex tests and maintained with additional intramuscular injections of ketamine upon reflex recovery. After anesthesia was confirmed, the animal was positioned in a stereotaxic head holder with hollow earbars to facilitate intraoperative electrophysiological recordings. Body temperature was maintained under anesthesia with a thermostatic water circulating pad and breathing and heart rate were monitored via pulse oximeter. After positioning in the stereotaxic head holder, the rat was shaved and the scalp was scrubbed for aseptic surgery.

An incision was made along the sagittal suture from bregma to lambda. The skin was loosened with blunt dissection and reflected to expose the dorsal face of the cranium. The right temporalis muscle was partially excised, with remaining portions reflected, to allow access to the cranium over the right auditory cortex. Four burr holes were drilled manually at positions rostral

to bregma and caudal to lambda, all 3-4mm from midline, such that the bones screws would not interfere with the two electrode headstages. After the burr holes were complete, the holes were widened manually with a #56 hand drill to accommodate 0-80x1/8" stainless steel screws which would serve as the reference and ground for the electrode arrays. For a dorsal approach to the medial geniculate body, an approximately 2mm diameter craniotomy was centered at -5.5mm bregma, 3.5mm right of midline. The ventral division of the medial geniculate body was primarily targeted for this experiment using a linear 16-channel array of 703μm^2 sites with 100µm site spacing (A1x16-Z16-10mm-100-703; NeuroNexus, Ann Arbor, MI), causing some of the sites (4-5) to reside in the dorsal division. These sites were never used for electrical stimulation, but recordings at these sites were analyzed along with sites from the ventral division. The 2mm diameter craniotomy over primary auditory cortex was performed caudally and dorsally to the squamosal suture. Primary auditory cortex was approached perpendicularly to the surface of the brain using a four shank electrode array with four, 703μm^2 sites per shank (A4x4-HZ16-3mm-100-125-703_21mm; NeuroNexus), such that each shank resided along a different cortical column. The cortical electrode array was manually positioned to a depth of 1mm such that the most superficial site recorded putatively from layer 4. Surgical placement of the electrodes in both cortex and auditory thalamus were verified via intraoperative electrophysiological recordings of evoked responses to Gaussian noise bursts at 80dB SPL delivered through hollow earbars. After electrode placement was validated, the electrodes were locked in place with a two-part silicone elastomer (Kwik-Sil; World Precision Instruments) and the headcap was secured with UV curable dental acrylic. The animal was then allowed to fully recover from unconsciousness and was returned to his home cage. Post-operative assessments of weight and wound care were completed for 5 days after surgery, and daily administrations of meloxicam (1 mg/kg) in saline were delivered for postoperative pain management.

2.2.2 Electrophysiological recordings

Beginning three days after surgery, electrophysiological recordings were used to measure neural responses to acoustic and electrical microstimulation in both the medial geniculate body and primary auditory cortex. Recordings were collected from an acoustically and electrically isolated chamber (Industrial Acoustics Corporation). On each day of recording, the rat underwent a full bout of conditions of consciousness: wake, sub-hypnotic, just hypnotic, and

recovery. For each drug condition, a loading period of 10 minutes was followed by an equilibration period. The next set of recordings only began after the animal had maintained a state of consciousness for a period of 10 minutes. One of two dosages of either isoflurane or dexmedetomidine induced altered states of consciousness while the rat was mildly restrained in a custom restraint apparatus (Fig. 2.1). Isoflurane (~0.6% for subhypnotic, ~0.9% for just hypnotic) was administered via vaporizer through a nosecone, while dexmedetomidine (0.08 mg/kg/hour 10 minute bolus + ~0.016mg/kg/hour dose for subhypnotic, 0.12 mg/kg/hour 10 minute bolus + ~0.024mg/kg/hour dose for just hypnotic) was delivered via tail vein catheterization, with only one drug being used on each recording day and isoflurane always being used on the day prior to dexmedetomidine. Approximately 20 hours passed between recording sessions. The animal's state of consciousness was confirmed before and throughout recording sessions. Sub hypnotic levels of consciousness were confirmed with the presence of a paw reflex and righting reflex, while just hypnotic unconsciousness was verified by a maintained paw withdrawal reflex accompanied by loss of the righting reflex. In the case of dexmedetomidine, a reversal agent (Atipamezole, 1 mg/kg s.q.) was delivered to induce rapid recovery from the drug effect.

Signals from recording electrodes were sampled at ~25kHz on a zif digitizing headstage (Tucker-Davis Technologies) and passed to a RZ2 bioamp processor (Tucker-Davis Technologies) for filtering. Local field potentials were band-pass filtered on-line between 10Hz and 500Hz, while multiunit data were similarly filtered between 300Hz and 5000Hz. Trials which contained pronounced movement artifact were detected via cross correlation between channels and changes in RMS voltage, and these trials were not included in future analyses. Spikes were detected and sorted offline with waveclus (Quiroga RQ et al. 2004), however, insufficient single unit clusters were identified for processing. Thus, all data were analyzed as multiunit clusters.

All of the electrodes used for this study underwent an activation protocol prior to implantation in order to deposit iridum oxide on their surfaces, thereby reducing impedance and increasing charge-carrying capacity (Robblee L et al. 1983). These features were necessary in order to stimulate on our electrodes while maintaining the integrity of the surrounding tissue and our electrode sites (Cogan SF et al. 2004; Merrill D et al. 2005), but the modification resulted in poorer unit isolation. Thus, in all recordings, multi-unit activity was analyzed.

2.2.3 Electrical stimulation

Electrical stimuli were sampled at ~25kHz and built in real time on a RX7 stimulator base station (Tucker-Davis Technologies) and delivered through an MS16 stimulus isolator (Tucker-Davis Technologies). Electrical pulses used for cortical stimulation composed of singular biphasic, symmetric, cathode-leading pulses of 205μs per phase in order to simulate corticothalamic feedback (Crandall SR et al. 2015). Electrical pulses used for thalamic stimulation were composed of a triplet of biphasic, symmetric, cathode-leading pulses of 205μs per phase at 300Hz, in order to simulate a thalamocortical burst volley (Swadlow HA and AG Gusev 2001). All electrical stimulation was performed on four sites in the cortical and thalamic arrays (Fig. 2.1A, gray circles). In the cortical arrays, the deepest sites on each array were selected such that the stimulated layers would be closest to cortical output layers. In the thalamic arrays, sites were selected with the intention of being equally spaced across the extent of the ventral division of the medial geniculate body to target the lemniscal auditory pathway, based on stereotaxic placement of the electrode array. This meant that the deepest site, along with three sites at 300μm intervals in the dorsal direction, were selected.

2.2.4 Information theoretic analysis

In order to study the raw spike trains, an incredibly large number of samples (~2^8 per stimulus) is encouraged in order to reduce the upward bias and variability in information estimates (Treves A and S Panzeri 1995; Panzeri S et al. 2007). Binning responses can help to drive the variability of the information estimates down, even at a lower sample count, through response compression. When combined with a bias correction scheme, error in the information estimate is further diminished. A reliable estimate of mutual information between a stimulus and its evoked response allows for the measurement of small changes in mutual information right on the boundary of consciousness.

Information theoretic analysis was performed by taking 10 millisecond binned spike counts for the first 100ms after stimulus onset. For each of the four stimulus channels in either thalamus or cortex, binned responses in the opposite structure were collected in response to 50 repetitions. Each bin formed a letter of a response word. These responses were fed into a custom Matlab program, which calculated an estimate of the mutual information between the stimulus condition and the response profiles with the following equation:

$$I_{est}(S;R) = \sum_{r,s} P(s)P(r|s)\log_2 \frac{P(r|s)}{P(r)} \qquad (1.1)$$

where S and R represent the stimuli and responses, respectively. To correct for bias in our MI estimate, the MI was calculated by removing the quadratic extrapolated bias (Treves A and S Panzeri 1995; Strong SP et al. 1998; Panzeri S *et al.* 2007) via the following equation:

$$I(S;R) = I_{est}(S;R) - \frac{a}{n} - \frac{b}{N^2} \qquad (2.2)$$

where *a* and *b* are parameters estimated by computing MI estimates (Equation 1) from fractions of the data, then fitting to a quadratic function of 1/*N*. Such was the case for estimates of MI for each channel (Fig. 2.4). In some cases, channels lacked a pronounced response to stimuli and drove the bias-corrected MI to near zero. When a channel displayed consistently low evoked rates (<0.5 Hz) across all states of consciousness and stimulus intensities, the channel was believed to be unresponsive and was excluded from future analysis.

2.2.5 Spike time tiling coefficient

Mutual information analyses are typically used to assess the information conveyed by the spike timing in a neural code, but these measures do not directly assess the precision and reliability of spike timing within or across channels. During the course of information theoretic analysis, it was determined that changing spike rates during loss of consciousness had a major effect on mutual information. For this reason, spike time tiling coefficients were explored as an alternative method to examine pairwise correlations in spike trains (Cutts CS and SJ Eglen 2014). Spike time tiling coefficients were determined for each of the recording channels by comparing responses to stimulation on sequential trials using the following equation:

$$STTC = \frac{1}{2}\left(\frac{P_A - T_B}{1 - P_A T_B} + \frac{P_B - T_A}{1 - P_B T_A}\right) \qquad (2.3)$$

where P_A and P_B represent spike probabilities, and T_A and T_B represent the fraction of tiled time analyzed per trial. For example, if trial *A* were being compared to trial *B*, spikes were first detected in *A* and *B* and a tiling window is set around each spike with a width of $2\Delta t$ (in this work, Δt=5ms). Using the duration of the trial, and the total duration of tiled time, T_A and T_B were calculated. Next, P_A was calculated by assessing the proportion of spikes in trial *A* that occur during the tiled time of trial *B*. The same was done for P_B. This process was repeated for every set of trials for a given channel and the result is averaged for that channel.

2.2.6 Statistical analysis

Statistical analyses were performed using the MATLAB Statistics Toolbox using linear mixed effects models. Initial exploration of the data revealed a significant intrasubject variance which was accounted for as a random effect in our model:

$$X \sim 1 + State + Drug + State * Drug + (1 \mid Rat) \qquad (2.4)$$

Where X was the dependent variable: mutual information or spike time tiling coefficient. Beyond the linear mixed effects models, regression analyses were performed to identify relationships between dependent variables, such as evoked rate and mutual information.

2.3 Results

In our experiment, data were collected in response to a range of stimulation intensities. The range (17µA to 100µA) was initially selected based on behavioral thresholds of perception of electrical stimulation collected from other rats (data not shown), with the intention of collecting some neural responses to sub-threshold stimulation and supra-threshold stimulation. In practice, the spike rasters revealed a suprathreshold neural response to all levels of stimulation, indicating that behavioral salience of electrical stimulation in our task requires greater stimulation intensity than low-level, focal activation of neural circuitry (Fig. 2.2D). In fact, the neural responses to 100uA stimulation, and often to 56uA stimulation, revealed prolonged inhibitory effects which we believed to be linked to wideband forward suppression (Fig. 2.2D). Further evidence of this effect can be seen in the average evoked rates in response to increasing levels of stimulation, where the responses to higher stimulus intensities were driven closer to

zero, sometimes below spontaneous rate, in both the thalamocortical and corticothalamic directions (Fig. 2.2C). We present data collected at the 31μA intensity for the remainder of the article, as it represented the highest stimulation intensity than did not evoke a strong inhibitory effect.

2.3.1 Changes in rate with drug and state

In our study, we elected to use multiple anesthetic or sedative drugs in order to identify common changes in information transfer between each drug condition. We found dexmedetomidine to induce a reduction of spontaneous rate in the just hypnotic condition, while isoflurane induced strong reductions of spontaneous rate in both drug levels (Fig. 2.3). These changes in spontaneous rate occurred in both the corticothalamic and thalamocortical directions. Dexmedetomidine didn't not exhibit a strong effect on evoked rate, and isoflurane's effect on evoked rate was only observed in the corticothalamic direction (Fig. 2.3). While the changes in spontaneous rate are supported by previous work, there is not a strong precedent in the literature for drug effects on firing rates evoked by direct activation of these network pathways.

2.3.2 Channel-specific mutual information

In order to assess channel-specific changes in mutual information, mutual information was calculated on each channel at each state of consciousness by analyzing the neural response to each of four stimulation channels. In figure 2.4, one channel per drug condition and network direction (each column) was selected to display some of the typical response profiles and how those profiles changed with brain state. In most cases, wake and recovery conditions exhibited the highest spontaneous rates and sometimes had stronger sustained response profiles to stimulation. In recordings of the sub- and just hypnotic levels of each drugs, responses either became more onset-driven or disappeared (Fig. 2.4).

2.3.3 Non-reciprocal reduction of corticothalamic mutual information

While many groups have assessed mutual information in auditory systems (Nelken I *et al.* 2005; Chechik G *et al.* 2006; Atencio CA et al. 2008; Gaucher Q et al. 2013), a large majority of the work is restricted to measuring the neural responses to natural stimuli. In our study, we sought to characterize changes in mutual information along feedforward and feedback pathways directly.

Our results show a non-reciprocal reduction of mutual information in the corticothalamic pathway, which was most significant under isoflurane-induced unconsciousness (Fig. 2.5). While the dexmedetomidine corticothalamic data was not found to be significant, the difference between the wake and just hypnotic level of unconsciousness approached significance ($p=.07$), and, if analyzed as a continuous trend from wake to unconsciousness (just hypnotic), the effect was found to be significant ($p<.05$). Further, we found a significant difference in how isoflurane modulated this mutual information change as compared to dexmedetomidine in both the corticothalamic and thalamocortical directions ($p<.001$). Due to the bin sizes used to calculate mutual information, we were concerned our metric might be highly sensitive to rate changes. Thus, we analyzed the change in mutual information versus the change in rate under each drug condition, comparing the sub- and just-hypnotic states to the wake state. We found a correlation between mutual information and rate changes (Fig. 2.6). Rate does drive the majority of the mutual information effect in most cases. However, the r^2 values indicate that at least 40% of the variance in these mutual information changes cannot be attributed to changes in rate.

We also note higher overall thalamocortical information than corticothalamic information at all states of consciousness. Due to our bin size and the differences in stimulation profiles (thalamocortical burst vs. single corticothalamic pulse), it is likely that cortical responses to the thalamocortical stimulation existed in the first two bins, rather than just the first bin as would be the case in thalamic responses. This is the likely cause of the difference in overall magnitude. Because of inherent experimental differences in stimulation profiles, we only examine differences between drug conditions and dosage levels for a given pathway, rather than comparing the pathways directly.

2.3.4 Pairwise dependencies of cortical responses increase with loss of consciousness

Due to the correlation between rate and mutual information, a rate-insensitive method to detect pairwise correlations and synchrony was selected to analyze the responses further. We found cortical spike time tiling coefficients to increase at the sub- and just- hypnotic levels of unconsciousness under both drugs (Fig. 2.7), however, this trend was not different between the two anesthetic drugs as it was using the mutual information metric. In auditory thalamus, the effects were far more variable and did not follow the same trend we saw in cortex, so it is possible that factors other than unconsciousness or anesthetic load are influencing these changes

in auditory thalamus. Generally speaking, wakeful responses have lower spike time tiling coefficients than anesthetized or drowsy responses, and it appears as though cortical circuits return to the wakeful response profile more readily than thalamic circuits.

While analyzing tiling coefficients within a channel's responses to different stimulus conditions gives us an understanding of the surrounding clusters response reliability, comparing between channels (as opposed to between trials) gives us an understanding of how network synchrony changes. During sub- and just-hypnotic levels of dexmedetomidine and isoflurane induced unconsciousness, thalamic networks became more synchronous (Fig. 2.8). Cortical networks responded similarly under isoflurane-induced unconsciousness, but dexmedetomidine induced unconsciousness did not follow a continuous trend with increasing sedative load.

2.3.5 Network response reliability decorrelated from mutual information

We found changes in mutual information and spike time tiling coefficients to be uncorrelated in our data (Fig. 2.9). As expected, channel-specific spike time tiling coefficients were generally found to be decorrelated from rate (not shown), and given the correlation between rate and mutual information, it is unsurprising that spike time tiling coefficient and mutual information would be uncorrelated in our data.

2.4 Discussion

This work represents a focused approach to assessing information flow and changes in network properties during loss of consciousness. To this end, we electrically activated one nucleus of the thalamocortical circuit and recorded the resultant effects on the other end of the circuit. Unlike typical studies which assess information between two anatomically connected neurons or networks by comparing two spike trains, we could directly manipulate the pathway in a way that allowed us to approach an deterministic experimental approximation of "effective information" (Tononi G 2004). This method also allowed us to assess changes in network synchrony and timing changes in response to brief, "wideband" stimulation.

We employed anesthetic drugs to achieve global brain state changes as a surrogate for natural loss of consciousness in a timely and repeatable manner. These drugs have known effects on neural circuitry at the single neuron and network levels. We chose to use two drugs,

the volatile anesthetic isoflurane and the sedative dexmedetomidine, such that we could examine the effects of changes in unconsciousness that transcend specific pharmacokinetics of each drug.

2.4.1 Drug-induced changes in firing rate

The general anesthetic isoflurane, which has diverse effects on GABA, glutamate, and glycine receptors (Antkowiak B 2001; Grasshoff C and B Antkowiak 2006; Franks NP 2008; Shelton KL and KL Nicholson 2010; Ogawa SK et al. 2011), is well-known for decreasing spontaneous and evoked firing rates at in neocortex (Hentschke H et al. 2005; Land R et al. 2012; Sitdikova G et al. 2014; Noda T and H Takahashi 2015). In our data, we see spontaneous and evoked rate reductions under sub- and just-hypnotic doses of isoflurane that are consistent with the body of previous work (Fig. 2.3). Changes in rate under isoflurane are representative of a generally inhibitory effect of the drug on neural activity. By contrast, the α2-adrenergic receptor agonist dexmedetomidine has been shown to have a much lesser effect on evoked firing rates in the auditory system (Ter-Mikaelian M et al. 2007). In our data, we see a small decrease in spontaneous rate at the sub-hypnotic dose of dexmedetomidine, and a far greater decrease at the just-hypnotic dose (Fig. 2.3). These changes do not appear in the evoked firing rate data, which is consistent with documented effects of the drug.

2.4.2 Change in mutual information and change in rate

Depending on how it is calculated, mutual information can be quite sensitive to changes in total firing rate. In our case, mutual information is computed by averaging spike count per 10 millisecond bin, and as such, higher firing rates may result in higher response entropy, and thus higher total information. Dexmedetomidine was selected to compare with isoflurane specifically due to differences of effect on firing rate in order to create a control for these known effects of rate on mutual information. In our data, we can assign approximately 60% of the changes in mutual information to evoked rate changes under loss of consciousness (Fig. 2.6), and in both the corticothalamic and thalamocortical pathways, we identified a significant effect of the drug used on resultant MI (Fig. 2.5). In the corticothalamic pathway, the interaction effect of Isoflurane on loss of consciousness was also significant ($p<.001$). We believe this interaction effect is due to the strong inverse correlation between Isoflurane concentration and firing rate, which we

document in our findings (Fig. 2.3). However, the remaining 40% or more of variance associated with mutual information changes, as well as the near-significant categorical trend of mutual information reduction in dexmedetomidine-induced loss of consciousness, suggests the non-reciprocal disruption of information flow is associated with loss of consciousness and is not specifically an effect of certain anesthetic drugs.

2.4.3 Validation of competing theories of consciousness

We hypothesized that the thalamocortical and corticothalamic pathways will be differentially affected by anesthesia, and specifically at doses causing loss of consciousness. Our previous work is consistent with both cognitive unbinding and loss of information integration as primary drivers of loss of consciousness, especially in isoflurane-induced unconsciousness (Raz A *et al.* 2014).

Our data reveal an increase in cortical response reliability during input volleys, in sub- and just- hypnotic concentrations of anesthetics drugs (Fig. 2.7). This change in cortical responses is indicative of a reduction of information integration, as sustained cortical processing of stimuli happens in networks distributed throughout a cortical column over several hundred milliseconds (Wehr M and AM Zador 2005; Sadagopan S and X Wang 2010). The proposed loss of sustained cortical processing is evidenced in reductions in gamma and high gamma band power observed in our acoustic data (Fig. 2.10) and by other groups. It is possible that this lack of sustained processing drives thalamic network synchrony up, as corticothalamic feedback becomes less differentiated between stimuli (Fig. 2.8). Further, these changes indicate that thalamic depression is an unlikely initiator of loss of consciousness, as thalamocortical information transmission was unchanged at the low doses of sedatives and anesthetics we used (Fig. 2.5). We should reiterate, however, that thalamus could (and likely does) play a role in loss of consciousness. In fact, it is possible that poorly informative feedback from cortex drives stronger, wideband feedforward suppression, disrupting normal feed-forward processing and driving the entire thalamocortical network deeper into unconsciousness.

2.4.4 Study limitations

While our work provides specific insight into the roles that ascending and descending pathways play in drug-induced loss of consciousness, using electrical stimulation to activate

these pathways introduced limitations to our study. Most notably, the stimulation artifact corrupted the local field potentials for tens of milliseconds after stimulus offset. This ringing artifact was due to our current-controlled stimulus with exceptionally sharp offset passing through our low-pass hardware filter. The only viable frequencies for local field potential analyses were approximately 15 Hz and above, and even at those frequencies, spectral analyses near the stimulus window were still heavily corrupted by the stimulus artifact. Thus, despite our initial interest in providing comparative results between local field and multiunit responses, our work was necessarily limited to the multiunit analysis.

In terms of the results that we were able to provide, however, the duration of each day's experiment was a critical limitation. As noted earlier, gathering a sufficient number of responses to each stimulus condition is critically important for mitigating bias in mutual information estimation. In this work, our desire to collect responses at multiple stimulation intensities, at multiple drug levels, in both network directions, caused experiments to run for exceedingly long periods of time even with non-ideal numbers of repetitions per stimulus. We recommend that future examination of this effect focus on a smaller number of independent variables, in order to reduce experiment duration and information bias.

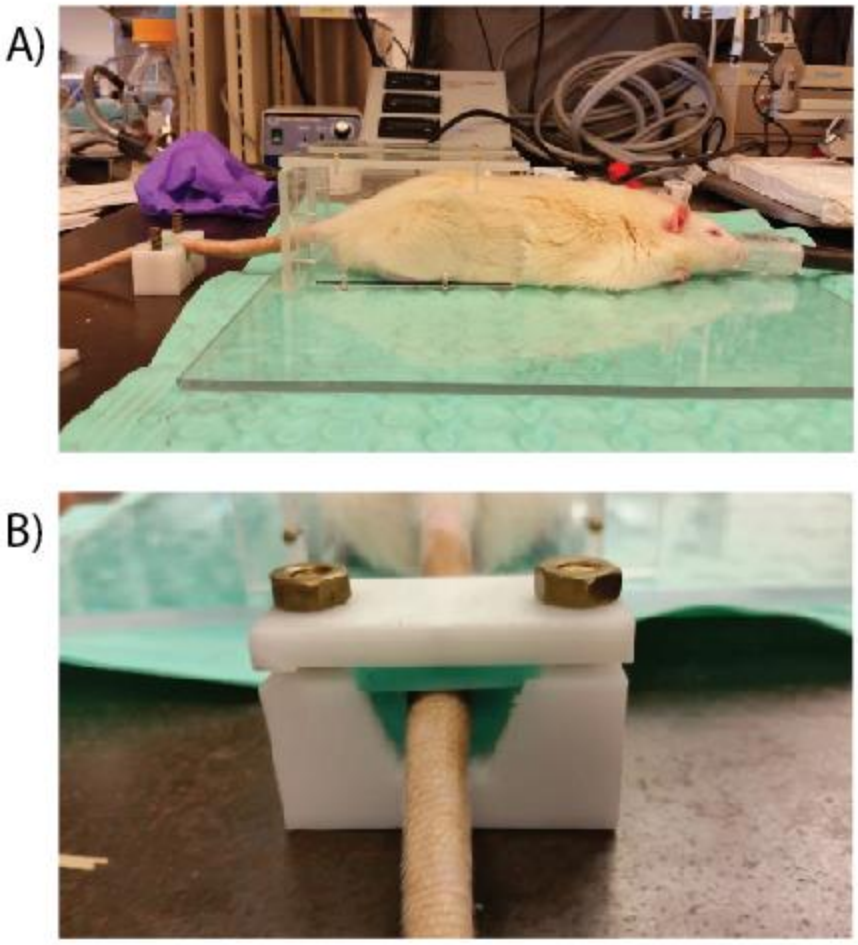

Figure 2.1: Custom Rodent Restraint for Wake Recordings with Tail Vein Access

A, A custom small animal restraint was built to aid in head localization, tail vein injections, and to limit animal mobility during recordings. The restraint consisted of an acrylic base unit which tightly housed the animal's hindquarters. This base unit had a small channel cut through the top that allowed a handler to pull an animal into the restraint from a tail grab. **B,** Once the animal was positioned in the restraint, the tail could be locked into position by a two-part clamp lined with a soft rubber mold. The angles of the clamping mechanism were specially designed to not obstruct the major blood vessels of the tail, and tests confirmed that the tail maintained satisfactory blood flow and responsiveness to stimuli (pin pricks).

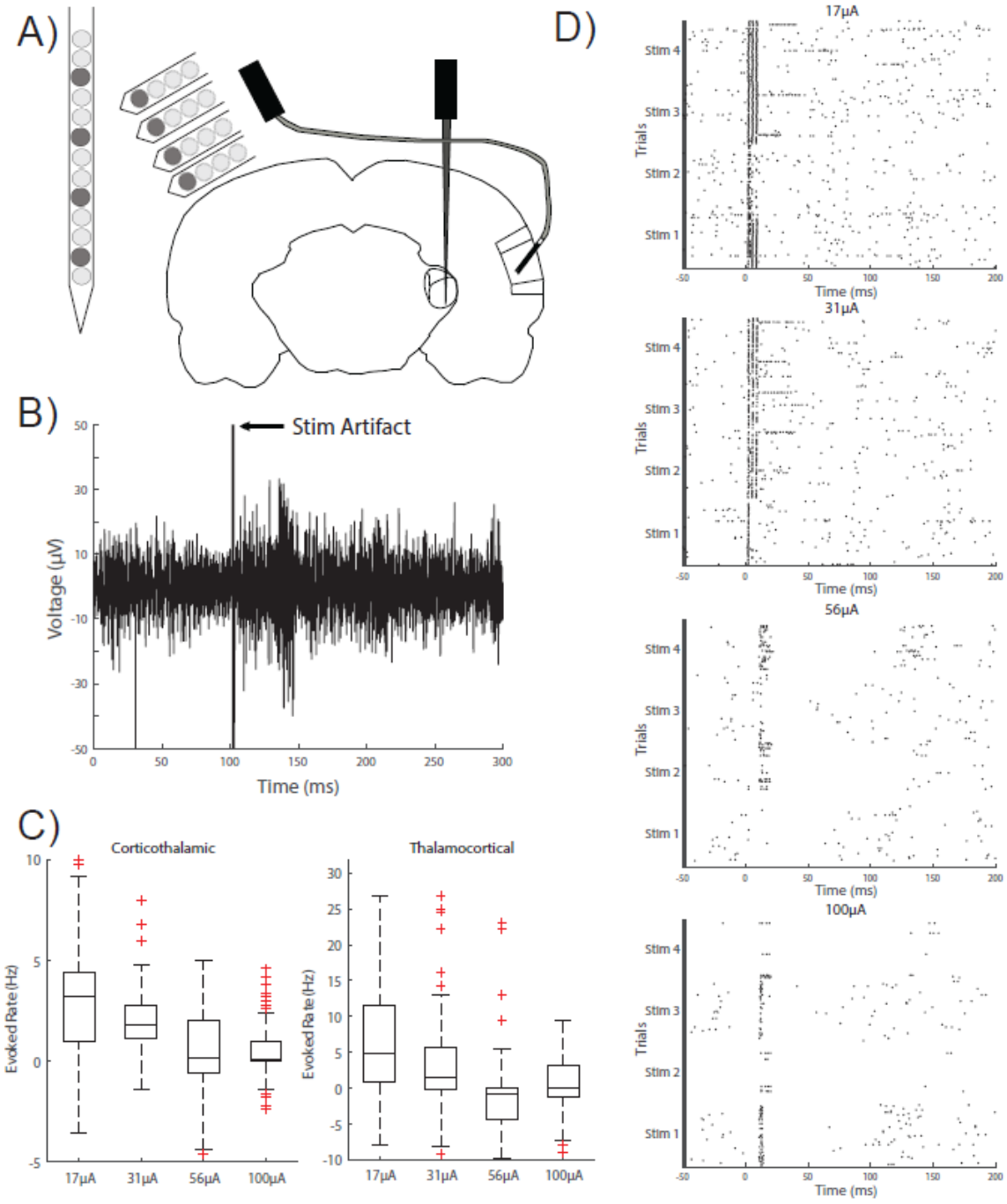

Figure 2.2: High intensity electrical stimulation invokes long-lasting suppression of responses

A, Electrodes were placed in primary auditory cortex and the ventral division of the medial geniculate body. Dark gray circles indicate stimulating electrodes (Stim 1-4, 1D), while responses were recorded on all electrodes from a given multichannel array. **B,** The stimulus artifact in our raw, multiunit activity data had excessively large amplitude compared to normal spiking data, and was easily detected and removed. **C,** Despite removal of the stimulus artifact, high intensity stimulation had a tendency to suppress responses to all stimulus channels. **D,** In extreme cases, such as at 56μA and 100μA, neural activity could be suppressed for over 100ms. For this reason, 31μA stimulation was used for future analysis.

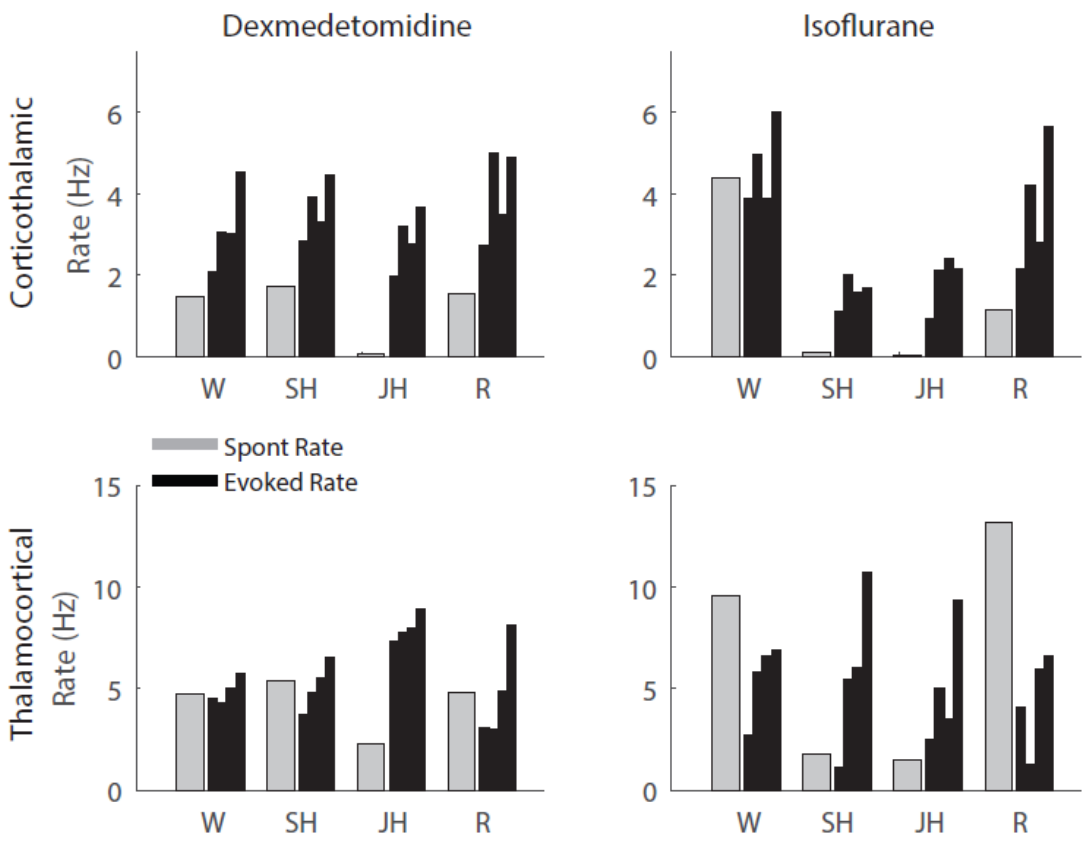

Figure 2.3: Isoflurane causes a characteristic reduction of spontaneous rate

Dexmedetomidine and Isoflurane were used in comparison in order to control for the known effects of Isoflurane on firing rates. Bars represent spontaneous (gray) or evoked (black) rates, where each black bar represents a rate response to a specifici stimulation channel. In both corticothalamic and thalamocortical directions, Isoflurane had a marked effect on rate at the sub- and just- hypnotic doses. These effects were not as prevalent in Dexmedetomidine-induced unconsciousness.

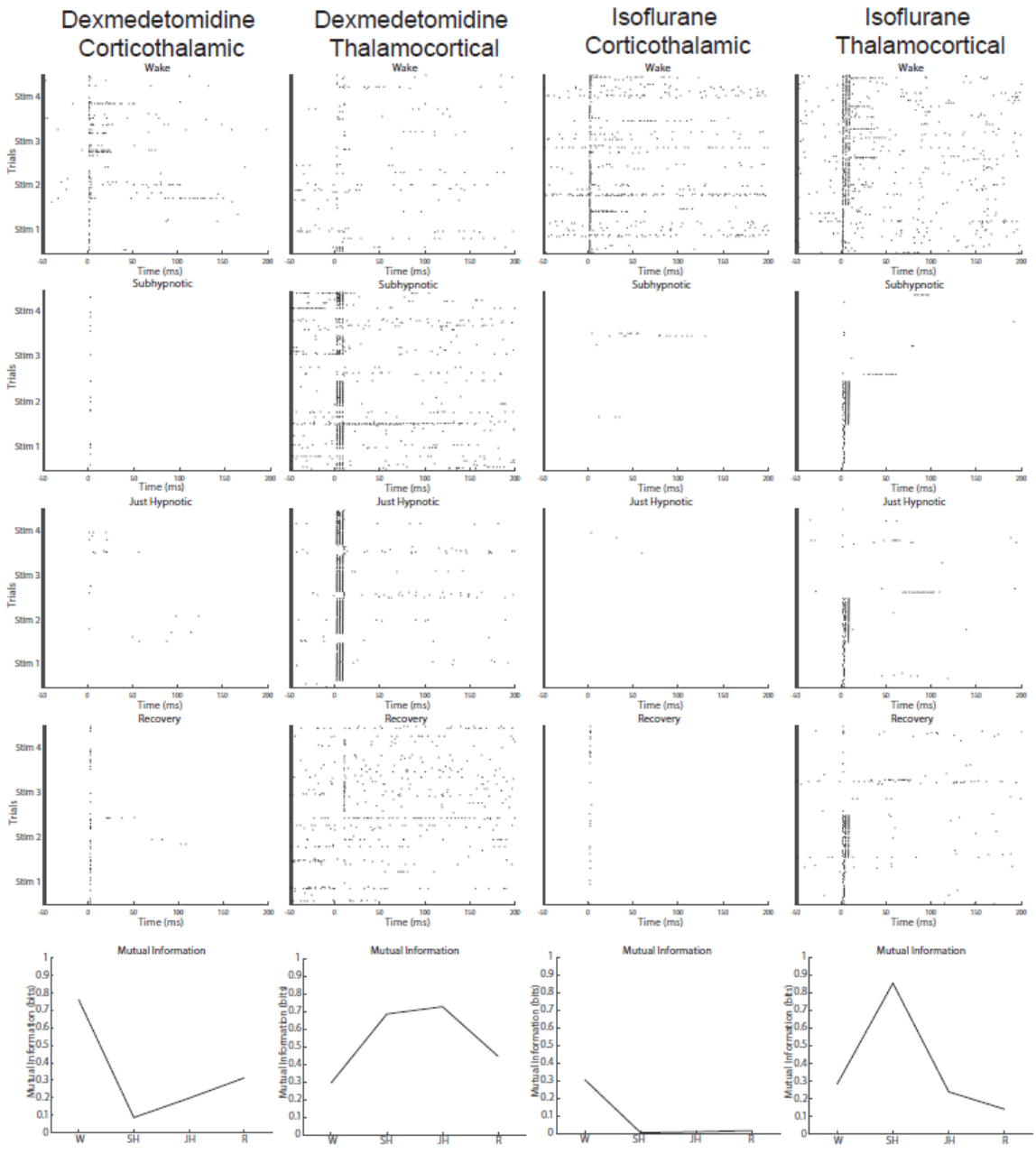

Figure 2.4: Calculation of channel-specific mutual information

For each channel, spike probabilities per bin were calculated for the first 100 milliseconds after stimulus onset. At each state of consciousness, for each channel, a mutual information was calculated. Generally, responses occurred in the first 2 bins (first 20ms), but in the wake and recovery conditions, responses were more distributed.

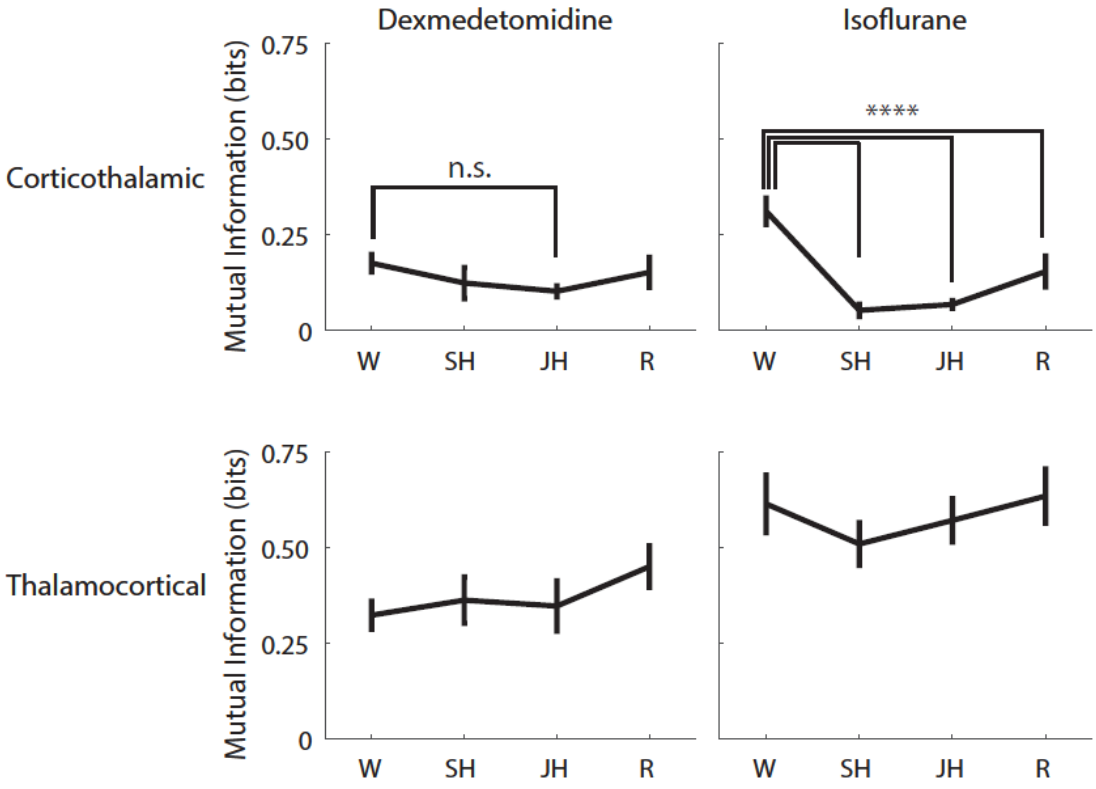

Figure 2.5: Corticothalamic mutual information decreases with loss of consciousness

In both cases of drug-induced loss of consciousness, corticothalamic information tended to decrease as the drug dose increased (top). In isoflurane induced unconsciousness, this effect was statistically significant ($p<.0001$), however, in the dexmedetomidine case, the effect was not significant when analyzed categorically. When analyzed as a continuous trend, the corticothalamic information was inversely proportional to dexmedetomidine dosage ($p<.05$). Thalamocortical information was unaffected by states of consciousness induced by either drug, at any dosage.

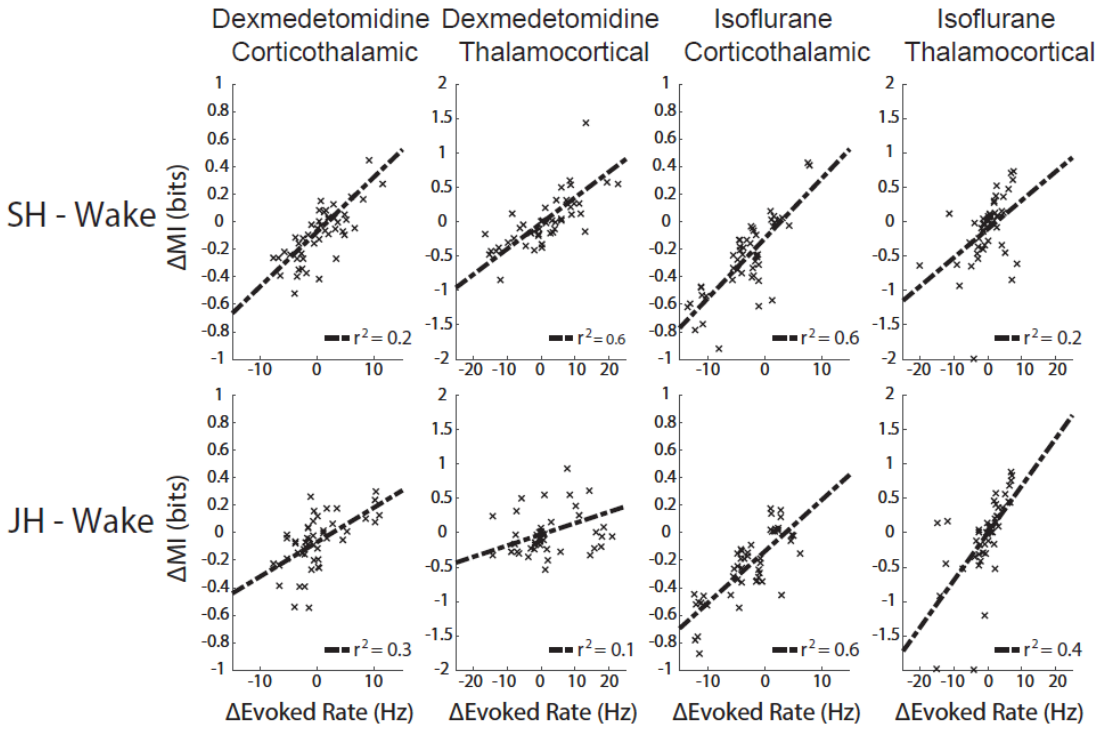

Figure 2.6: Changes in mutual information correlate with changes in rate

Our assessment of mutual information used relatively large bin sizes, and as such, our estimate of mutual information was largely dependent on evoked firing rate. In dexmedetomidine-induced unconsciousness, the rate effect on mutual information was less informative (lower r^2), however, in isoflurane-induced unconsciousness, rate changes more reliably explained mutual information changes (higher r^2), especially in the corticothalamic direction.

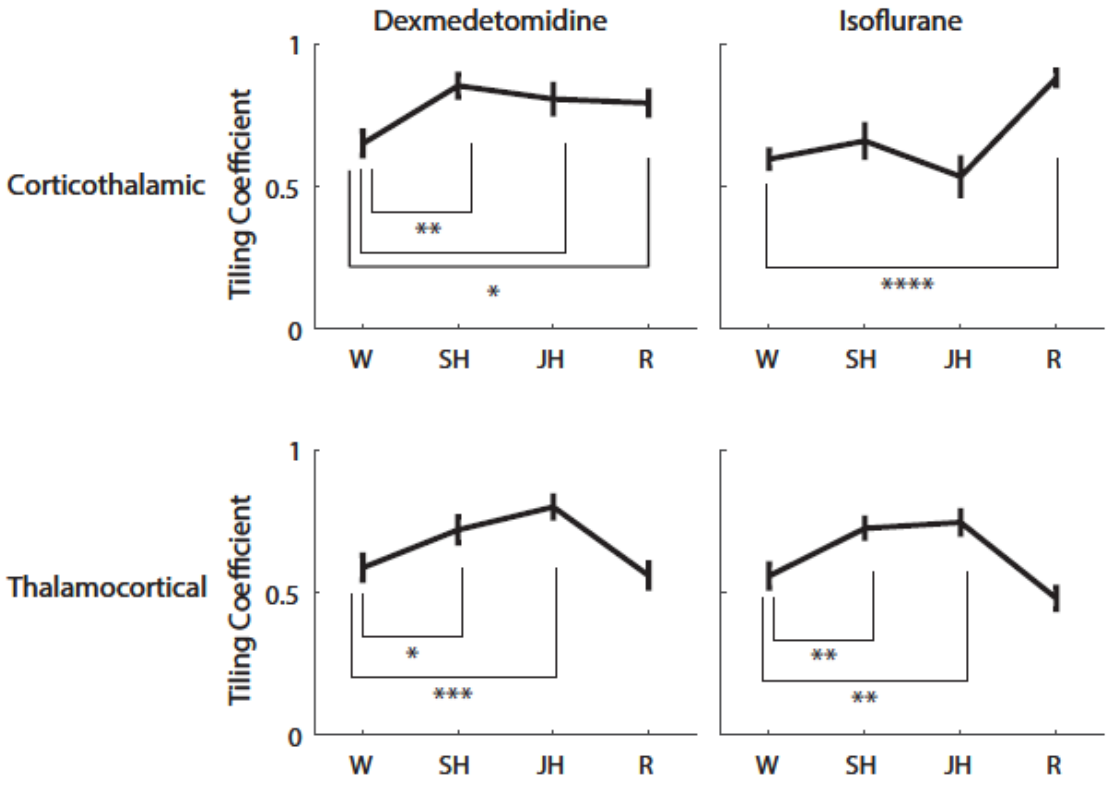

Figure 2.7: Cortical spike time tiling coefficient increases with loss of consciousness

Spike time tiling coefficients were calculated in the first 100 milliseconds after stimulus onset, for each channel. We found thalamocortical tiling coefficients to significantly increase in the sub- and just-hypnotic levels of both dexmedetomidine and isoflurane before recovering, however, we found the corticothalamic changes to be less predictable. In the dexmedetomidine case, thalamic tiling coefficients seemed to increase, but not recover completely, while in the isoflurane case, the tiling coefficient only increased significantly during the recovery session.

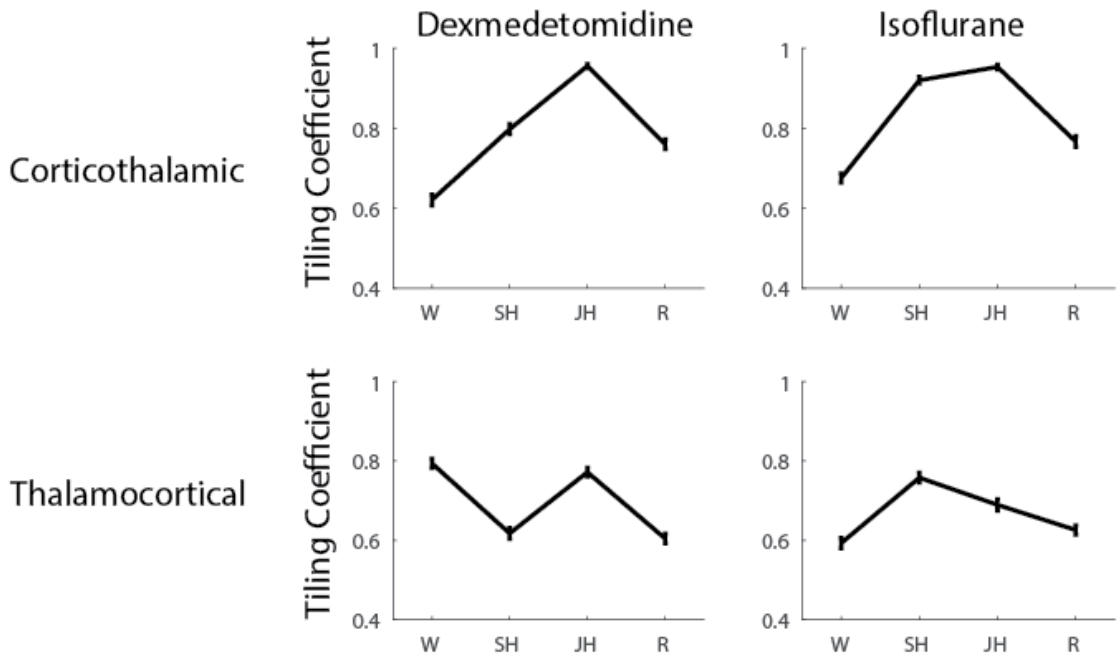

Figure 2.8: Interchannel spike time tiling coefficient

Spike time tiling coefficients were also calculated across multiple recordings channels, as opposed to across trials, in order to understand network synchrony as opposed to a multiunit cluster's response reliability. Network synchrony in thalamus was found to increase with loss of consciousness derived from both drugs, however, cortical network synchrony only appeared in reliably increase in response to isoflurane-induced unconsciousness.

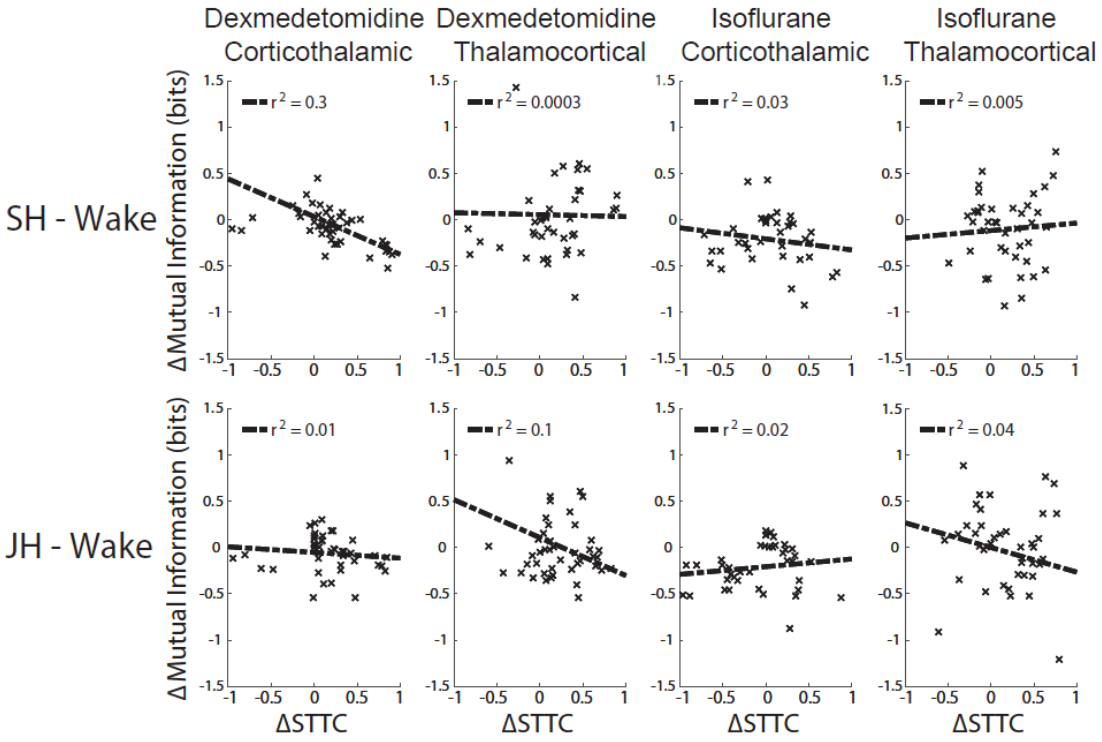

Figure 2.9: Changes in mutual information and spike time tiling coefficient are not correlated

Based on previous work (Cutts CS and SJ Eglen 2014), we did not expect the changes we observed in spike time tiling coefficient to be correlated with changes in mutual information, as mutual information was correlated with rate (Fig. 5) and spike time tiling coefficient was not (not shown). Except in the case of subhypnotic levels of dexmedetomidine, changes in spike time tiling coefficient did not reliably predict changes in mutual information.

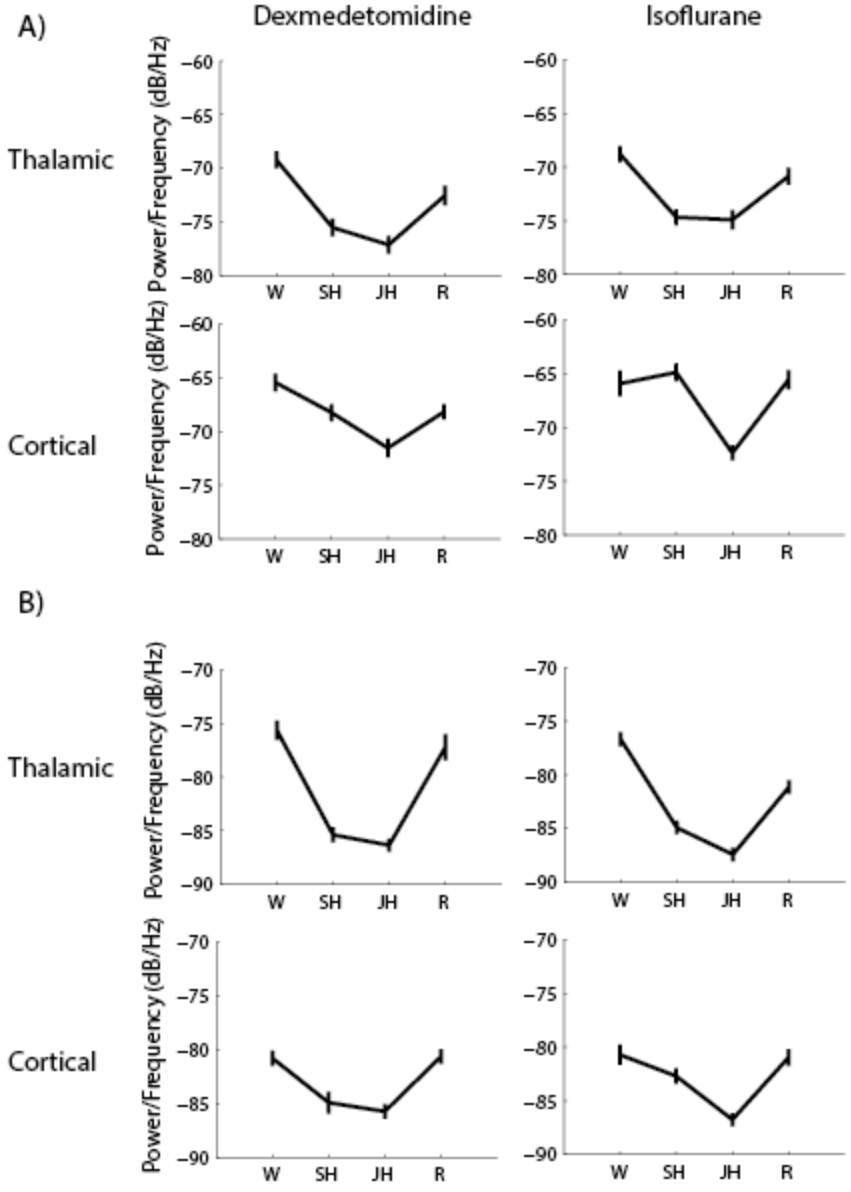

Figure 2.10: Gamma and high gamma band power decrease with loss of consciousness

In both thalamic and cortical networks, average power in the **A** gamma and **B** high gamma bands during stationary acoustic stimuli (band-passed noise) were reduced with loss of consciousness. While both drugs instigated this change, subhypnotic levels of isoflurane appeared to have less of an effect than dexmedetomidine in cortical networks.

3. THRESHOLD STABILITY AND CHRONIC STIMULATION EFFECTS

3.1 Introduction

Sensory neuroprostheses offer the possibility of partial or complete sensory restoration to patients. The success of cochlear implants suggests the vast potential for restoration in other sensory systems (Zeng FG and RV Shannon 1992, 1994; Shannon RV et al. 1995). Unfortunately, not all etiologies of chronic sensory deprivation can be addressed with a peripheral neuroprosthetic such as neurofibromatosis type 2 (NF2) (Asthagiri AR et al. 2009). The central nervous system offers many desirable target nuclei for these devices, but the invasiveness of the electrode arrays tend to cause a pronounced immune response and prohibits frequent surgical modifications.

The intensity of electrical microstimulation from these devices is typically calibrated to a behavioral or neural threshold and changes over time primarily due to electrical impedance changes. Impedance changes around the active electrode site require a larger voltage to deliver the desired current-controlled pulse (Williams JC *et al.* 2007). These impedance changes are believed to be caused by the changing cell population around the electrode site, specifically a marked increase in activated microglia and reactive astrocytes (Woodroofe MN et al. 1991; Giulian D, J Li, B Leara, et al. 1994; Giulian D, J Li, X Li, et al. 1994; Babcock AA et al. 2003), and can be verified by a lumped circuit model (Williams JC *et al.* 2007). In devices implanted longer than several weeks, microglia and reactive astrocytes have been observed forming a glial sheath around the device in an attempt at phagocytosis, reducing the efficacy of current delivery (Polikov VS et al. 2005). Many groups have attempted to lessen the immune response to these devices with the hope of reducing chronically high impedances and encourage acceptance of the device into the local circuitry. Recently, many groups have been exploring the effects of reducing device surface area (Skousen JL *et al.* 2011), adding electroactive coatings (Wilks SJ et al. 2009; Venkatraman S et al. 2011; Wilks SJ et al. 2011), delivering anti-inflammatory drugs through dissolvable coatings (Zhong Y and RV Bellamkonda 2007; Pierce AL et al. 2009; Kozai TD *et al.* 2012; Rao L *et al.* 2012), and changing the mechanical stiffness of the device (Takeuchi S et al. 2005; Kozai TD and DR Kipke 2009; Ejserholm F et al. 2015). Fortunately, all of these well-studied methods are applicable to multiple types of stimulation modalities and

neural target structures, and are thus easily translatable to future interface designs. Fluctuations in behavioral or neural thresholds can also be caused by neurotoxic effects of implanted devices and stimulation paradigms (Merrill D *et al.* 2005), which have been implicated in driving healthy neurons away over time (Biran R et al. 2005).

Studies of chronic microelectrode performance have invariably shown that implants fail over time, often on a channel-by-channel basis (Williams JC *et al.* 1999). Device failure is linked to losing the ability to interact with the surrounding neural population. In auditory cortical neuroprostheses, increased threshold stability and lower chronic thresholds were found in deeper electrodes (Koivuniemi A and K Otto 2012). However, it is unknown whether the depth-related threshold changes found in auditory cortex are causative, or merely correlative. The explanation of this finding is confounded by increased axon density in deeper tissue layers (Woolley AJ *et al.* 2011), accompanied by a decreased immune response (Woolley AJ et al. 2013), both of which could result in lower intensities required to elicit behavioral responses.

Daily or monthly calibration of chronically implanted devices can help patients maintain device efficacy, but changing thresholds over time can also change perceptual relevance. Increasing the intensity of microstimulation, given a constant impedance, also increases the volume of affected tissue, and as such, intensity increases should not simply be associated with the loudness of a percept. Furthermore, when these threshold fluctuations occur between calibration sessions, patients could be left without access to the full range of sensory input. In this paper, we characterize threshold stability based on behavioral relevance in a chronically implanted rat model. We target the two highest level processing centers of the lemniscal auditory pathway, the ventral division of the medial geniculate body (MGV) and primary auditory cortex (A1), in order to determine which location might be more appropriate for chronic microstimulation. Cortical and thalamic microstimulation are being actively explored for sensory restoration (Romo R *et al.* 1998; Torab K et al. 2011; Berg JA et al. 2013; Thomson EE et al. 2013; Atencio CA et al. 2014), and our hypothesis is that MGV stimulation and A1 stimulation could be used interchangeably as treatments for chronic deafness in cases which cannot be helped with cochlear implants, without the risk of non-auditory stimulation that is prevalent in ABIs. However, we also hypothesize that the encoding of stimulus features into thalamic microstimulation waveforms will be more efficacious, as thalamic neurons encode for less specific stimulus features than cortical neurons (see Chapter 1). We suspect that in some patients,

preference toward either a cortical or thalamic prosthetic might be made by a clinician, taking into account patient specific factors such as the presence of other devices or surgical complications. In both structures, we examined the longitudinal effects of chronic stimulation, as well as the effects of stimulation over the course of a given experimental session.

3.2 Methods

The following experiments were performed using male Sprague Dawley rats in accordance with procedures approved by the Purdue Animal Care and Use Committee (PACUC 1204000631).

3.2.1 Surgical preparation

Following induction with isoflurane in air (5%), an initial injection of 80mg/kg ketamine and 0.2mg/kg dexmedetomidine was administered. The animal was then positioned in a stereotaxic head holder. Heart rate and blood oxygenation was monitored via a pulse oximeter, and body temperature was regulated with a recirculating water bath. Areflexia was maintained with 30-minute assessments of the paw withdrawal reflex, and a visible reflex was accompanied by an i.m. injection of ketamine.

An initial incision was performed along the sagittal suture from bregma to lambda. Blunt dissection was then performed to increase the diameter of the opening, and periosteal tissue was elevated from the cranium to provide access for four bone screws. For thalamic electrode insertion, a rectangular craniotomy of approximately 3x2 mm was centered 6 mm caudal to bregma, approximately 3.5 mm from midline (Paxinos G et al. 1980). Through this craniotomy, a multichannel electrode (NeuroNexus A1x16-10mm-100-703) was driven 6 mm ventrally into the brain through the dura mater. To confirm placement of the thalamic electrode, intraoperative recordings were performed to assess neural responses to Gaussian noise bursts at 80 dB SPL delivered through hollowed earbars. For cortical electrode insertion, the temporalis muscle was reflected to allow access to primary auditory cortex. Auditory cortex was approached via a 3 mm oval craniotomy positioned dorsal to the squamosal suture. In order for the electrode used in cortical stimulation to penetrate the brain, the dura mater was cut and partially reflected to allow for a small insertion site. The cortical electrode (NeuroNexus A4x4-3mm-100-125-703_21mm) was then manually driven to a depth of approximately 1 mm, such that the deepest channel

would reach layer VI, but the most superficial channel would sit at the bottom edge of layer IV (Games KD and JA Winer 1988), to allow for the lowest intensity and most consistent behavioral thresholds (Koivuniemi A and K Otto 2012). After placement of each electrode, the craniotomy was covered in a quick curing silicone elastomer (Kwik-Sil, World Precision Instruments), and the electrode circuit boards were cemented to the cranium using a UV-curable dental acrylic (UV Fusio, Pentron).

After surgeries, animals were monitored for 3-5 days to confirm recovery of lost weight, and pain was managed with daily injections of 0.1 mg/kg meloxicam s.q.. Later histological analysis revealed qualitatively that electrode sites were adequately positioned in A1 and MGV by anatomical landmarks and stereotaxic measurements (Paxinos G *et al.* 1980).

3.2.2 Behavioral training

Behaviors executed in this work were based on previously modeled conditioned avoidance behaviors in various rodents (Heffner HE and RS Heffner 1985; Heffner HE and RS Heffner 1995). More recently, this behavior has been modeled in Sprague-Dawley rats (Koivuniemi A and K Otto 2011; Koivuniemi A *et al.* 2011; Koivuniemi A and K Otto 2012), and it is this experimental protocol which we repeat in our study. Water deprived rats were introduced to the experimental chamber, which contained an electrically active water spout and a metal cage floor. Early in the training process, the desired behavior was simply initiating contact with the water spout, which was rewarded with ad libitum access to water in the experimental chamber. After 2 days of habituation, or when rats would reliably use the water spout for drinking, ad libitum access was replaced with behavioral trials. When rats began drinking from the water spout, they completed a circuit inside a custom built lick detection box. Presence on the water spout initiated a trial, which consisted initially of the presence of lowpassed (< 8 kHz) noise (“warning”) or absence of a sound (“safe”). In warning trials, the animals were conditioned to cease the licking behavior on the water spout. Persistent licking behavior during the warning trial resulted in a mild cutaneous shock (<1.6mA) on the tongue. After the animal achieved sufficient mastery of the task, defined by a behavioral d’ of 2 or greater, which typically took approximately 2-3 weeks of daily training, the task became adaptive. In these adaptive trials, correct behaviors resulted in future trials becoming more difficult (reduced

loudness of noise), while incorrect behaviors resulted in future trials becoming easier (increased volume) by the following equation:

$$Level(next\ trial) = Level\ (previous\ trial) \pm \frac{Adapt\ Range}{20 * \sqrt[6]{Trial\ Number}} \quad (3.1)$$

Where the adapt range was the difference between the warning and safe levels (-100 dB SPL and the starting level). Rats typically achieved auditory thresholds in the range of 25-35 dB SPL during this task, over the course of approximately 60-80 trials. Behavioral series were controlled by custom MATLAB code and a microprocessor circuit on Tucker-Davis Technologies hardware.

After implantation, these same behavioral paradigms were performed with electrical pulse trains acting as substitutes for acoustic stimulation. Thresholds on multiple electrode sites were collected each day, and aspects of the pulse trains were manipulated for experimental purposes, such as the leading phase and pulse rate. These experiments were all performed using the adaptive paradigm, and as such, the thresholds reported are from series where the false alarm rate was less than 20% to control for guessing behavior.

3.2.3 Electrical stimulation

Electrical stimulation on both the thalamic and cortical electrodes consisted of monopolar, biphasic, symmetric pulses arranged in a 650ms pulse train at 100 pulses per second (Fig. 3.1A), which was the same stimulus duration as the acoustic noise burst used for training. Leading phase and pulse rate were experimental variables in some cases, however, thresholds reported for the longitudinal experiment were derived from cathode-leading trains at 100 pulses per second. Electrical waveforms were generated in a custom microprocessor circuit written on an RX7 (TDT) and delivered through an MS16 stimulus isolator (TDT) configured for milliamp mode. In order to achieve electrical impedances optimal for chronic stimulation, all electrodes were electrochemically coated with a thin-film of iridium oxide to achieve a 1 kHz impedance of less than 150 kΩ prior to implantation(Weiland JD and DJ Anderson 2000). There was no correlation between *ex vivo* electrical impedance of the sites (provided they indicated the site was functional) and first day behavioral thresholds.

3.2.4 Thick-slice immunohistochemistry

After the last day of behavioral thresholds, rats were perfusion fixed with 4% paraformaldehyde at 4ºC and the brain was extracted. The brains were then immersed in PBS at 4ºC and sliced using a Vibratome into 250-400µm sections and individually placed into wells of a 24 well plate in cold PBS, with special note taken of the slices around the electrode tracts. No more than 3 days after slicing, the slices then received three sequential five minute washes of Hepes Buffered Hanks Solution with Sodium Azide (for recipes, see Table 1), were briefly incubated in a Sodium Borohydride solution for 30 minutes, then washed three more times at five minutes per wash with a Wash Solution (WS). Slices were blocked in WS for two hours prior to a 48 hour incubation in primary antibodies (Mouse anti-NeuN [Abcam ab104224], Rabbit anti-Iba1 [Abcam ab178847], and Chicken anti-GFAP [Abcam ab4674]) at a 1:400 dilution. After incubation in primaries, the slices were quickly washed in WS six times, then washed six more times at one hour intervals, to ensure that excess primary antibodies had been fully removed from the well. Slices were then incubated in secondary antibodies (Goat anti-mouse Alexa Fluor 488 [Abcam ab150117], Goat anti-rabbit Alexa Fluor 555 [Abcam ab150086], and Goat anti-chicken Alexa Fluor 647 [Abcam ab150175]) and subsequently washed using the same dilution factor, incubation period, and wash protocol as the primary antibodies. Slices were then incubated in a U2/Scale clearing solution for approximately one week before imaging on a Zeiss LSM 710 Confocal Microscope. Images were collected under 10x magnification for a pixel dimension of 2.77µm^2. For each slice, a full tile scan across the width and height of the slice was taken and was stitched in Zen 10. In each tile, a Z-dimension stack (z-thickness 25µm) was taken through the visible range of the slice, typically approximately 250µm, which were then projected into a single plane for display and analysis.

3.2.5 Statistical analysis

Standard frequentist analyses, such as ANOVAs, and regression model analyses via f-tests were performed in Matlab with a significance criteria of $p < 0.05$. For behavioral analysis, channels from all rats were pooled. Regression analysis was performed on pooled threshold data due to intrachannel threshold trends, despite high interchannel variance.

3.3 Results

Behavioral results and statistical analyses were prepared using custom software in MATLAB (MathWorks, Natick, MA). Image analysis was performed in Image J.

3.3.1 Threshold stability

Of interest in this study was the comparison between auditory thalamus and primary auditory cortex as a stimulation target for chronically implanted auditory prostheses. In order to understand how these two interface targets perform over time, thresholds on multiple sites were collected once every three days at minimum. While post-operative behavioral thresholds in both targets were similar shortly after implantation, we found that thalamic thresholds increased over time at a faster rate than cortical thresholds (Fig. 3.2A). In fact, the cortical thresholds were not found to have significantly increased at all over the course of the experimental timeframe, whereas the thalamic thresholds did show a significant increase via an F-test ($p=0.0042$).

In cortical devices, previous work has shown cathode leading pulses to be optimal for achieving lower behavioral thresholds (Koivuniemi A and K Otto 2011). We performed a short experiment to verify that this result was consistent in thalamus, as differences in anatomic position, orientation, and density of axons may have influenced a network preference for anode-leading pulses (Ranck J 1975). Consistent with previous cortical results, we found thresholds derived from cathode leading trains to be lower than those from anode leading pulse trains (Fig. 3.2B).

3.3.2 Intraday threshold adaptation

During our experiment, all subjects were additionally used for a separate behavioral protocol between days of dedicated threshold collection. During some of these days, subjects received an additional amount of stimulation on a single electrode to execute an experiment in electrical stimulus intensity discrimination (Chapter 4). In order to find a sufficient range for intensity discrimination, a threshold experiment was performed on the target site prior to the discrimination task. After the task, during which the subject would receive a suprathreshold level of electrical stimulation on every trial, another threshold experiment was performed.

We found that both cortical and thalamic sites adapted to repeated stimulation by increasing the intensity of stimulation required to elicit a behavioral response (Fig. 3.3, $p<<.001$,

t-test). Thalamic adaptation was found to be more variable than cortical adaptation, but was not found to increase more than cortical adaptation.

3.3.3 Synaptic fatigue follows extended bouts of stimulation

Data collected in chapter 2 were used to examine the possibility of synaptic fatigue occurring during prolonged behavioral stimulation sessions. Thalamocortical burst stimulation was assessed over the course of a 3 minute experimental series. During this period, we found first spike latencies to increase in all rats (example shown, Fig 3.4).

3.3.4 Immunohistochemistry of the electrode-tissue interface

Rats were sacrificed 41 days after implantation and their brains were explanted for histological analyses. Our thick-slice, triple-label preparation allowed us to identify intact glial scar formation around several devices (Fig. 3.5, see Study Limitations). Normalized gray scale values from maximum intensity projections were analyzed up to 500μm away from around each device (Fig. 3.6). For these profiles, a distance of 500μm from each device's tip, along the implant, was selected for analysis such that the width of each probe would be approximately similar at the point of analysis. From that point, a pixel gray value profile was plotted perpendicularly from the device for each label. Only one side of the implant was used for analysis, and the side selected was always the side closer to midline.

We found that profiles for microglia and reactive astrocytes were elevated compared to the contralateral hemisphere, but that these profiles were not significantly different between the cortical and thalamic devices. We did find a significant loss of neurons in the proximity of the thalamic probes ($p<<.001$).

3.4 Discussion

The purpose of this chapter was to define the potential of an auditory thalamic neuroprosthetic in terms of chronic efficacy and stability of the device-tissue interface. To this end, we characterized the intraday and inter-day threshold stability of electrodes positioned in both auditory thalamus and auditory cortex. We found significant increases in auditory thalamic thresholds which we did not identify on cortical electrodes over the course of one month; however, we also found that the behavioral threshold of both auditory thalamic and auditory

cortical electrodes significantly increased over the course of one day of stimulation. In order to ascertain the source of these changes, brains were fixed and labelled for various proteins related to glial encapsulation. Both auditory nuclei exhibited a strong response to the implanted devices, and we found the glial response to cortical and thalamic probes to not be significantly different. However, we did find increased neuron death in thalamus as compared to cortex. While this could explain the longitudinal increase in behavioral thresholds in auditory thalamus, it does not sufficiently explain the intraday effect.

3.4.1 Increased thresholds in response to repeated electrical stimulation

In both auditory cortex and auditory thalamus, we found a significant increase in intraday thresholds, many of which occurred over the course of 10 minutes or less, in response to repeated stimulation on the same channel (Fig. 3.3). In several neural pathways, long-term depression (LTD) can be instigated by prolonged low-frequency stimulation (Chen R et al. 1997; Doyle CA et al. 1997; Mockett B et al. 2002; Bartlett TE et al. 2007; Izumi Y et al. 2013). Typically, this depression can be induced by stimulation frequencies in the range of 1-10 Hz, but the required parameters tend to be affected by the circuit being tested, level of anesthesia, and duration of the stimulation (Chen R *et al.* 1997; Doyle CA *et al.* 1997). In our data, rats typically received stimulation at frequencies less than 1 Hz, and responses did not persist between days, leading us to believe that prolonged low-frequency stimulation induced LTD was not the cause of these increased thresholds.

In the auditory cortex and thalamus, forward suppression or forward masking is an inhibitory response which lasts for hundreds of milliseconds after stimulus offset and is believed to be related to synaptic depression (Bartlett EL and X Wang 2005; Wehr M and AM Zador 2005). If synaptic depression is the cause of the changes we see in these data, we believe presynaptic fatigue, where rapid firing rates at the presynaptic terminal and slow neurotransmitter reuptake limit the efficacy of synaptic transmission, is the source of this short-term plasticity, and evidence of the frequency dependency of synaptic transmission is well documented (Tsodyks MV and H Markram 1997; Markram H et al. 1998; Tsodyks M et al. 2000; Swadlow HA and AG Gusev 2001; Swadlow HA et al. 2002; Swadlow HA et al. 2005). Electrical stimulation at our pulse rate produces tetanic stimulation in a shell of influence surrounding the electrode site (Ranck J 1975). Axons in the affected region that lead to

excitatory and inhibitory terminals are causing excitatory and inhibitory neurotransmitter release events simultaneously. Given the inter-trial duration of approximately 1.5 seconds (mediated by the animal's trial initiation), both excitatory and inhibitory presynaptic terminals are unlikely to have recovered a significant portion of the released neurotransmitters (Ryan TA et al. 1996; Armbruster M and TA Ryan 2011). If excess GABA has not been cleared from the synaptic cleft, a slow buildup of inhibitory neurotransmitters will drive postsynaptic excitability down. While this effect is more frequently observed in cortical networks, auditory thalamus has been shown to exhibit the same behavior, although it does recover faster (Wehr M and AM Zador 2005). One could argue that excitatory synaptic events with similar reuptake kinetics are also occurring in this model which would mitigate synaptic depression, such as excess glutamate in the synaptic cleft. However, using presynaptic fatigue as our model already compensates for this effect. If excitatory synapses are fatigued by previous bouts of stimulation, then future bouts of stimulation will cause less glutamate release. Incorporating all aspects of excitation and inhibition into this explanation, the postsynaptic terminal is held in a state of fluctuation, excitatory and inhibitory events caused by a bath of neurotransmitters in the cleft that can't be cleared quickly enough. When each bout of stimulation occurs, the excitatory postsynaptic events increase in frequency at a faster rate than inhibitory events across multiple synapses due to the ratio of excitatory to inhibitory neocortical neurons. This is not functionally different than when the system is not in a fatigued state, however, the excitatory effect is reduced due to increased latent inhibition and weaker transient excitation.

This theory allows for a biomimetic interpretation of the effects of electrical stimulation in other sensory systems as well, as forward suppression has analogous representations in the somatosensory (Chung S et al. 2002) and visual systems (Carandini M et al. 2002; Freeman TC et al. 2002). Unfortunately, our experiment was not originally designed to examine the mechanism of this adaptation, so we cannot draw any conclusions about how therapeutic electrical stimulation can be improved to compensate for this effect. At the most basic level, it would seem that interfacing with sensory systems in regions with minimal inhibitory feedback would be ideal, which explains the clinical success of the cochlear implant.

However, it should be noted that many sensory systems undergo active adaptation to repetitive stimuli. It is also possible that the effect we see here, which is similarly transient, is simply an active adaptation mechanism. Unfortunately, due to the length of our stimulus trains

and short intertrial interval, it was difficult for us to ignore the possibility of synaptic fatigue as an explanation for this change in behavior.

3.4.2 Pronounced neuron death in auditory thalamus

The longitudinal increase in behavioral thresholds in auditory thalamus, while cortical thresholds did not significantly increase, could likely be explained by differences in the device-tissue interface. Unfortunately, our experiment was designed to test ventral division channels only, so electrode sites in the dorsal division, which qualitatively displayed less neural cell death, were not tested and cannot be used for comparison. Implant design and insertion characteristics are known to have a profound effect on the local immune response to microelectrodes, such as device tethering, cross-sectional area and surface area, and insertion depth (Subbaroyan J et al. 2005; Biran R et al. 2007; Skousen JL *et al.* 2011; Woolley AJ *et al.* 2013; Ejserholm F *et al.* 2015). In our study, the cortical electrodes outperformed the thalamic electrodes in almost all of these areas. Regardless of the probe geometry differences, cortical electrodes and thalamic electrodes started with relatively similar behavioral thresholds, and as such, we attribute changes in behavioral thresholds which we observed to changes in the local cellular environment.

In terms of tethering, our cortical electrodes were only mildly cemented to the acrylic headcap due to the presence of a long, flexible polyamide cable that connected the electrode shanks to the circuit board. This cable was covered in a silicone elastomer prior to being coated in dental acrylic, allowing the cortical electrode to be somewhat flexible around the insertion site. By comparison, the thalamic electrode lacked this polyamide cable, so the electrode shank was directly connected to its circuit board and fully tethered into the dental acrylic headcap. This electrode design was required for easy and repeatability of stereotaxic insertion of the thalamic electrode, as auditory thalamus is a relatively small (~1.5μm^3) and deep brain structure (6mm from dorsal surface) in the rat.

The thalamic electrode's cross-sectional area at its widest aspect, near the most superficial site, was 6150μm^2, and the tip was 3400μm^2. The cortical electrode's dimensions in equivalent locations were 825μm^2 and 495μm^2, respectively. While the thalamic electrode's cross-sectional area was almost an order of magnitude higher than the cortical probe's through its entire length, it is important to note that they were not the same thickness, and as such the thalamic probe's surface area in the longest dimension was only twice that of the cortical probe.

Regardless, this nearly order of magnitude difference in cross-sectional area should be expected to have a strong effect on immune response. Again, the choice of thalamic probe was by requirement, as a sufficiently stiff electrode was required to penetrate two layers of dura mater which were surgically inaccessible in order to reach auditory thalamus.

Insertion depth obviously varied between the two devices and was unavoidable. Neural devices have been shown to elicit immune responses which are inversely correlated with increasing insertion depth, at least in cortical devices (Woolley AJ *et al.* 2013). This depth-related effect could be caused by many factors, including changing device flexibility, changing cross-sectional or surface areas, distance from damage to the dura mater and blood-brain-barrier, or changing neural cell morphologies. In our data, we identified a depth-related immune response in each probe, as well as a trend that the cortical probes generally exhibited a smaller immune response than the thalamic probes. Due to confounding variables of device dimensioning and tethering, we could not separate the effects of insertion depth or distance from major damage to the blood-brain-barrier. Unfortunately, there are insufficient microelectrode studies in which deep brain structures were targeted, and most deep brain stimulatory devices utilize devices that are too dissimilar for adequate comparison to microelectrode arrays, so we are unable to draw further conclusions by addressing the literature.

Thus, we would like to call attention to the inherent challenges of device implantation into sensory thalamic structures. While our data suggest that the device-tissue interface in auditory thalamus was more prone to damaging local neuron populations than the cortical probes we tested, more advanced probe designs which allow for more tip flexibility with smaller cross-sectional areas or surgical techniques which avoid damage to the blood-brain-barrier near thalamus could reduce this effect.

3.4.3 Study limitations

Devices with such pronounced differences in physical characteristics should not evoke a similar immune response in both thalamus and cortex, especially considering the marked difference in neuron death, so why are our device's quantitative glial profiles so similar? We believe that our thick-slice preparation, and coronal slicing orientation, are partially at fault for this result. In 2 out of 3 of our thalamic slices, the multinucleated glial sheath became detached from the slice. We believe it is possible that if the slice was fully intact, we might have

identified a significant difference in microglial and astrocytic activity in the first 25-50μm around the device. Frozen-fixed sections, thinly sliced on a cryotome, would likely have eliminated this experimental limitation.

Further, rats used for this work were implanted with dual electrode arrays for use in other experiments – one in primary auditory cortex and one in the dorsal and ventral divisions of auditory thalamus. We would like to note that cellular and network changes may have been evoked by the device which was not used for stimulation in this experiment, and may have had an effect on behavioral thresholds or histological results.

In two animals, cortical devices were implanted without thalamic devices due to a limited number of available implants. In these rats, histology was performed even though their implant hemispheres would not be directly comparable to the other rats used in the study. We found qualitative and quantitative evidence that thalamic devices may not have been the source of all of the thalamic neuron death observed in our data (Fig. 3.7). In these animals, we found preferential death of neurons in the medial and dorsal division of the medial geniculate body (Table 3.1). This evidence suggests that our study's histological result in thalamus may be confounded by long-range neurotoxic effects from the cortical probe. We hypothesize this medial and dorsal division neuron death to be related to loss of a large portion of feedback from cortical layers 5 and 6, which might drive thalamic neurons in these regions to modify their network properties through apoptosis, but we cannot confirm this hypothesis with the available data.

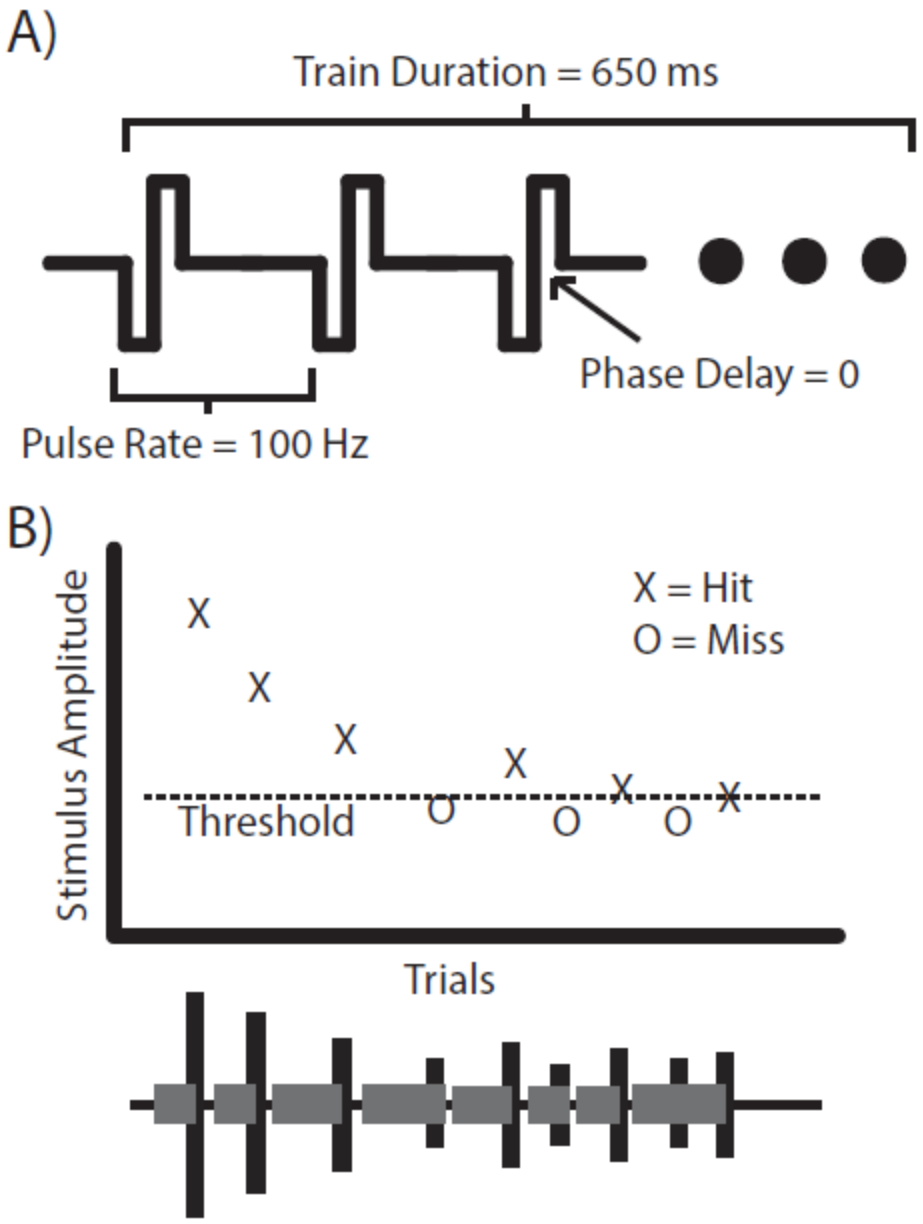

Figure 3.1: Stimulus waveforms delivered in an adaptive paradigm to determine behavioral thresholds

A Electrical microstimulation in both auditory cortex and auditory thalamus was comprised of trains of cathode-leading, symmetric, biphasic square pulses with no phase delay at 100 pulses per second in a monopolar configurations to a grounded bone screw. **B, Upper** These stimuli were delivered throughout a behavioral series in an adaptive fashion, where correct responses ("hits") resulted in reduced intensity in subsequent trials and incorrect responses ("miss") resulted in increased intensity. **B, Lower** Hits and misses were determined by the subjects' failure to cease normal licking behavior in the presence of a stimulus. Grey boxes indicate licking behavior, while black boxes indicate the presence of stimulation at a given amplitude.

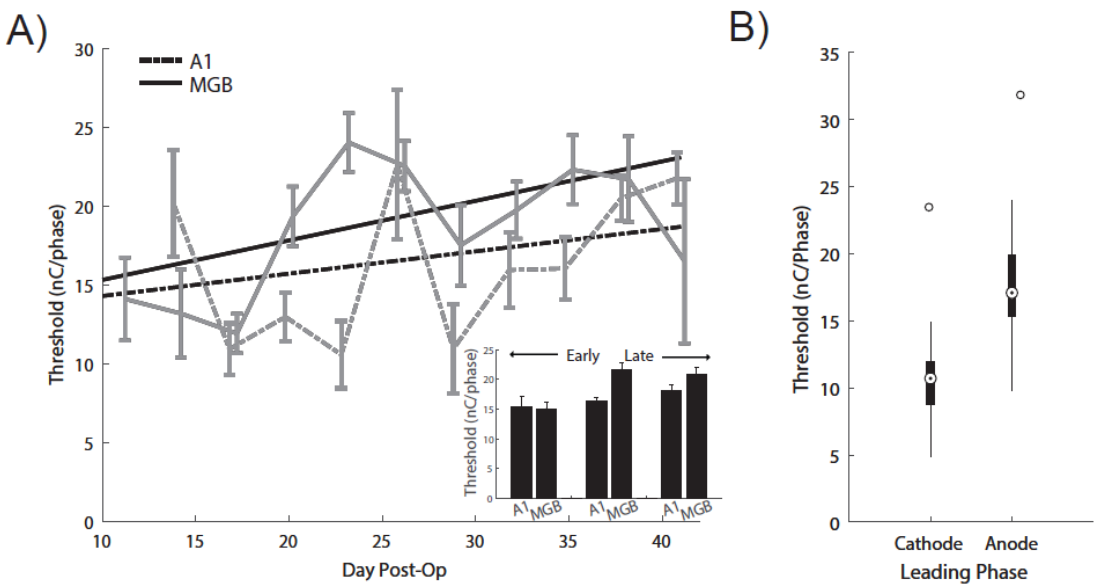

Figure 3.2: Behavioral thresholds increase over time in auditory thalamus

A Behavioral thresholds in response to cortical and thalamic both appeared to increase of the course of the 30 days of our study, however, only the thalamic thresholds were found to increase significantly ($p=0.0042$, F-test). Error bars indication standard error of the mean. Due to interday variability, the trend is more apparent in a 10-day moving average (inset), where each set of bars corresponds to average thresholds for the first, second, and last 10 days of the experiment. **B** Leading phase of the waveform was analyzed in auditory thalamus to confirm that cathode leading pulses elicited lower thresholds ($p<.001$, two-sample t-test), as is the case for other target regions.

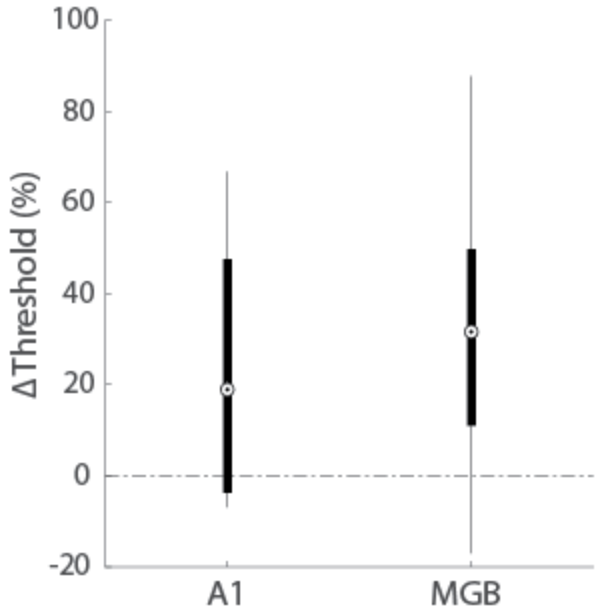

Figure 3.3: Thresholds in auditory cortex and auditory thalamus adapt to repeated stimulation

Cortical and Thalamic thresholds increased over the course of a single day after repeated stimulation at a duty cycle of approximately 1 Hz ($p<<.001$, one-sample t-test). Thalamic and Cortical thresholds were not found to increase at significantly different rates.

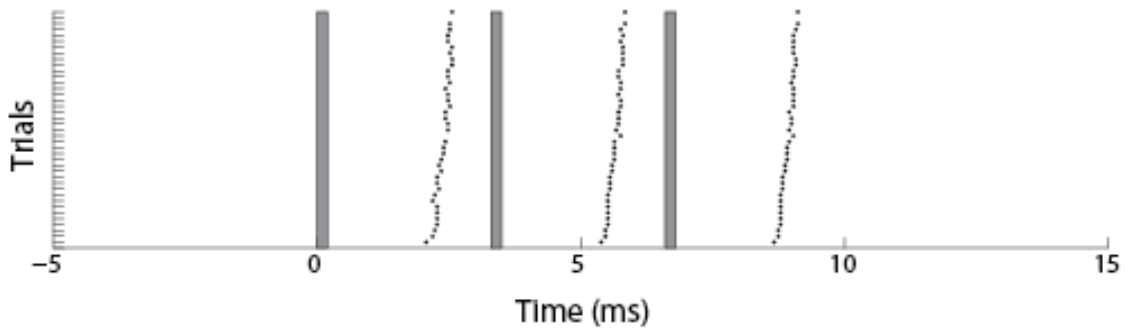

Figure 3.4: Extended periods of stimulation induce response latency changes

In this example, ITMS was delivered on one of four stimulus channels over the course of a 3 minute experiment, using the same paradigm from chapter 2. Latency of cortical responses to thalamic input increased over the course of the 3 minute experiment (responses to one channel shown). Gray boxes indicate the timing of each stimulus pulse.

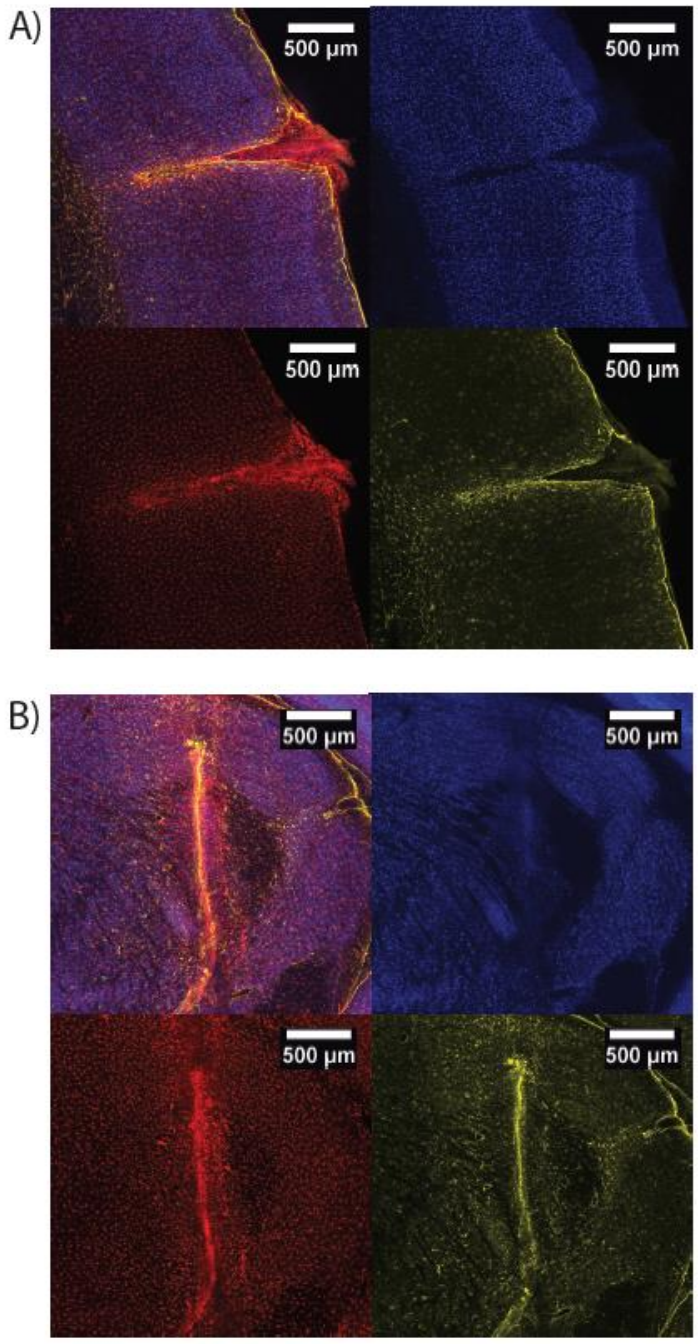

Figure 3.5: Auditory cortex and auditory thalamus exhibit glial encapsulation at the chronic implant site

A The observed corical immune response shows characteristic dimpling around the implant site, along with astrocytic (GFAP, Yellow) and microglial (Iba1, Red) proliferation and migration toward the implant. Microglial multinucleation in frustrated phagocytosis is also observed. **B** A similar response is also qualitatively observed in the medial geniculate body, however, neural death (NeuN, Blue) is noted by decreased NeuN intensity.

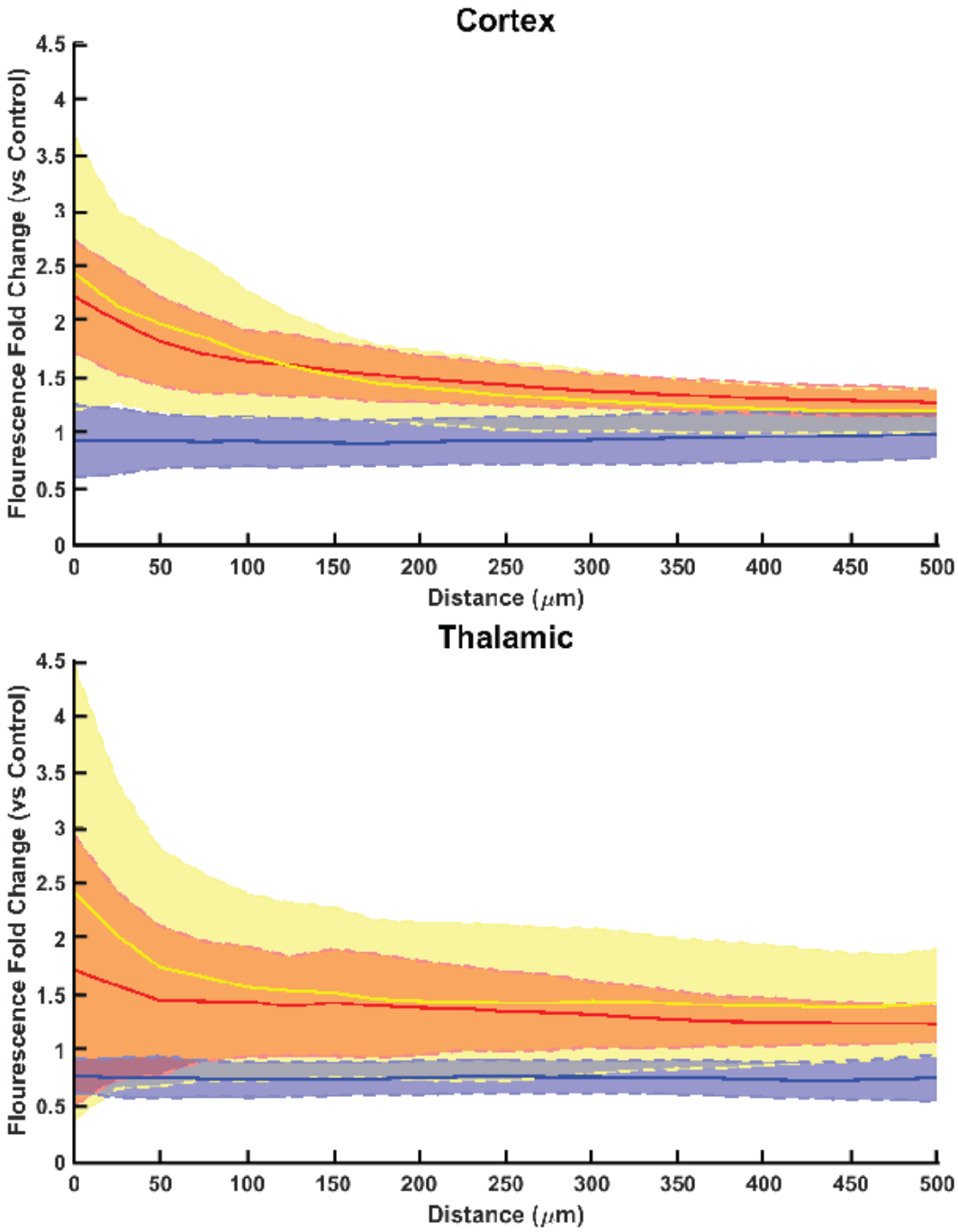

Figure 3.6: Neural death in auditory thalamus

Cortical and thalamic implants provoke a strong immune response close to the implant which decays with distance away from the implant site, as expected. Qualitatively, variance in the thalamic glial response (Red, Activated Microglia, Iba1; Yellow, Reactive Astrocytes, GFAP) is greater than in cortex. We identified a significant loss of neurons (Blue, Neuronal Nuclei, NeuN) in both cortex ($p<.05$, one-sample t-test) and thalamus ($p<<.0001$, one-sample t-test) compared to the contralateral hemisphere control, however, the neuron death in thalamus decreased more so than in cortex ($p<<.0001$, two-sample t-test). Error bars are standard deviation.

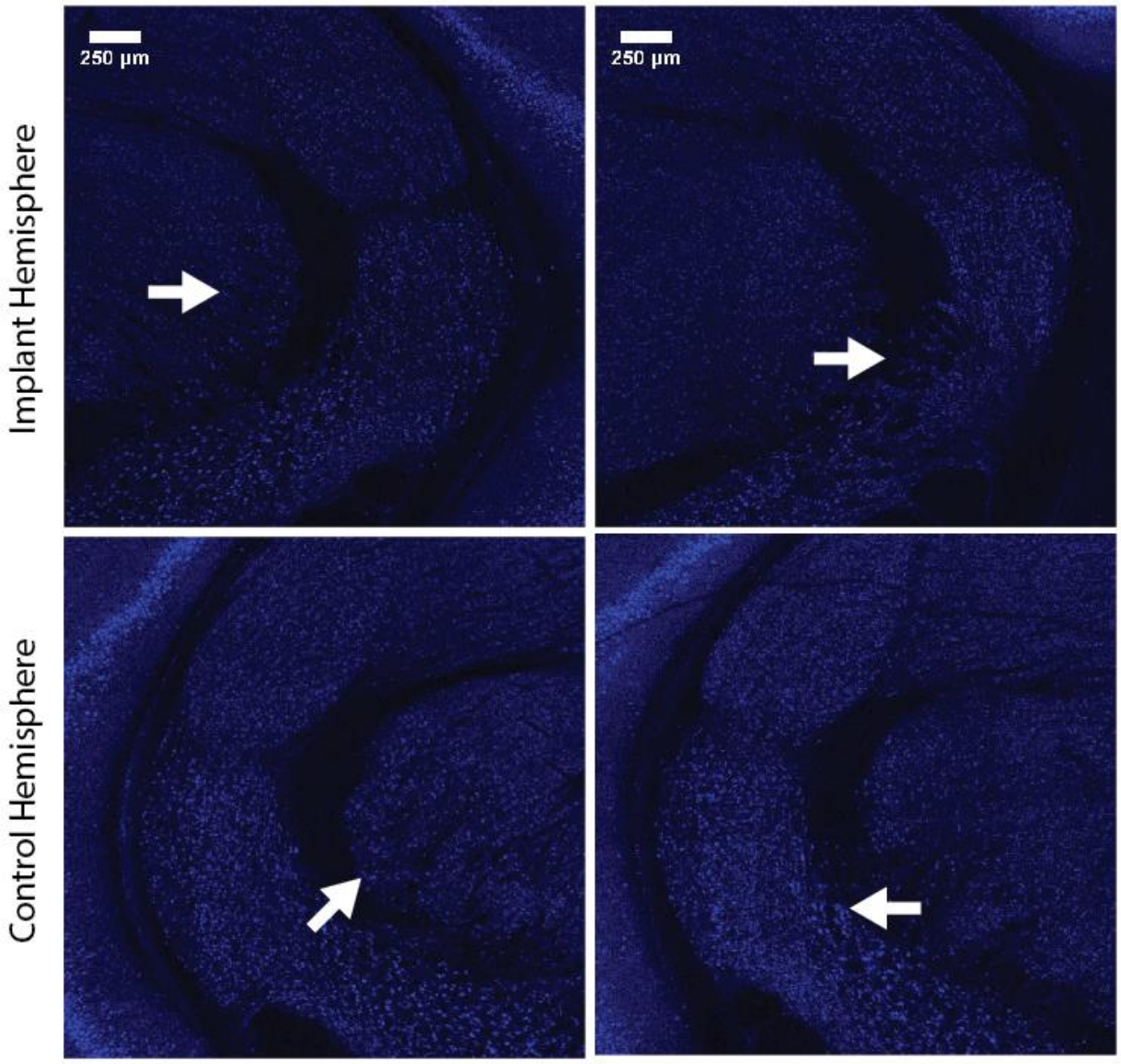

Figure 3.7: Thalamic neuron death in response to cortical implants

In two rats (left and right images), thalamic devices were not implanted along with cortical devices. In these animals, neuron decay was identified both qualitatively and quantitatively (Table 1) in the medial division of the medial geniculate body. Bottom row displays the control hemisphere thalamic region, with larger numbers of well-labelled neurons throughout. Arrows draw attention to regions of large differences between the images, typically in the MGM or medial-facing MGV.

Table 3.1: Cortical implants cause neuron death in medial and dorsal MGB

When normalized by contralateral control regions, rats with cortical devices only showed pronounced neuron death in layers 4, 5, and 6. In MGB, neuron death was found primarily in the dorsal and medial divisions, which receive substantial corticothalamic feedback.

Cortex	
L2/3	1.07
L4	0.64
L5	0.41
L6	0.40
MGB	
Medial	0.52
Ventral	0.85
Dorsal	0.71
MGMZ	0.75

4. ICMS PROVIDES PERCEPTUAL ADVANTAGES

4.1 Introduction

Cochlear implants have been the flagship neuroprosthetic treatment for chronic deafness since the early 1970s. These devices offer permanent, high-fidelity restoration of audition in almost every patient (Shannon R 1992; Shannon RV *et al.* 1995; McDermott HJ 2004; Wu CC and X Luo 2014). Unfortunately, these devices aren't indicated in all etiologies of chronic deafness, such as in cases of Neurofibramatosis Type II (NF2), where surgical removal of the schwannomas typically necessitates transection of one or both of the patient's eighth cranial nerves. In these patients, early treatments of deafness typically indicated implantation of an auditory brainstem implant. In many of these cases, patients reported lower quality speech perception than cochlear implant users, and surgeons reported difficulty implanting the device appropriately on the cochlear nucleus (Brackmann DE *et al.* 1993). In fact, in some cases of NF2, surgical removal of the tumors occasionally would cause damage to the cochlear nucleus (Colletti V and RV Shannon 2005), making the nucleus inefficacious as a neuroprosthetic target. Thus, recent work in the field of auditory neuroprostheses have focused on collicular (Lim HH and DJ Anderson 2006, 2007; Lim HH et al. 2008; Lim HH and T Lenarz 2015) and cortical targets (Otto K et al. 2005, 2005; Koivuniemi A and K Otto 2011, 2012; Regele O et al. 2013).

Inferior colliculus is the target nucleus of the auditory midbrain implant, which is currently undergoing clinical trials. While the clinical trial has been largely successful in terms of safety and efficacy, many patients report difficulty understanding speech stimuli (Lim HH and T Lenarz 2015). This difficulty is likely linked to the challenge of encoding temporal modulation information in higher-level auditory nuclei, as temporal information begins to become encoded more commonly with a rate code (Rouiller E *et al.* 1981; Ter-Mikaelian M *et al.* 2007; Wang X *et al.* 2008; Wang H et al. 2011) and neurons change from having generalized responses for level and rate at their characteristic frequency to more specific and diversified responses to stimulus features (Atencio CA *et al.* 2007; Atencio CA *et al.* 2008; Zhou Y and X Wang 2010). In fact, auditory cortical neuroprostheses experience these effects in even greater magnitude, as cortical neurons can have an even more specific set of responses to spectral stimuli (Atencio CA *et al.* 2007), can have center frequencies that do not correspond to their tonotopic

location (Bandyopadhyay S *et al.* 2010), and often simultaneously code for temporal and amplitude information with firing rate, however, these rate codes can often be nonmonotonic (Sadagopan S and X Wang 2008). Because electrical microstimulation is known for being relatively non-specific (Ranck J 1975; Tehovnik EJ 1996), the randomized location of neurons that code for highly specific elements of a natural stimulus make neuroprosthetic restoration of hearing in these nuclei challenging. Thus, we suggest auditory thalamus, a highly segregated auditory processing center with less diversified feature encoding (Bartlett EL and PH Smith 1999; Bartlett EL *et al.* 2000; Bartlett EL and X Wang 2011; Bartlett EL 2013), as an alternative nucleus for neuroprosthetic restoration of hearing in patients who would not benefit from a cochlear implant.

Thalamus was traditionally thought of as a relay center for ascending sensory information, however, recent work has revealed the auditory thalamus plays a significant role in auditory processing. Tonotopically organized neurons in the MGV are tuned for narrow bandwidths and are optimal for spectral processing (Bartlett EL and X Wang 2011), with approximate intralaminar spacing of ~10 octaves/mm (Winer JA et al. 1999), compared to 2.14 octaves/mm in A1 (Sally S and J Kelly 1988), assuming MGV tonotopy preserves the ratio of frequency to area found in A1. The MGV is also known to be rate sensitive in the rostrocaudal plane (Rouiller EM *et al.* 1989), and this rostrocaudal organization plays a role in thalamocortical signaling of temporal information to A1 (Read HL *et al.* 2011). MGV also sends excitatory signals to the thalamic reticular nucleus (TRN) (Conley M *et al.* 1991; Crabtree JW 1998), which is a GABAeric center believed to be associated with temporal feedback (de Biasi S et al. 1986). Most importantly, however, the ventral thalamocortical pathways innervate tonotopic regions of A1. Cells in MGB encode stimulus intensity with either a monotonic or non-monotonic rate code (Aitkin LM and SM Prain 1974). Depending on a neuron's connectivity within MGB, it may exhibit strong tonic activity, strong phasic activity followed by inhibition, or be completely inhibited in the presence of a stimulus of any suprathreshold amplitude (Yu YQ *et al.* 2004). This variability in sustained responses properties is pervasive across sensory systems and poses a significant technical challenge for all CNS neuroprostheses.

Neurons in anterior MGD are not tonotopically organized, but they do exhibit exceptional temporal synchrony and are optimized for the processing of temporally modulated signals (Bartlett EL and X Wang 2011) along with MGM (Anderson LA *et al.* 2009). MGD neurons

have broad tuning properties, though some neurons in the posterior MGD are completely ignorant of tone or noise, responding only to specific stimulus features such as modulation rates (Bartlett EL and X Wang 2011). This segregation of analysis between two regions allows for more specialization in later cortical processing, as MGV connects to A1 and MGD connects to A2, although the highly specialized neurons in posterior MGD connect only to secondary auditory cortex (Bartlett EL and X Wang 2011). Early electrophysiological work in MGB revealed thalamic cells to be more reliable at temporal coding than cortical cells (Creutzfeldt O *et al.* 1980), and in a study of ascending best temporal modulation frequencies for amplitude modulated tones in squirrel monkeys, best temporal modulation frequency median ranges decreased from 32-64 Hz in IC (Müller-Preuss P 1986), to 4-32 Hz in MGB (Preuss A and P Müller-Preuss 1990), and 4-16 Hz in cortex (Fastl H *et al.* 1986; Gaese B and J Ostwald 1995). This finding suggests that temporal information of the stimulus is either extracted prior to cortical processing or that the temporal information is transformed from temporal coding to rate coding as the signal approaches cortex.

In this chapter, we aim to characterize the behavioral discriminability of electro-auditory percepts in both auditory cortex and auditory thalamus. Specifically, we examine the behavioral discriminability of electrical stimulation intensity and the spatial distance between two electrodes along the tonotopic axis. In humans, changes in electrical intensity are typically reported as changes in loudness, and changes in stimulation location along the tonotopic axis are reported as pitch. Further, we explore the connectivity of cortical stimulation versus thalamic stimulation using a c-Fos immunohistochemistry assay in order to understand the complexity of activating such a highly interconnected feedback network. We hypothesize that ITMS will activate a more biologically natural circuit than ICMS, due to the organization of the feedforward and feedback pathways in medial, dorsal, and ventral divisions of the medial geniculate body. This biomimetic activation profile will be verified by preferential activation of the lemniscal auditory pathway in thalamus and cortex.

4.2 Methods

The following experiments were performed using 6 male Sprague Dawley rats (Envigo) in accordance with procedures approved by the Purdue Animal Care and Use Committee (PACUC 1204000631).

4.2.1 Surgical implantation

Animals initially induced with 5% isoflurane in air were subsequently anesthetized via i.p. injection of 80mg/kg Ketamine and 0.2 mg/kg Dexmedetomidine and positioned in a stereotaxic head holder. Anesthetic plane was monitored throughout surgery via paw withdrawal reflex testing every 30 minutes, heart rate and blood oxygenation were monitored constantly with a pulse oximeter, and body temperature was controlled with a recirculating heated water pad.

During the surgery, four bone screws were placed near the edges of the crown at bregma and lambda. For thalamic electrode placement, a craniotomy was centered at -6 mm to bregma and 3.5mm from midline. For cortical electrode place, the temporalis muscle was reflected such that a craniotomy could be performed dorsally to the squamosal suture. Due to dimensional differences between the thalamic and cortical implants, a small opening was created in the dura mater over primary auditory cortex for allow for insertion without damaging the device. After device placement, position in each auditory nucleus was verified via intraoperative neural recordings in response to Gaussian noise bursts. When the device was confirmed to be well positioned around auditory responsive neurons, the electrode was sealed in place with a fast curing two-part silicone elastomer (Kwik-Sil) and UV curable dental acrylic.

Post-operative monitoring consisted of weight maintenance with soft food and saline injections, and pain was managed with daily injections of 0.1mg/kg Meloxicam (Metacam).

4.2.2 Behavioral training

Animals were initially trained similarly to methods presented in Chapter 3, however, after habituation and threshold training, discrimination training was performed as follows. Our behavioral model is based on previous work in acoustic amplitude modulation detection (Kelly JB et al. 2006; Cooke JE et al. 2007), which we found to provide insight into stimulus discriminability.

Behaviors performed in this chapter fall into two categories: Detection and Discrimination. For the detection task, animals were initially trained to discern the presence of lowpassed noise (a “warning” trial) versus no acoustic stimulus (a “safe” trial). The desired behavior in the presence of the warning stimulus was cessation of licking behavior, and animals who persisted in licking behavior received a mild cutaneous shock (<1.6mA) through the water

spout. For discrimination tasks, animals were trained to discern the difference between amplitude modulated noise ("warning") and unmodulated noise ("safe"). In both cases, proficiency in the task was measured with a behavioral d' of 2. In the detection task, proficient animals were sometimes presented with an adaptive analog of the task, where correct behaviors caused future trials to become more difficult to detect, and incorrect behaviors resulted in easier future trials. These adaptive series asymptotically approached the animal's behavioral threshold level of detection.

4.2.3 Electrical stimulation

After implantation, acoustic stimuli were replaced with electrical pulse trains delivered from either the thalamic or cortical electrode. In all experiments, electrical waveforms were cathode-leading biphasic, symmetric pulse trains of 200μs per phase at 100 pulses per second for 650ms, with no delay between phases, delivered in a monopolar configuration. Electrical stimuli were generated on an RX7 (TDT) and delivered through an MS16 Stimulus Isolator configured for milliampere stimulation. In order to chronically stimulate through these microelectrodes, electrical impedance on each site was lowered to less than 150kΩ by electrochemical deposition of a thin iridium oxide layer.

4.2.4 Amplitude discrimination

For amplitude discrimination experiments, the behavioral threshold of electrical stimulation was first collected on a single site, for a given day. Then, a discrimination experiment was performed on that site, where the safe trials consisted of stimulation at +3dB from the behavioral threshold, and warning trials consisted of stimulation of a higher intensity than the safe trials (Fig. 4.1B). Only one direction was selected for testing in our experiment because direction specificity in amplitude discrimination tasks is known to be dependent on the amplitude difference of the two stimuli, at least for acoustic tasks (Syka J *et al.* 1996). The "upward" direction (warning has higher intensity) was selected in our experiment in order to limit the number of high intensity pulses a rat received during a given experimental session.

4.2.5 Interchannel discrimination

For interchannel discrimination experiments, behavioral thresholds were collected on two electrode sites at the same depth (for cortical electrodes) or within the ventral division of

auditory thalamus (for thalamic electrodes), for a given day. Then, a discrimination experiment was performed where stimulation on one of the sites was considered the warning trial, and stimulation on the other site was considered the safe trial (Fig. 4.1A). On both channels, stimulation occurred at +3dB over the predetermined threshold on that channel. Furthermore, amplitudes were roved between 0 and +1dB to eliminate response bias for amplitude cues.

4.2.6 Thick-slice c-Fos immunohistochemistry

After the last day of behavioral thresholds, rats were placed in a quiet, acoustically-isolated chamber for 1 hour before being sedated with dexmedetomidine (0.2 mg/kg). After sedation, rats were reconnected to the RX7 stimulus isolator and subjected to 90 minutes of behaviorally suprathreshold stimulation intensities (as confirmed by previously collected thresholds) at a 1 Hz repetition rate. These stimulation waveforms were "biologically inspired" and consisted of either singular pulses in the case of cortical stimulation or a 300 Hz triplet in the case of thalamic stimulation (Swadlow HA and AG Gusev 2001). After 90 minutes of stimulation, rats were disconnected from the stimulator and allowed to wait in the sound chamber for 30 more minutes prior to perfusion. From this moment forward, immunohistochemistry methods were performed as described in detail in earlier work (for details, see (Woolley AJ *et al.* 2011). Rats were perfusion fixed with 4% paraformaldehyde and the brains were extracted. The brains were then sliced into 250-400μm sections and individually placed into wells of a 24 well plate, with special note taken of the slices around the electrode tracts. The slices then received three sequential five minute washes of Hepes Buffered Hanks Solution with Sodium Azide (for recipes, see Table 1), were briefly incubated in a Sodium Borohydride solution for 30 minutes to reduce endogenous autofluoresence, then washed thoroughly in Wash Solution (WS). Slices were blocked in WS for two hours prior to a 48 hour incubation in primary antibodies (Mouse anti-NeuN [Abcam ab104224], Rabbit anti-c-Fos [Abcam ab190289], and Chicken anti-GFAP [Abcam ab4674]) at a 1:400 dilution. After incubation in primary antibodies, the slices were thoroughly washed in WS to ensure that excess primary antibodies had been fully removed from the well (for details, see Chapter 3). Slices were then incubated in secondary antibodies (Goat anti-mouse Alexa Fluor 488 [Abcam ab150117], Goat anti-rabbit Alexa Fluor 555 [Abcam ab150086], and Goat anti-chicken Alexa Fluor 647 [Abcam ab150175]) and subsequently washed using the same dilution factor,

incubation period, and wash protocol as the primary antibodies. Slices were then incubated in a U2/Scale clearing solution for approximately one week before imaging on a Ziess LSM 710 Confocal Microscope. Images were collected under 10x magnification for a pixel dimension of 2.77μm^2. For each slice, a full tile scan across the width and height of the slice was taken and was stitched in Zen 10. In each tile, a Z-dimension stack (z-thickness ~25μm) was taken through the visible range of the slice, typically approximately 250μm, which were then projected into a single plane for display and analysis. Cell counts were collected in each layer of auditory cortex and division of the medial geniculate body based on estimated stereotaxic position of the slice and anatomic markers using a rat atlas. For cell counting, an open source plugin for ImageJ was used (cell_counter.jar), which detects cells based on size and shape of a given template cell. Templates used for cells were simply circular labeled areas of less than 15μm diameter, as NeuN and c-Fos are nuclear labels, which were manually selected as a training set for the ImageJ plugin. We were unable to differentiate neuron types (pyramidal vs. interneurons) due to the label localization.

4.3 Results

4.3.1 Intensity discriminability in auditory cortex and auditory thalamus

During threshold collection, we found that behaviorally salient intensities of stimulation could be variable across channels or days (See Chapter 3 Results, Discussion, Fig. 3.2). Due to the correlation between stimulation intensity and electric field radius, we chose to present our results as a ratio or percentage difference between the warning stimulus and the safe stimulus, as stimuli delivered on electrode sites with higher thresholds may result in perceptual differences compared to stimuli delivered on sites with lower thresholds. We found that in auditory cortex and auditory thalamus, electrical intensity discriminability was similarly poor at differences of less than 25%, but that cortical stimulation exhibited significant advantage over thalamic stimulation at differences greater than 40% (Fig. 4.2). Further, we found the thalamic data to not significantly increase over the range of amplitudes tested, whereas cortical stimulation did after 50% intensity difference.

4.3.2 Interchannel discriminability in auditory cortex and auditory thalamus

It would be expected that behavioral salience of differences between stimulus channels would increases as interchannel distance increased, due to the tonotopic mapping of A1 and MGV. Counterintuitively, our rats performed worse on the interchannel discrimination task as interchannel distance increased in both target structures (Fig. 4.3A). As preliminary experiments in auditory cortex had indicated that randomization of stimulus intensities was an important factor for reducing behavioral bias, we elected to examine the correlation of interchannel discrimination d' and the difference between thresholds on each channel (Fig. 4.3B). We found no significant correlation between interchannel threshold difference and behavioral salience under the cortical microstimulation regime, however, we did find a significant effect of interchannel threshold difference in the thalamic microstimulation data ($p < 0.05$, F-test).

4.3.3 c-Fos immunohistochemistry

C-Fos labeling in auditory cortex following thalamocortical stimulation appeared across layers and in a high proportion of neurons upon visual inspection. Conversely, corticothalamic stimulation did not appear to activate c-fos labeling in MGB (Fig. 4.4). Cortical stimulation appeared to activate both hemispheres, and c-fos labeling populated the boundary between ventral and dorsal medial geniculate body in both hemispheres. However, stimulation in auditory thalamus evoked a very tight stimulation profile (Fig. 4.5) in that structure and did not broadly excite auditory cortex (Fig. 4.4). This thalamic activation can be seen more clearly when magnified, and appears to spread to a diameter of approximately 300 microns (Fig. 4.5). Contralateral thalamic activation was observed in the ventral-facing MGMZ.

After images were collected on our confocal microscope, cell counts were performed using available plugins in ImageJ (cell_counter.jar). We found thalamocortical stimulation produced c-fos labeling large portions of ipsilateral and contralateral auditory cortex, with the only noticeable difference in activation occurring in layer 6, determined by depth estimation from the pial surface (Games KD and JA Winer 1988) (Table 4.2). Thalamic stimulation was found to preferentially activate ipsilateral auditory cortex, with the strongest difference in activation occurring in layers 2 and 3. In thalamus, cortical stimulation did not evoke strong c-fos labeling, except for possibly in the medial division. Thalamic stimulation of auditory

thalamus, however, evoked specific activation of the ipsilateral ventral and dorsal medial geniculate body, including the MGMZ at the edges of those structures (Table 4.2).

4.4 Discussion

In our study, we hoped to identify fundamental strengths and weaknesses of ICMS versus ITMS, and corroborate those findings with histological results that characterized the network activated by each type of stimulation. We hypothesized that ITMS would activate a more biologically natural circuit than ICMS, due to the organization of the feedforward and feedback pathways in medial, dorsal, and ventral divisions of the medial geniculate body. Further, we proposed that this more biomimetic circuit activation would correlate with better behavioral salience of stimulation in thalamus. However, while our histology results supported our hypothesis, our behavioral results did not.

4.4.1 ICMS outperforms ITMS in delivery of intensity cues

The fundamental principle behind electrical stimulation of nervous tissues is the generation of a spatiotemporal electric field. The size and strength of this field drives the movement of ions in the tissue, creating voltage gradients and driving action potentials in nearby neurons. One inherent flaw of electrical stimulation of nervous tissue is that waveform intensities, which are required to change with sound loudness, as well as behavioral (Wood N and N Cowan 1995; Conway AR et al. 2001; Hawley ML et al. 2004; Elhilali M 2013), biological (Giulian D, J Li, X Li, *et al.* 1994; Turner JN et al. 1999; Biran R *et al.* 2005), and electrochemical factors (Weiland JD and DJ Anderson 2000; Cogan SF *et al.* 2004; Vetter RJ *et al.* 2004; Williams JC *et al.* 2007), conflate electric field magnitude or size with firing probability or rate in the sphere of influence. Thus, neurons around an electrode delivering more charge aren't just more likely to fire faster at higher stimulus intensities, but neurons further from the electrode are likely to start firing as well (Ranck J 1975). Further confounding this issue is the pulse rate of a stimulus train, which neurons are likely to phase-lock to, if possible, has been shown to correlate with a level detection effect in ICMS percepts, but may be confounded by total charge delivery (Koivuniemi A and K Otto 2012). Also, factors such as calcium-gated potassium channels and the balance of excitation and inhibition can limit neuronal excitability, particularly after the first round of stimulation. Neurons in many auditory nuclei code level

information with rate codes (Wang X *et al.* 2008; Huetz C *et al.* 2011; Wang H *et al.* 2011), which might suggest that neurons which phase lock to a given electrical pulse rate at two different stimulus intensities are unlikely to code additional level information. However, human subjects have reported perceived volume changes associated with increased stimulus intensities (Zeng FG and RV Shannon 1992, 1994). Two explanations of our results must be considered. One option is that the increase in stimulus intensity causes a larger area of neurons to become activated, and the other is that the firing rate or probability of neurons increases with increasing stimulus intensity. It is likely that both of these occur simultaneously, and in fact both are necessary for the result that we observe in cortex.

First, we consider ICMS, where significant intensity discriminability was observed. We propose that in the presence of the higher intensity stimulus, a wider area of cortex was activated by the stimulation, and that neurons closer to the electrode have a higher firing probability and possibly rate. In primary auditory cortex, there is a diversity of level-sensitive neurons with monotonic, non-monotonic, and level-invariant firing profiles (Sadagopan S and X Wang 2008), with a majority of these neurons encoding level information with nonmonotonic codes (Pfingst BE and TA O'Connor 1981; Polley DB et al. 2006; Sadagopan S and X Wang 2008). We propose that in cortex, the addition of any amount of level-encoding neurons (both monotonic and non-monotonic coders) to the firing population is what drives the discriminable response, and the increased firing rate of monotonic rate/level neurons with traditional, V-shaped frequency response areas enhances the broadband spectral content of the stimulus. Of critical importance, however, is feedback. While stimulating in Layers 4, 5, and 6, we are likely to drive excitatory and inhibitory feedback in early auditory nuclei (Winer JA 1984; Hefti BJ and PH Smith 2000; Crandall SR *et al.* 2015). This feedback is designed to refine level and pitch information, but in our case, there is no ascending information. This feedback does not operate on the signal we put into the brain, and as such, the increased stimulus intensity we provide simply translates to highly discriminable percept of “louder”, “wider band” noise in these subcortical regions.

So if this is the case for auditory cortex, why do we not see the same response in thalamus? Stimulating in the ventral division of auditory thalamus allows for a physiological feedback circuit to activate, as we had hoped (Fig. 1.1). This inhibitory feedback refines the edges of the excited neural population, and higher stimulation intensities only drive stronger

inhibition. Further, thalamic neurons code level with monotonic and non-monotonic rate codes, with a strong preference for nonmonotonic codes in cat and monkey, but rats are not as clear (Rouiller E et al. 1983), so increasing firing rate in a given area might not even correlate to a "louder" percept. Non-monotonic neurons often have a strong offset response that could be a behavioral cue also. It is likely that changing the pulse rate of stimulus trains in this region would evoke a more reliable percept for loudness cues.

4.4.2 ITMS evokes more focal activation, but poor best-frequency selectivity

Our histological results suggest that ITMS evokes a more focal pattern of activation than ICMS (Figures 4.4 and 4.5, Table 4.2). These results suggest that the lack of excitatory connectivity between ventral and dorsal thalamic cells and ample top-down center-surround inhibition provides an opportunity to present best-frequency specific percepts along the tonotopic map (Gross NB et al. 1974; Edeline JM and NM Weinberger 1991). However, our rats exhibited equally poor interchannel discriminability from both ICMS and ITMS evoked percepts (Fig. 4.3A). In fact, perceptual salience of the signal *decreased* with increasing interchannel distance. One potential explanation for this result is the activation of long-lasting, wideband inhibition (Bartlett EL and PH Smith 2002; Bartlett EL and X Wang 2005; Gaucher Q *et al.* 2013). In cortical networks, this would exist through interneuron networks, and in thalamus, through corticothalamic or corticocolliculothalamic pathways.

In thalamus, we found that our rats were able to use intensity differences between the two stimulation channels to aid in interchannel discrimination, which might account for the ability of our rats to discriminate interchannel cues on adjacent sites better than interchannel cues from sites separated by several hundred microns. It is possible that this bias also existed in cortex, but that most of our stimulation channels had similar enough thresholds to mask the weak correlation. However, due to the sensitivity of cortical networks to stimuli of differing intensities, we believe the interchannel discriminability we observe at adjacent electrode sites to be due to discriminating amplitude cues, despite our attempt to mask that bias.

4.4.3 Study limitations

The primary limitation of ICMS and ITMS is the interplay between pulse rate, stimulation intensity, and total charge delivery. It is fortunate that cochlear implants interface

with a structure which can phase lock to very high rates (Dynes SB and B Delgutte 1992) and thus avoid this issue. In our work, we followed the work of previous studies in assessing electrical intensity discriminability as a proxy for level discrimination, but our results suggest that this assumption may be under the conditions that we studied invalid for central nervous system targets and should be studied further. In order to properly address the issue, however, further work is necessary to explore the relationship between perceived level and total charge delivered, charge per phase, and pulse rate.

For clinical prostheses, such as the cochlear implant, it is important to calibrate the device for each patient. In the case of the cochlear implant, this requires collecting auditory brainstem responses to cochlear microstimulation, then tuning the dynamic range of current output of the device to match the acoustic dynamic range (Raggio MW and CE Schreiner 1994). Such techniques are impossible in our preparation due to the proximity of the electrical stimulation site and the recording electrode. Instead, dynamic range in these structures may need to be assessed behaviorally, or in using a stimulation methodology that does not generate such a large electrical artifact.

Our assessment of network activation using c-Fos was inspired by a large body of successful work with this label, especially recently (Jakob TF et al. 2015; Ouda L et al. 2016; de Hoz L et al. 2017; Pernia M et al. 2017). However, our application of the method in a thick-slice preparation left much to be desired. Most notably, there were many situations where the labeled slice did not contain tissue near the electrode site which was stimulated prior to sacrifice. Due to the application of other labels to neighboring slices bound for other experiments, the activation profiles around these electrodes were lost. Using a thin-slice preparation, and devoting more slices to the c-Fos immunolabelling protocol, would have yielded far more information about the differences between ICMS and ITMS near the electrode site. While our results were helpful in revealing the broad, network level impact of microstimulation in each of these auditory structures, we had initially hoped to identify changes in local activation profiles. Most notably, little work has been done to functionally characterize the activation profile of electrical stimulation outside of mathematical modelling (Ranck J 1975; Joucla S and B Yvert 2009), and the experimental data that does exist uses stimulation parameters that are far removed from our parameters (Histed MH et al. 2009). A series of images similar to our result in Figure 4.5 would be ideal for examining this question experimentally.

4.4.4 Conclusion

Our histological data suggest that the activation feedforward and feedback circuits during ITMS optimizes information delivery in the network. However, our results for ITMS intensity and interchannel discriminability (Figure 4.2 and 4.3) imply that current stimulation parameters do not take advantage of this network adequately, as behavioral salience of these cues was poor (d'<1). We believe our work provides evidence that further study is required to design waveforms which properly convey level and spectral cues to this target structure.

Table 4.1: Solution formulae for immunohistochemistry protocol

Solution	Recipe
Phosphate Buffered Saline (PBS)	in g/l; 9 g NaCl, 1.44 g KH_2PO_4, 7.95 g Na_2HPO_4, at pH 7.4
4% Paraformaldehyde	in ml/l; 202 ml Sodium phosphate dibasic solution (0.4 M Na_2HPO_4), 48 ml Sodium phosphate monobasic solution (0.4 M NaH_2PO_4), 500 ml 8% formaldehyde solution, 250 ml Mili Q DDi water, at pH 7.4
HEPES Buffered Hank's Saline with Sodium Azide	in g/l; 7.5 g NaCl, 0.3 g KCl, 0.06 g KH_2PO_4, 0.13 g Na_2HPO_4, 2 g Glucose, 2.4 g HEPES, 0.05 g $MgCl_2$ 6 parts H_2O, 0.05 g $MgSO_4$ 7 parts H_2O, 0.165 g $CaCl_2$, 0.09 g NaN_3 at pH 7.4
Wash Solution (WS)	in Vol/Vol; 1% Normal Goat Serum, 0.3% Triton X-100, in HBHS with Sodium Azide (NaN_3). Refrigerate the WS at 4°C before use.
U2 Scale Solution	4 M Urea, 30% Vol/Vol Glycerol and 0.1% Vol/Vol Triton X-100

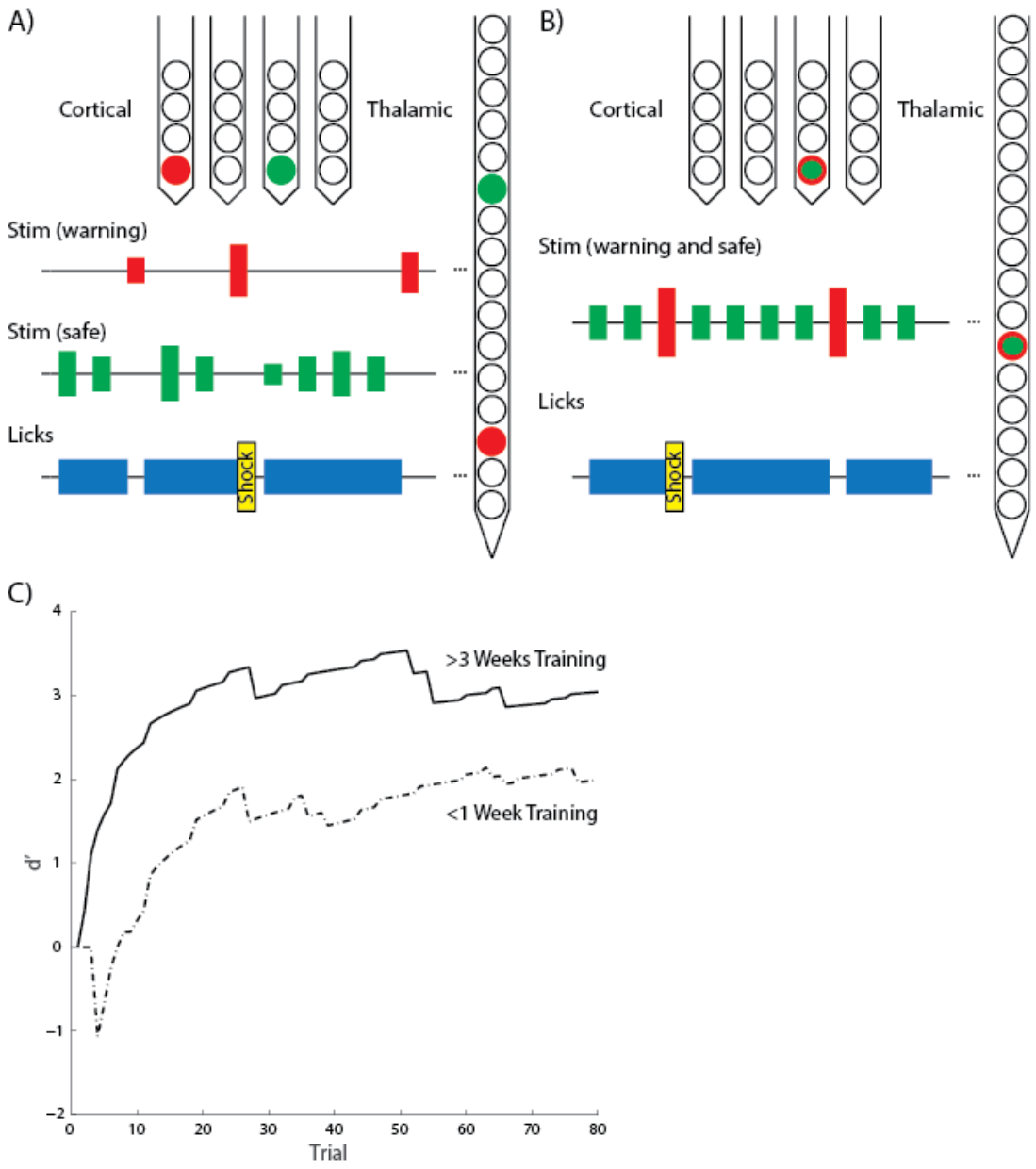

Figure 4.1: Interchannel and intensity discrimination behavioral paradigms

Rats were presented with two types of behavioral paradigms to estimate ability to discriminate between channel-specific stimulation and different intensities. **A** Interchannel discrimination was performed by stimulating on two different sites, controlling for each site's behaviorally salient threshold and roving amplitudes to control for bias. **B** Intensity discrimination was performed by stimulating on a single channel at two intensities, one slightly above the behaviorally salient threshold for that channel, and the other at some higher intensity. Animals were punished with a mild cutaneous shock for failed detection of the warning stimulus. **C** Example of acoustic sinusoidal amplitude modulation discrimination results from an example rat. An example series from the first week of AM discrimination is shown (dashed) as compared to a similar series from the same rat several weeks later (solid).

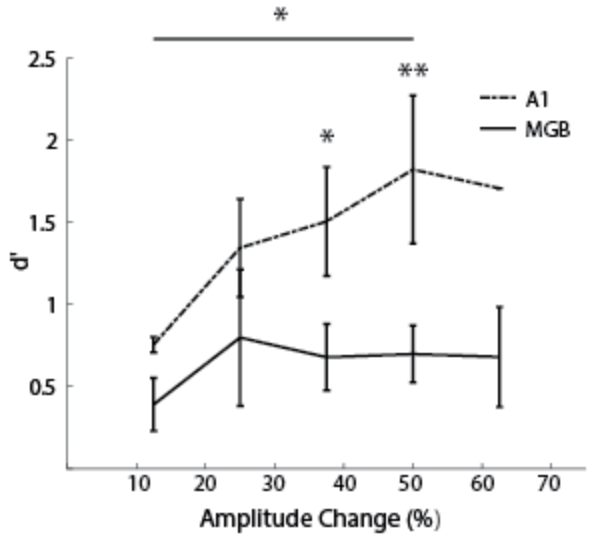

Figure 4.2: Cortical microstimulation offers superior discriminability of intensity cues

Rats presented with ICMS performed better than rats presented with ITMS in the intensity discrimination task, particularly at intensity differences greater than 30% of the baseline stimulation intensity. At 37.5% and 50% amplitude change, cortical behavioral d' was significantly higher than respective thalamic behavioral d'. Within cortical results, only 50% amplitude change results were found to be significantly different from the 12.5% results. Error bars represent the standard error of the mean. * corresponds to $\alpha = 0.05$; ** corresponds to $\alpha = 0.01$.

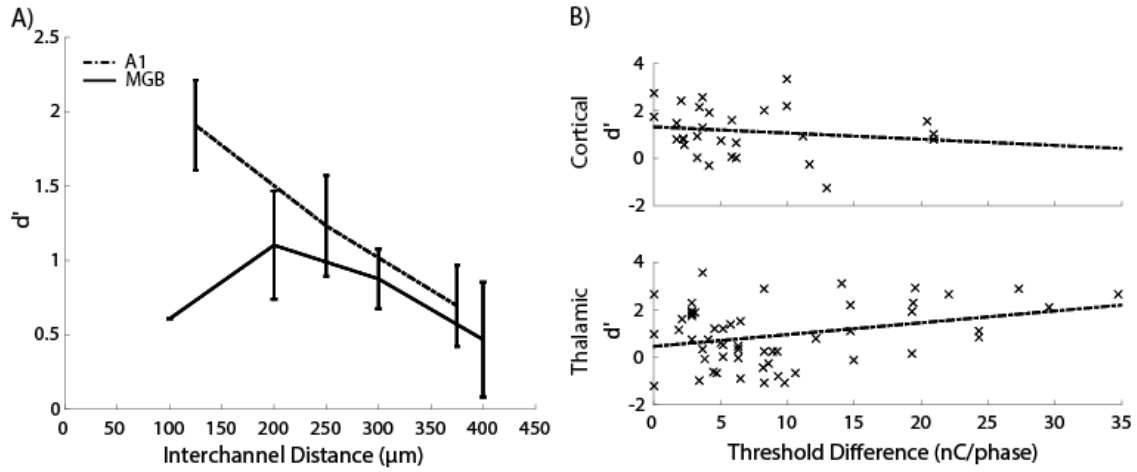

Figure 4.3: ITMS and ICMS offer similarly inadequate interchannel discriminability

A Both ICMS and ITMS show decaying behavioral salience as interchannel distance increases. Error bars display standard error of the mean. **B** Control of behavioral bias of intensity cues in ICMS was adequate, as significant correlations did not exist. However, in auditory thalamus, behavioral salience of the interchannel cues was confounded by a weak correlation between behavioral d' and the interchannel threshold difference ($p < .05$, $r^2 = 0.1$).

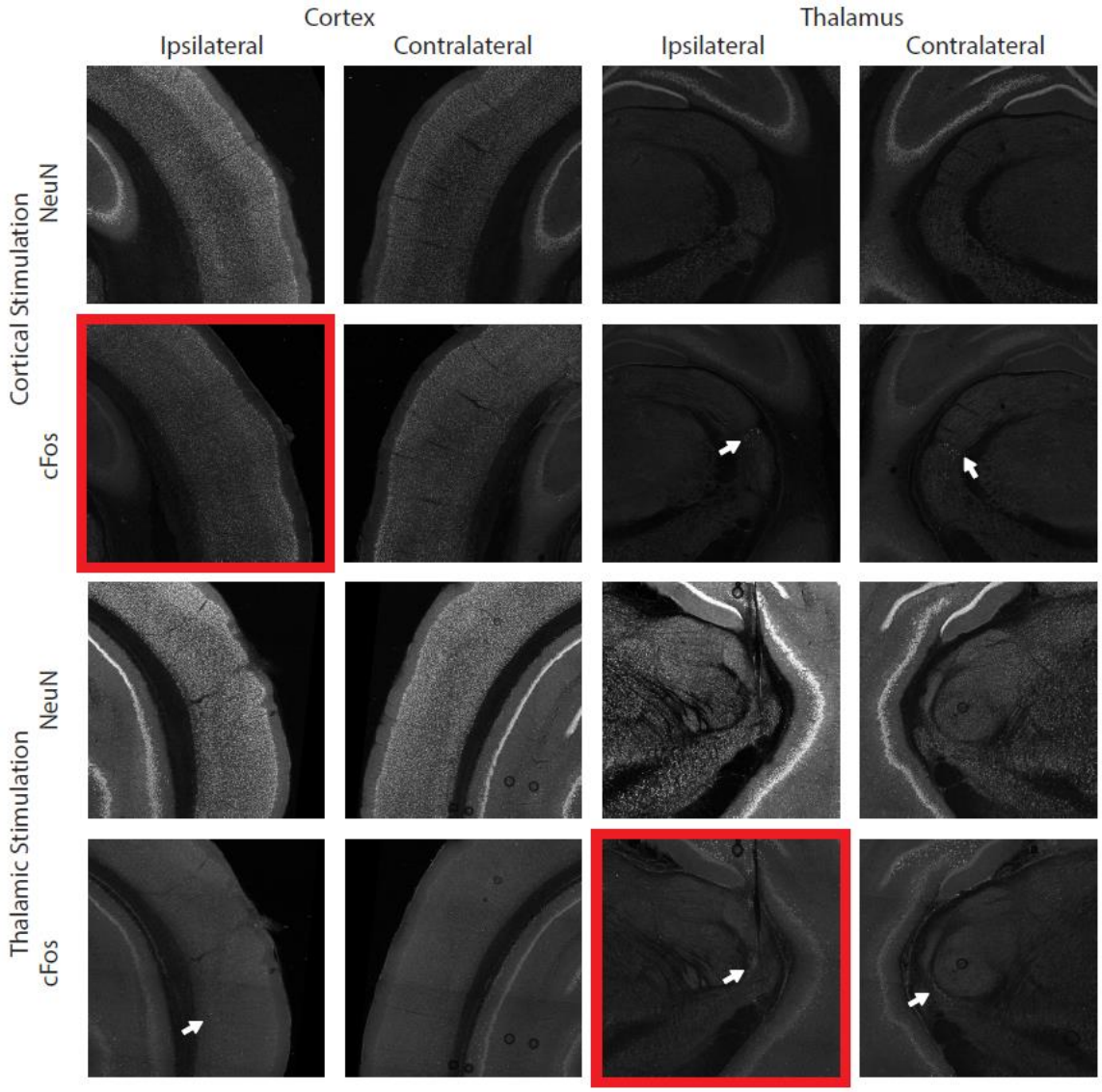

Figure 4.4: c-Fos Immunoreactivity demonstrates network activation

Rats were triple-labeled with c-Fos, NeuN, and GFAP following a stimulation procedure prior to sacrifice. In this figure, each row displays NeuN or c-Fos immunoreactivity, while each column represents where the image was collected from the slice. Ipsilateral (implant side) and contralateral (control hemisphere) images were analyzed. ICMS appeared to activate wide-band cortical networks in both hemispheres, while ITMS appeared to activate narrow-band thalamic networks in ipsilateral thalamus (white arrows). Red boxes indicated slices where the stimulus channel existed.

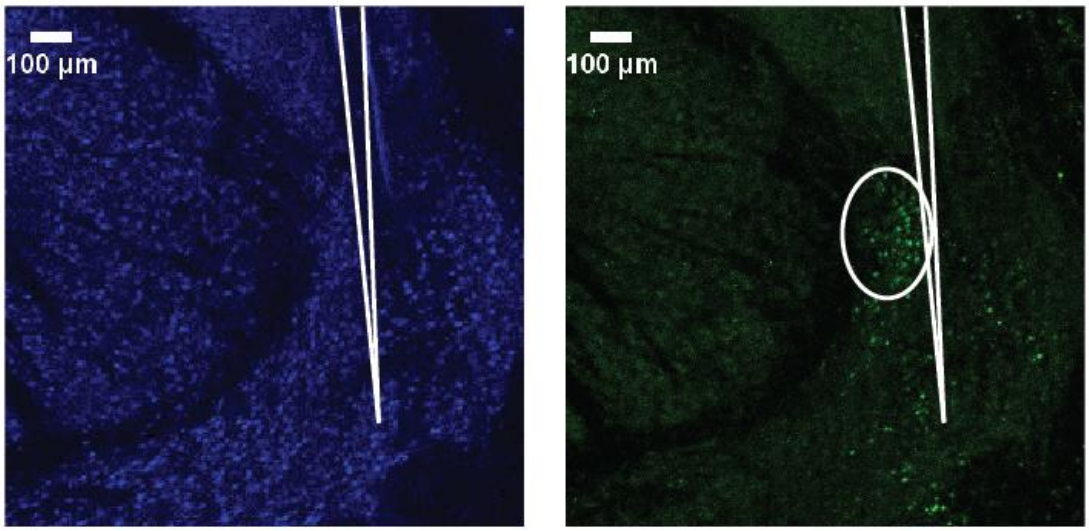

Figure 4.5: Thalamic c-Fos activity in response to single channel electrical stimulation

In one of our thalamic slices, we were able to precisely capture the area around the stimulation channel in the width of the slice. The area activated by this stimulation appears to be spherical and approximately 300 microns in diameter, facing away from the electrode site. White lines indicate the electrode tract in each image, while the white oval indications the region of stimulation around the electrode site.

Table 4.2: ITMS activates biomimetic auditory networks

Cells were counted in each anatomic subdivision of ipsilateral and contralateral auditory cortex and auditory thalamus in response to stimulation. The cell counts of c-Fos immunoreactive neurons were divided by the cell counts of NeuN immunoreactive neurons in order to normalize the activation of each region. We identified preferential ipsilateral activation of neural circuits by ITMS, specific in the ventral and dorsal divisions of the MGB and layers 2, 3, and 4 of auditory cortex. By contrast, ICMS evoked broadband cortical activation in both hemispheres, without strong hemispheric differences in the thalamic activation.

		Cortical Stimulation		Thalamic Stimulation	
		Implant	Control	Implant	Control
Cortex	L2/3	73.50%	74.00%	51.50%	24.00%
	L4	74%	64.10%	20.00%	11.80%
	L5	56.60%	51.60%	23.30%	14.10%
	L6	78.80%	54.20%	23.50%	16.80%
MGB	Medial	8.80%	4.60%	15.20%	5.70%
	Ventral	11.70%	10.70%	42.50%	13.60%
	Dorsal	23.10%	18.00%	41.80%	20.40%
	MGMZ	6.00%	5.90%	35.10%	8.60%

5. CONCLUSIONS

5.1 Impact

Globally, over 60,000 individuals have been implant with cochlear implants to relieve the symptoms of chronic deafness (McDermott HJ 2004). Despite the clinical power of these devices, they cannot help all patients, especially those without functional auditory nerves as a result of trauma or gliomas. Over 1 in 25,000 children in the US are born with neurofibromatosis type 2, which often results in bilateral gliomas on the auditory nerves, with 100% penetrance by age 60 (Asthagiri AR *et al.* 2009). For these patients, the only clinical option for relief of their deafness is the ABI. Of over 500 implanted ABIs, in tumor or non-tumor patients, limited success has been noted (Colletti V and RV Shannon 2005). Clinical trials of Auditory Midbrain Implants (AMIs) have begun in Germany, and preliminary data from patients with AMIs is slightly more hopeful that what has been seen in ABIs (Lim HH and DJ Anderson 2006, 2007; Lim HH *et al.* 2008). However, AMIs are still not as efficacious as cochlear implants.

Our work toward the development of a thalamocortical auditory neuroprosthetic offers the possibility of multimodal stimulation, where sensory stimulation of the visual and auditory centers of thalamus might be linked to offer more information to the subject. It has been shown that visual attention to the source of a sound contributes to comprehension, and we hope to achieve that someday with our device. Also, a thalamus-targeted prosthetic requires a simpler surgical approach which is commonly applied to the implantation of deep brain stimulating electrodes. For these reason, we believe a thalamocortical prosthetic will outperform AMIs in patient safety and ease of implantation, and hope to develop its capabilities in overall sound and speech perceptibility.

Beyond the clinical possibilities of auditory thalamic microstimulation as a solution for chronic deafness, our preliminary work in targeting thalamus for sensory stimulation may be beneficial for other neuroprosthetic applications, such as bidirectional interfaces for upper and lower limb prostheses. What we learn about stimulation of primary and multimodal thalamic targets, and the activation of thalamocortical networks, may assist in the delivery of the much sought after pressure percept, which continues to be an active area of research.

5.2 The Visual Thalamocortical System: A Comparable Model of Microstimulation

When assessing our results, it is valuable to view the in the context of other successful thalamic and cortical microstimulatory prostheses. The most notable examples of this work where there is comparable data in both cortical and thalamic structures are in the visual system.

Central nervous system neuroprostheses first targeted visual cortex, similarly to how early auditory prostheses in the central system targeted primary auditory cortex. In many of these studies, electrical stimulation parameters were cathode-leading biphasic pulses in the range of 0-100nC delivered per phase, either during pulse trains or within a single pulse (Tehovnik EJ 1996), despite the fact that these ranges often surpassed a limit of safety suggested by Asanuma and Arnold (Asanuma H and AP Arnold 1975). In fact, in the visual cortex, primates were capable of displaying a behavioral indication of noxious stimulation which provided evidence that such high intensity stimulation was altering the cortical system (Bartlett JR et al. 1977). Such pulses, even at low intensities, have been shown to activate sparse networks both near the stimulating electrode and far from the device (Histed MH *et al.* 2009). All of these findings, taken together, are remarkably similar to the results we find in auditory cortex. We identified increases in behavioral thresholds in response to prolonged electrical stimulation above the level of safety specified by Asanuma, Arnold, and later by generalized by Robert Shannon and others. We also identified activation of widely distributed neural networks in response to cortical stimulation in our c-Fos study.

It was for these reasons, and surgical reasons, that visual thalamus was sought as a new stimulation target. In our work, auditory thalamic stimulation offered many similar benefits to visual thalamic stimulation: ease of access/adoption, modular macroscopic processing structure, less stimulus encoding complexity (than cortex), and the possibility of stimulating smaller populations of neurons around the electrode site. In the lateral geniculate nucleus, visuoelectic percepts evoked reliable behavioral responses which were similar to responses to optical stimuli in terms of response latencies, error, and scatter (Pezaris JS and RC Reid 2007). A noteworthy difference between this study and ours is the waveform structure. Pezaris utilized 80-200ms long pulse trains of 1ms sinusoidal pulses, typically at 200Hz. Thus, this strong behavioral result was created by shorter train durations, longer pulse durations, and faster pulse rates than what we used. In fact, the only waveform parameter that mimicked our data was stimulation intensity, which was approximately 40μA. It is for these reasons that we advise future study of behavioral

salience of auditory thalamic stimulation focus on waveform parameterization, rather than attempting to match thalamic stimulation parameters to those of other structures.

5.3 The Thalamocortical System and Neuroprostheses

In order to develop an effective biomimetic neuroprosthetic, it is important for encoding and decoding algorithms to compensate for global brain state changes. To assess how our stimulus encoding might change with global brain state, we prepared an electrophysiological assessment of the thalamocortical network during drug-induced loss of consciousness. We found that corticothalamic feedback diminishes during loss of consciousness, as evidenced by a reduction of mutual information between cortically delivered electrical stimulation and thalamic responses (Fig. 2.5). Further, we found that both cortical and thalamic networks become more onset responsive (Fig. 2.7 and 2.8), and network responses became more paired to the stimulus, rather than distributing firing over a sustained or spontaneous response pattern. This was further characterized by a reduction in the gamma band in both thalamus and cortex (Fig. 2.10), which represents polysynaptic activity and implies that there is less network activity occurring during loss of consciousness.

These findings have strong implications for the perceptibility of central nervous system neuroprostheses, as network connectivity is critical to the perception and interpretation of sounds. In thalamic neuroprostheses, a reduction of stimulus specificity in corticothalamic feedback pathways could result in electrically delivered percepts becoming less discriminable despite ascending input remaining unaffected. The same could be said for cortically delivered stimulation. However, we argue that the perceptual difference would be far more pronounced. Cortical networks are very complex, and our data suggest that cortical microstimulation during dexmedetomidine induced unconsciousness broadly activates cortical structures in both hemispheres. This wholesale activation of cortical structures, in multiple layers, would be very ineffective at mimicking natural stimulus features. Thus, we conclude that thalamic stimulation offers biomimetic network activation, even under altered global brain states, such as state changes induced by consciousness-altering drugs.

5.4 Synaptics of ICMS/ITMS Pulse Trains

Electrical stimuli in central nervous system neuroprostheses are commonly delivered as pulse trains lasting hundreds of milliseconds. Our data strongly suggest that this stimulation is unwise in the central nervous system, despite its success in stimulating peripheral structures. We found that 650 millisecond pulse trains delivered at behaviorally salient stimulation intensities evoked long-term suppression, likely through inhibitory interneuron networks. Unfortunately, our work did not include direct recordings of neural activity resultant from these prolonged pulse trains, so we have no knowledge of the neural response profiles over the course of a stimulus train. Over the course of 10-20 minutes, thalamic and cortical behavioral thresholds increased significantly (Fig. 3.3), which we attributed to synaptic fatigue caused by the long pulse train, coupled with the short intertrial interval. In fact, even over the course of 3 minutes, we observed latency changes in first spike latency following behaviorally subthreshold stimulation intensities. The general, non-specific activation of neural networks in central nervous system targets which are not designed for rapid, repetitive firing is not functional and actually decreases the salience of percepts over time. Thus, we conclude that stimulation paradigms in central nervous system neuroprostheses should consist of multiple electrode sites firing at physiologically relevant pulse rates and behaviorally subthreshold intensities, such that networks can activate in a more natural manner.

5.5 Discriminability of ICMS/ITMS Pulse Trains

Discriminability of percepts is critically important to the clinical success of a sensory neuroprosthetic. For this reason, we pursued a line of experiments with the intention of understanding the behavioral discriminability of percepts delivered on different channels and at different intensities. Our hope was that this experiment would mimic the natural percept dimensions of pitch and loudness.

Realistically, electrical stimulation intensity has a muddied relationship with perceived loudness of a percept, as increasing stimulation intensity is also associated with activating a larger area of tissue, which is in turn associated with activating a larger portion of the tonotopic map (in the auditory system). We found that this distinction was quite important, as discriminability of percepts at differing intensities was superior in cortical stimulation as

compared to thalamic stimulation (Fig. 4.3). We believe this advantage that cortical stimulation seems to have is a side-effect of stimulation of larger cortical regions, as evidenced by c-Fos labelling results (Fig. 4.4) and our understanding of the corticothalamic network.

As for interchannel discriminability, our result reveals a significant weakness for central neuroprostheses as compared to cochlear implants. Our inability to present salient perceptual differences when stimulating on two different channels separated by a given distance in the central system represents a major challenge and area for improvement. A key weakness of the field of afferent neuroprostheses is that much of the central nervous system work is done using parameters and methods generated in clinical settings with peripheral prostheses. The reason this is so detrimental is that the neurons in the central and peripheral system are markedly different. Peripheral sensing organs are designed to fire rapidly, have excellent temporal precision, and remodel quickly and efficiently after being damaged. As interfaces move closer to cortical structures, all of these features break down *and* the network becomes more distributed and heterogeneous. It is our opinion that these problems can be solved with better optimized waveform parameters or electrode pulsing protocols, as well as stimulation paradigms that don't rely on such long pulse trains in order to elicit behavioral responses. We found in Chapter 2 that neural activation can occur with as little as a singular pulse, and often at intensities lower than those used on some channels in Chapters 3 and 4. Studying the networks activated by pulse trains of given amplitude is an important next step for the development of central nervous system stimulating neuroprostheses. Fortunately, imaging techniques now exist that can allow us to explore these relationships *in vivo*, and in real time, such as *in vivo* calcium and two-photon imaging.

5.6 Longevity of Thalamic Interfaces

We identified some confounding findings in previous work regarding the relationship of electrode site depth and threshold stability which lead us to initially question whether thalamic or cortical implants would provide a more stable brain interface. In our data, we found thalamic behavioral thresholds to rise more quickly than cortical thresholds (Fig. 3.2), despite similar glial responses to each implant. However, we also identified significant neuron death in the proximity of the thalamic devices (Fig. 3.6) which was unfortunately confounded by a certain amount of thalamic neuron death induced by the presence of a cortical device (Fig. 3.7). Neuron death in

the area of the thalamic probe would undoubtedly result in increasing behavioral thresholds, and we hope future work will explore the possibility of using state-of-the-art neural probes with smaller profiles, so that the stability of the thalamic interface can be explored beyond the limitations of the neural probes that were selected for this dissertation.

5.7 Functional Limits of Safety and Device Integrity for ITMS/ICMS

In the field of microstimulation, there are known noxious effects of electrical pulsing such as local pH changes and the evolution of redox reaction byproducts including but not limited to gases and free radicals (Lilly J et al. 1955; Bartlett JR *et al.* 1977; Shannon R 1992; Merrill D *et al.* 2005). Fortunately, these effects only occur above a certain stimulation intensity, and that intensity has been modelled mathematically and confirmed experimental for a number of electrode sizes and shapes (Merrill D *et al.* 2005). Recent stimulation waveforms utilize a reversing pulse, or biphasic waveform, in order to capture many of the negative byproducts of overpulsing and reduce the noxious effects of electrical stimulation on local tissue, and in the case of high frequency deep brain stimulation, completely mitigates the lesioning effect at a given amplitude (Piallat B et al. 2009). However, the functional safety limit of biphasic pulsing on microelectrodes has not be experimentally confirmed. Outside of the risk of tissue damage, overpulsing on electrodes with iridium oxide deposition can cause delamination of the double layer, often in an irreversible fashion (Troyk PR et al. 2004). Fortunately, this risk can be partially mitigated by short pulse durations, such as the 205μs pulses used in our work, as the risk to the integrity of the double layer capacitance only occurs over long charging cycles or short charging cycles at exceptionally high current levels.

During our discrimination experiments, we tested both interchannel and intensity discriminability at a defined suprathreshold level of +3dB. This level was selected to ensure the rats were performing a discrimination experiment where they could sense a stimulus in every trial, while also maintaining access to a wide range of suprathreshold stimuli below the risk of damage to the tissue or our device. While the thresholds we detected throughout the study were found to increase over the course of our month long study, particularly in thalamus, by assessing the channel-specific thresholds on a daily basis we hoped to compensate for this effect. Regarding the intraday threshold increases we noted in Chapter 3, we don't have sufficient data to assess the time course of those threshold changes during the intensity discrimination trial, and

as such cannot be certain that the lower intensity stimulation remained suprathreshold for the duration of the intensity discrimination trial. Unfortunately, the upper limit of this functional range has not been experimentally defined for our devices and we did not perform that experiment ourselves, so we arbitrarily limited ourselves to a small dynamic range between the animal's behavior threshold (typically <100µA) and 300µA. Thus, specifically in our intensity discrimination work, a relatively small range of intensities were used for testing. The 300µA level was selected based on experience in our lab in overpulsing on our electrodes, as stimulation near that level could sometimes cause behavioral expressions of distress in our animals. When these behaviors were enacted, the stimulation was immediately discontinued on that channel. If these behaviors persisted between days, the channel was no longer used for any stimulation. Furthermore, in 2/3 of our ICMS rats, prolonged stimulation at high stimulus intensities had a tendency to kindle seizure activity, with an onset which varied widely between 10 and 20 days.

However, using stimulus amplitudes in our discrimination tasks which were close to threshold had the potential added benefit of reducing the size of our electrical field of influence (Ranck J 1975; Tehovnik EJ 1996), which we hoped might aid in interchannel discriminability. Early models of this area modelled the shaped of the potential field as a sphere around a simple point charge, however, in our disk shaped electrodes, this model changes to a more conical shape modelled by the following function, derived from Poisson's Equation:

$$V(b,z) = \frac{1}{2\pi\varepsilon_o\varepsilon_r}\iint \frac{\sigma(a) * a}{r}\,da\,d\theta \qquad (5.1)$$

Where *b* and *z* represent the distance from the center of the disk in the radial and orthogonal directions, respectively. Taking advantage of radial symmetry, *r* represents the distance away from the electrode's center to a given point in space:

$$r = \sqrt{a^2 + b^2 + z^2 - 2a\sqrt{b^2 + z^2}\cos(\theta)} \qquad (5.2)$$

Where *a* is the distance from the center of the disk to an infinitely small, radially symmetric element of charge *σ(a)*, where most of the charge resides on the edge of the disk:

$$\sigma(a) = \frac{4V_o\varepsilon_o}{\pi\sqrt{R^2 - a^2}} \qquad (5.3)$$

Where V_o represents the voltage on the disk, and *R* represents the radius of the disk. Despite the specificity of charge localization in our model, we cede that local topography of the iridium oxide layer as well as potential anisotropy of local dielectric properties of neural tissue could

affect the shape of this field. Due to our study limitation of using thick-slice histology for our c-Fos study, we were not able to experimentally validate our model or determine the potential level required to activate nearby neurons, however, in the c-Fos data that we do have, it appeared as though suprathreshold levels (+3dB from threshold, ~177μA) of ITMS evoked an area of neural activation of approximately 150μm from the site in most directions. While we expected the activation to extend further from the site orthogonally than radially, the tissue section in question faced the anatomical border of MGM, which experienced substantial neuronal death. Similar stimulation amplitudes of ICMS activated broad networks in both hemispheres, and a preference for sparse local activation consistent with results in visual ICMS (Histed MH *et al.* 2009). Based on these findings, we believe the activation of sparse local cortical networks, broad activation of distributed cortical networks, and the significant level of neuronal death in auditory thalamus, are all primary contributors to the poor salience of interchannel cues in our behavioral study.

5.8 Final Conclusions

We initially hypothesized that cortical structures would be more heavily modified by drug-induced loss of consciousness than thalamic structures, and suggested that this difference would make thalamus a superior stimulation target for a central neuroprosthetic. We found that both cortical and thalamic structures undergo significant changes during loss of consciousness, specifically in decreasing polysynaptic network interconnectivity and increasing preference to stimulus-linked onset response profiles. We also found that corticothalamic information flow diminished with loss of consciousness, which is indicative of a decrease in feedback specificity. Thus, we conclude that both thalamic and cortical microstimulation must account for the network effects of brain state changes, and that thalamic stimulation may prove superior to cortical stimulation due to the minimal effect of brain state on ascending information flow.

We initially hypothesized that thalamic prostheses would provide an optimal interface with the thalamocortical network and allow for the stimulation of a more physiologically natural network. Further, we implied that activation of a more physiologically natural network would result in superior interchannel and intensity discriminability. Unfortunately, while we did find the network activated by thalamic microstimulation to be more biomimetic, it did not lead to the expected success in discriminability of thalamic microstimulation. In fact, we found thalamic microstimulation to be very poor at delivering behavioral cues, with behavioral d' values

typically less than 1. We hypothesize that ITMS-induced corticothalamic feedback limits the ability of ITMS rats to discriminate percepts of differing intensity, whereas the lack of ICMS-induced thalamocortical feedforward suppression allowed ICMS rats to discriminate intensity percepts based on broadband spectral content.

REFERENCES

Aitkin LM, Prain SM. 1974. Medial geniculate body: unit responses in the awake cat. J Neurophysiol 37:512-521.
Alkire MT, Haier RJ, Fallon JH. 2000. Toward a unified theory of narcosis: brain imaging evidence for a thalamocortical switch as the neurophysiologic basis of anesthetic-induced unconsciousness. Conscious Cogn 9:370-386.
Alkire MT, Hudetz AG, Tononi G. 2008. Consciousness and anesthesia. Science 322:876-880.
Anderson LA, Christianson GB, Linden JF. 2009. Stimulus-specific adaptation occurs in the auditory thalamus. J Neurosci 29:7359-7363.
Antkowiak B. 2001. How do general anaesthetics work? Naturwissenschaften 88:201-213.
Antunes FM, Nelken I, Covey E, Malmierca MS. 2010. Stimulus-specific adaptation in the auditory thalamus of the anesthetized rat. PLoS One 5:e14071.
Armbruster M, Ryan TA. 2011. Synaptic vesicle retrieval time is a cell-wide rather than individual-synapse property. Nat Neurosci 14:824-826.
Asanuma H, Arnold AP. 1975. Noxious effects of excessive currents used for intracortical microstimulation. Brain Res 96:103-107.
Asthagiri AR, Parry DM, Butman JA, Kim HJ, Tsilou ET, Zhuang Z, Lonser RR. 2009. Neurofibromatosis type 2. Lancet 373:1974-1986.
Atencio CA, Blake DT, Strata F, Cheung SW, Merzenich MM, Schreiner CE. 2007. Frequency-modulation encoding in the primary auditory cortex of the awake owl monkey. J Neurophysiol 98:2182-2195.
Atencio CA, Schreiner CE. 2008. Spectrotemporal processing differences between auditory cortical fast-spiking and regular-spiking neurons. J Neurosci 28:3897-3910.
Atencio CA, Schreiner CE. 2010. Laminar diversity of dynamic sound processing in cat primary auditory cortex. J Neurophysiol 103:192-205.
Atencio CA, Schreiner CE. 2012. Spectrotemporal processing in spectral tuning modules of cat primary auditory cortex. PLoS One 7:e31537.
Atencio CA, Sharpee TO, Schreiner CE. 2008. Cooperative nonlinearities in auditory cortical neurons. Neuron 58:956-966.
Atencio CA, Shih JY, Schreiner CE, Cheung SW. 2014. Primary auditory cortical responses to electrical stimulation of the thalamus. J Neurophysiol 111:1077-1087.
Atiani S, Elhilali M, David SV, Fritz JB, Shamma SA. 2009. Task difficulty and performance induce diverse adaptive patterns in gain and shape of primary auditory cortical receptive fields. Neuron 61:467-480.
Babcock AA, Kuziel WA, Rivest S, Owens T. 2003. Chemokine expression by glial cells directs leukocytes to sites of axonal injury in the CNS. J Neurosci 23:7922-7930.
Bandyopadhyay S, Shamma SA, Kanold PO. 2010. Dichotomy of functional organization in the mouse auditory cortex. Nat Neurosci 13:361-368.
Bartlett EL. 2013. The organization and physiology of the auditory thalamus and its role in processing acoustic features important for speech perception. Brain Lang 126:29-48.
Bartlett EL, Sadagopan S, Wang X. 2011. Fine frequency tuning in monkey auditory cortex and thalamus. J Neurophysiol 106:849-859.
Bartlett EL, Smith PH. 1999. Anatomic, intrinsic, and synaptic properties of dorsal and ventral division neurons in rat medial geniculate body. J Neurophysiol 81:1999-2016.

Bartlett EL, Smith PH. 2002. Effects of paired-pulse and repetitive stimulation on neurons in the rat medial geniculate body. Neuroscience 113:957-974.
Bartlett EL, Stark JM, Guillery RW, Smith PH. 2000. Comparison of the fine structure of cortical and collicular terminals in the rat medial geniculate body. Neuroscience 100:811-828.
Bartlett EL, Wang X. 2005. Long-lasting modulation by stimulus context in primate auditory cortex. J Neurophysiol 94:83-104.
Bartlett EL, Wang X. 2007. Neural representations of temporally modulated signals in the auditory thalamus of awake primates. J Neurophysiol 97:1005-1017.
Bartlett EL, Wang X. 2011. Correlation of neural response properties with auditory thalamus subdivisions in the awake marmoset. J Neurophysiol 105:2647-2667.
Bartlett JR, Doty RW, Lee BB, Negrão N, Overman WH. 1977. Deleterious effects of prolonged electrical excitation of striate cortex in macaques. Brain Behav Evol 14:46-66.
Bartlett TE, Bannister NJ, Collett VJ, Dargan SL, Massey PV, Bortolotto ZA, Fitzjohn SM, Bashir ZI, Collingridge GL, Lodge D. 2007. Differential roles of NR2A and NR2B-containing NMDA receptors in LTP and LTD in the CA1 region of two-week old rat hippocampus. Neuropharmacology 52:60-70.
Berg JA, Dammann JF, Tenore FV, Tabot GA, Boback JL, Manfredi LR, Peterson ML, Katyal KD, Johannes MS, Makhlin A, Wilcox R, Franklin RK, Vogelstein RJ, Hatsopoulos NG, Bensmaia SJ. 2013. Behavioral Demonstration of a Somatosensory Neuroprosthesis. IEEE Transactions on Neural Systems and Rehabilitation Engineering 21:500-507.
Biran R, Martin DC, Tresco PA. 2005. Neuronal cell loss accompanies the brain tissue response to chronically implanted silicon microelectrode arrays. Exp Neurol 195:115-126.
Biran R, Martin DC, Tresco PA. 2007. The brain tissue response to implanted silicon microelectrode arrays is increased when the device is tethered to the skull. J Biomed Mater Res A 82:169-178.
Boly M, Moran R, Murphy M, Boveroux P, Bruno MA, Noirhomme Q, Ledoux D, Bonhomme V, Brichant JF, Tononi G, Laureys S, Friston K. 2012. Connectivity changes underlying spectral EEG changes during propofol-induced loss of consciousness. J Neurosci 32:7082-7090.
Brackmann DE, Hitselberger WE, Nelson RA, Moore J, Waring MD, Portillo F, Shannon RV, Telischi FF. 1993. Auditory brainstem implant: I. Issues in surgical implantation. Otolaryngol Head Neck Surg 108:624-633.
Carandini M, Heeger DJ, Senn W. 2002. A synaptic explanation of suppression in visual cortex. J Neurosci 22:10053-10065.
Carney LH, Zilany MS, Huang NJ, Abrams KS, Idrobo F. 2014. Suboptimal use of neural information in a mammalian auditory system. J Neurosci 34:1306-1313.
Chechik G, Anderson MJ, Bar-Yosef O, Young ED, Tishby N, Nelken I. 2006. Reduction of information redundancy in the ascending auditory pathway. Neuron 51:359-368.
Chen R, Classen J, Gerloff C, Celnik P, Wassermann EM, Hallett M, Cohen LG. 1997. Depression of motor cortex excitability by low-frequency transcranial magnetic stimulation. Neurology 48:1398-1403.
Chung K, Wallace J, Kim SY, Kalyanasundaram S, Andalman AS, Davidson TJ, Mirzabekov JJ, Zalocusky KA, Mattis J, Denisin AK, Pak S, Bernstein H, Ramakrishnan C, Grosenick L, Gradinaru V, Deisseroth K. 2013. Structural and molecular interrogation of intact biological systems. Nature 497:332-337.
Chung S, Li X, Nelson SB. 2002. Short-term depression at thalamocortical synapses contributes to rapid adaptation of cortical sensory responses in vivo. Neuron 34:437-446.

Clerici WJ, Coleman JR. 1990. Anatomy of the rat medial geniculate body: I. Cytoarchitecture, myeloarchitecture, and neocortical connectivity. J Comp Neurol 297:14-31.
Clerici WJ, McDonald AJ, Thompson R, Coleman JR. 1990. Anatomy of the rat medial geniculate body: II. Dendritic morphology. J Comp Neurol 297:32-54.
Cogan SF, Guzelian AA, Agnew WF, Yuen TG, McCreery DB. 2004. Over-pulsing degrades activated iridium oxide films used for intracortical neural stimulation. J Neurosci Methods 137:141-150.
Colletti V, Shannon RV. 2005. Open set speech perception with auditory brainstem implant? Laryngoscope 115:1974-1978.
Conley M, Kupersmith AC, Diamond IT. 1991. The Organization of Projections from Subdivisions of the Auditory Cortex and Thalamus to the Auditory Sector of the Thalamic Reticular Nucleus in Galago. Eur J Neurosci 3:1089-1103.
Conway AR, Cowan N, Bunting MF. 2001. The cocktail party phenomenon revisited: the importance of working memory capacity. Psychon Bull Rev 8:331-335.
Cooke JE, Zhang H, Kelly JB. 2007. Detection of sinusoidal amplitude modulated sounds: deficits after bilateral lesions of auditory cortex in the rat. Hear Res 231:90-99.
Crabtree JW. 1998. Organization in the auditory sector of the cat's thalamic reticular nucleus. J Comp Neurol 390:167-182.
Crandall SR, Cruikshank SJ, Connors BW. 2015. A corticothalamic switch: controlling the thalamus with dynamic synapses. Neuron 86:768-782.
Creutzfeldt O, Hellweg FC, Schreiner C. 1980. Thalamocortical transformation of responses to complex auditory stimuli. Exp Brain Res 39:87-104.
Cutts CS, Eglen SJ. 2014. Detecting pairwise correlations in spike trains: an objective comparison of methods and application to the study of retinal waves. J Neurosci 34:14288-14303.
de Biasi S, Frassoni C, Spreafico R. 1986. GABA immunoreactivity in the thalamic reticular nucleus of the rat. A light and electron microscopical study. Brain Res 399:143-147.
de Hoz L, Gierej D, Lioudyno V, Jaworski J, Blazejczyk M, Cruces-Solís H, Beroun A, Lebitko T, Nikolaev T, Knapska E, Nelken I, Kaczmarek L. 2017. Blocking c-Fos Expression Reveals the Role of Auditory Cortex Plasticity in Sound Frequency Discrimination Learning. Cereb Cortex:1-11.
Doyle CA, Cullen WK, Rowan MJ, Anwyl R. 1997. Low-frequency stimulation induces homosynaptic depotentiation but not long-term depression of synaptic transmission in the adult anaesthetized and awake rat hippocampus in vivo. Neuroscience 77:75-85.
Dräger UC. 1975. Receptive fields of single cells and topography in mouse visual cortex. J Comp Neurol 160:269-290.
Dynes SB, Delgutte B. 1992. Phase-locking of auditory-nerve discharges to sinusoidal electric stimulation of the cochlea. Hear Res 58:79-90.
Edeline JM, Weinberger NM. 1991. Thalamic short-term plasticity in the auditory system: associative returning of receptive fields in the ventral medial geniculate body. Behav Neurosci 105:618-639.
Edelman GM. 2003. Naturalizing consciousness: a theoretical framework. Proc Natl Acad Sci U S A 100:5520-5524.
Ejserholm F, Stegmayr J, Bauer P, Johansson F, Wallman L, Bengtsson M, Oredsson S. 2015. Biocompatibility of a polymer based on Off-Stoichiometry Thiol-Enes + Epoxy (OSTE+) for neural implants. Biomater Res 19:19.

Elhilali M. 2013. Bayesian inference in auditory scenes. Conf Proc IEEE Eng Med Biol Soc 2013:2792-2795.
Eliades SJ, Wang X. 2008. Chronic multi-electrode neural recording in free-roaming monkeys. J Neurosci Methods 172:201-214.
Fastl H, Hesse A, Schorer E, Urbas J, Müller-Preuss P. 1986. Searching for neural correlates of the hearing sensation fluctuation strength in the auditory cortex of squirrel monkeys. Hear Res 23:199-203.
Ferrarelli F, Massimini M, Sarasso S, Casali A, Riedner BA, Angelini G, Tononi G, Pearce RA. 2010. Breakdown in cortical effective connectivity during midazolam-induced loss of consciousness. Proc Natl Acad Sci U S A 107:2681-2686.
Franks NP. 2008. General anaesthesia: from molecular targets to neuronal pathways of sleep and arousal. Nat Rev Neurosci 9:370-386.
Freeman TC, Durand S, Kiper DC, Carandini M. 2002. Suppression without inhibition in visual cortex. Neuron 35:759-771.
Gaese B, Ostwald J. 1995. Temporal Coding of Amplitude and Frequency Modulation in the Rat Auditory Cortex. European Journal of Neuroscience 7:438-450.
Games KD, Winer JA. 1988. Layer V in rat auditory cortex: projections to the inferior colliculus and contralateral cortex. Hear Res 34:1-25.
Gaucher Q, Huetz C, Gourévitch B, Edeline JM. 2013. Cortical inhibition reduces information redundancy at presentation of communication sounds in the primary auditory cortex. J Neurosci 33:10713-10728.
Giulian D, Li J, Leara B, Keenen C. 1994. Phagocytic microglia release cytokines and cytotoxins that regulate the survival of astrocytes and neurons in culture. Neurochem Int 25:227-233.
Giulian D, Li J, Li X, George J, Rutecki PA. 1994. The impact of microglia-derived cytokines upon gliosis in the CNS. Dev Neurosci 16:128-136.
Grasshoff C, Antkowiak B. 2006. Effects of isoflurane and enflurane on GABAA and glycine receptors contribute equally to depressant actions on spinal ventral horn neurones in rats. Br J Anaesth 97:687-694.
Graybiel AM, Moratalla R, Robertson HA. 1990. Amphetamine and cocaine induce drug-specific activation of the c-fos gene in striosome-matrix compartments and limbic subdivisions of the striatum. Proc Natl Acad Sci U S A 87:6912-6916.
Grill WM, Norman SE, Bellamkonda RV. 2009. Implanted neural interfaces: biochallenges and engineered solutions. Annu Rev Biomed Eng 11:1-24.
Gross NB, Lifschitz WS, Anderson DJ. 1974. The tonotopic organization of the auditory thalamus of the squirrel monkey (Saimiri sciureus). Brain Res 65:323-332.
Hack M. 1971. Auditory Intensity Discrimination in the Rat. Journal of Comparative and Physiological Psychology 74:315-318.
Hawley ML, Litovsky RY, Culling JF. 2004. The benefit of binaural hearing in a cocktail party: effect of location and type of interferer. J Acoust Soc Am 115:833-843.
He J, Hu B. 2002. Differential distribution of burst and single-spike responses in auditory thalamus. J Neurophysiol 88:2152-2156.
Heffner HE, Heffner RS. 1985. Hearing in two cricetid rodents: wood rat (Neotoma floridana) and grasshopper mouse (Onychomys leucogaster). J Comp Psychol 99:275-288.
Heffner HE, Heffner RS. 1995. Conditioned Avoidance. In: Klump GM, Dooling RJ, Fay RR, Stebbins WC, editors. Methods in Comparative Psychoacoustics Basel: Birkhäuser Basel p 79-93.

Hefti BJ, Smith PH. 2000. Anatomy, physiology, and synaptic responses of rat layer V auditory cortical cells and effects of intracellular GABA(A) blockade. J Neurophysiol 83:2626-2638.
Hentschke H, Schwarz C, Antkowiak B. 2005. Neocortex is the major target of sedative concentrations of volatile anaesthetics: strong depression of firing rates and increase of GABAA receptor-mediated inhibition. Eur J Neurosci 21:93-102.
Histed MH, Bonin V, Reid RC. 2009. Direct activation of sparse, distributed populations of cortical neurons by electrical microstimulation. Neuron 63:508-522.
Hu E, Mueller E, Oliviero S, Papaioannou VE, Johnson R, Spiegelman BM. 1994. Targeted disruption of the c-fos gene demonstrates c-fos-dependent and -independent pathways for gene expression stimulated by growth factors or oncogenes. EMBO J 13:3094-3103.
Huetz C, Gourévitch B, Edeline JM. 2011. Neural codes in the thalamocortical auditory system: from artificial stimuli to communication sounds. Hear Res 271:147-158.
Huetz C, Philibert B, Edeline JM. 2009. A spike-timing code for discriminating conspecific vocalizations in the thalamocortical system of anesthetized and awake guinea pigs. J Neurosci 29:334-350.
Imas OA, Ropella KM, Ward BD, Wood JD, Hudetz AG. 2005. Volatile anesthetics disrupt frontal-posterior recurrent information transfer at gamma frequencies in rat. Neurosci Lett 387:145-150.
Izumi Y, O'Dell KA, Zorumski CF. 2013. Metaplastic LTP inhibition after LTD induction in CA1 hippocampal slices involves NMDA Receptor-mediated Neurosteroidogenesis. Physiol Rep 1:e00133.
Jakob TF, Döring U, Illing RB. 2015. The pattern of Fos expression in the rat auditory brainstem changes with the temporal structure of binaural electrical intracochlear stimulation. Exp Neurol 266:55-67.
Jeong J, Gore JC, Peterson BS. 2001. Mutual information analysis of the EEG in patients with Alzheimer's disease. Clin Neurophysiol 112:827-835.
Jones EG. 1998. Viewpoint: the core and matrix of thalamic organization. Neuroscience 85:331-345.
Joucla S, Yvert B. 2009. Improved focalization of electrical microstimulation using microelectrode arrays: a modeling study. PLoS One 4:e4828.
Kelly JB, Cooke JE, Gilbride PC, Mitchell C, Zhang H. 2006. Behavioral limits of auditory temporal resolution in the rat: amplitude modulation and duration discrimination. J Comp Psychol 120:98-105.
Kerssens C, Hamann S, Peltier S, Hu XP, Byas-Smith MG, Sebel PS. 2005. Attenuated brain response to auditory word stimulation with sevoflurane: a functional magnetic resonance imaging study in humans. Anesthesiology 103:11-19.
Kilgard M, Merzenich M. 1999. Distributed Representation of Spectral and Temporal Information in Rat Primary Auditory Cortex. Hearing Research 134:16-28.
Kimura A, Donishi T, Okamoto K, Tamai Y. 2005. Topography of projections from the primary and non-primary auditory cortical areas to the medial geniculate body and thalamic reticular nucleus in the rat. Neuroscience 135:1325-1342.
Koivuniemi A, Otto K. 2011. Asymmetric Versus Symmetric Pulses for Cortical Microstimulation. IEEE Transactions on Neural Systems and Rehabilitation Engineering 19:468-476.
Koivuniemi A, Otto Keditors. Year Published|. Title|, Conference Name|; Year of Conference Date|; Conference Location| Place Published|:Publisher|. Pages p|.

Koivuniemi A, Regele O, Brenner J, Otto K. 2011. Rat Behavioral Model for High-Throughput Parametric Studies of Intracortical Microstimulation. In. 33rd Annual International Conference of the IEEE Engineering in Medicine and Biology Society. Boston, MA, USA: IEEE Xplore. p 7541-7544.
Kozai TD, Kipke DR. 2009. Insertion shuttle with carboxyl terminated self-assembled monolayer coatings for implanting flexible polymer neural probes in the brain. J Neurosci Methods 184:199-205.
Kozai TD, Langhals NB, Patel PR, Deng X, Zhang H, Smith KL, Lahann J, Kotov NA, Kipke DR. 2012. Ultrasmall implantable composite microelectrodes with bioactive surfaces for chronic neural interfaces. Nat Mater 11:1065-1073.
Land R, Engler G, Kral A, Engel AK. 2012. Auditory evoked bursts in mouse visual cortex during isoflurane anesthesia. PLoS One 7:e49855.
Lilly J, Hughes J, Alvord E, Galkin T. 1955. Brief, Noninjurious Electric Waveform for Stimulation of the Brain. Science 121:468-469.
Lim HH, Anderson DJ. 2006. Auditory cortical responses to electrical stimulation of the inferior colliculus: implications for an auditory midbrain implant. J Neurophysiol 96:975-988.
Lim HH, Anderson DJ. 2007. Spatially distinct functional output regions within the central nucleus of the inferior colliculus: implications for an auditory midbrain implant. J Neurosci 27:8733-8743.
Lim HH, Lenarz T. 2015. Auditory midbrain implant: research and development towards a second clinical trial. Hear Res 322:212-223.
Lim HH, Lenarz T, Anderson DJ, Lenarz M. 2008. The auditory midbrain implant: effects of electrode location. Hear Res 242:74-85.
Liu X, Lauer KK, Ward BD, Rao SM, Li SJ, Hudetz AG. 2012. Propofol disrupts functional interactions between sensory and high-order processing of auditory verbal memory. Hum Brain Mapp 33:2487-2498.
Lu T, Liang L, Wang X. 2001. Temporal and Rate Representations of Time-Varying Signals in the Auditory Cortex of Awake Primates. Nature Neuroscience 4:1131-1138.
Lu T, Wang X. 2000. Temporal Discharge Patterns Evoked by Rapid Sequences of Wide- and Narrowband Clicks in the Primary Auditory Cortex of Cat. Journal of Neurophysiology 84:236-246.
Malmierca MS, Merchán MA, Henkel CK, Oliver DL. 2002. Direct projections from cochlear nuclear complex to auditory thalamus in the rat. J Neurosci 22:10891-10897.
Markram H, Gupta A, Uziel A, Wang Y, Tsodyks M. 1998. Information processing with frequency-dependent synaptic connections. Neurobiol Learn Mem 70:101-112.
Mashour GA. 2013. Cognitive unbinding: a neuroscientific paradigm of general anesthesia and related states of unconsciousness. Neurosci Biobehav Rev 37:2751-2759.
Mashour GA. 2013. Consciousness, anesthesia, and neural synchrony. Anesthesiology 119:7-9.
Mashour GA, Alkire MT. 2013. Consciousness, anesthesia, and the thalamocortical system. Anesthesiology 118:13-15.
Massimini M, Ferrarelli F, Huber R, Esser SK, Singh H, Tononi G. 2005. Breakdown of cortical effective connectivity during sleep. Science 309:2228-2232.
McConnell GC, Rees HD, Levey AI, Gutekunst CA, Gross RE, Bellamkonda RV. 2009. Implanted neural electrodes cause chronic, local inflammation that is correlated with local neurodegeneration. J Neural Eng 6:056003.

McDermott HJ. 2004. Music perception with cochlear implants: a review. Trends Amplif 8:49-82.
Merrill D, Bikson M, Jefferys J. 2005. Electrical Stimulation of Excitable Tissue: Design of Efficacious and Safe Protocols. Journal of Neuroscience Methods 141:171-198.
Miller LM, Escabí MA, Read HL, Schreiner CE. 2001. Functional convergence of response properties in the auditory thalamocortical system. Neuron 32:151-160.
Miller LM, Escabí MA, Read HL, Schreiner CE. 2002. Spectrotemporal receptive fields in the lemniscal auditory thalamus and cortex. J Neurophysiol 87:516-527.
Miller LM, Escabí MA, Schreiner CE. 2001. Feature selectivity and interneuronal cooperation in the thalamocortical system. J Neurosci 21:8136-8144.
Mockett B, Coussens C, Abraham WC. 2002. NMDA receptor-mediated metaplasticity during the induction of long-term depression by low-frequency stimulation. Eur J Neurosci 15:1819-1826.
Molander C, Hongpaisan J, Grant G. 1992. Changing pattern of c-FOS expression in spinal cord neurons after electrical stimulation of the chronically injured sciatic nerve in the rat. Neuroscience 50:223-236.
Monzée J, Lamarre Y, Smith A. 2003. The Effects of Digital Anesthesia on Force Control Using a Precision Grip. Journal of Neurophysiology 89:672-683.
MOREST DK. 1964. THE NEURONAL ARCHITECTURE OF THE MEDIAL GENICULATE BODY OF THE CAT. J Anat 98:611-630.
Müller-Preuss P. 1986. On the mechanisms of call coding through auditory neurons in the squirrel monkey. Eur Arch Psychiatry Neurol Sci 236:50-55.
Nelken I, Chechik G, Mrsic-Flogel TD, King AJ, Schnupp JW. 2005. Encoding stimulus information by spike numbers and mean response time in primary auditory cortex. J Comput Neurosci 19:199-221.
Nelken I, Rotman Y, Bar Yosef O. 1999. Responses of auditory-cortex neurons to structural features of natural sounds. Nature 397:154-157.
Nichols CD, Sanders-Bush E. 2002. A single dose of lysergic acid diethylamide influences gene expression patterns within the mammalian brain. Neuropsychopharmacology 26:634-642.
Noda T, Takahashi H. 2015. Anesthetic effects of isoflurane on the tonotopic map and neuronal population activity in the rat auditory cortex. Eur J Neurosci 42:2298-2311.
Ogawa SK, Tanaka E, Shin MC, Kotani N, Akaike N. 2011. Volatile anesthetic effects on isolated GABA synapses and extrasynaptic receptors. Neuropharmacology 60:701-710.
Otto K, Rousche P, Kipke D. 2005. Cortical Microstimulation in Auditory Cortex of Rat Elicits Best-Frequency Dependent Behaviors. Journal of Neural Engineering 2:42-51.
Otto K, Rousche P, Kipke D. 2005. Microstimulation in Auditory Cortex Provides a Substrate for Detailed Behaviors. Hearing Research:112-117.
Ouda L, Jílek M, Syka J. 2016. Expression of c-Fos in rat auditory and limbic systems following 22-kHz calls. Behav Brain Res 308:196-204.
Panzeri S, Senatore R, Montemurro MA, Petersen RS. 2007. Correcting for the sampling bias problem in spike train information measures. J Neurophysiol 98:1064-1072.
Paxinos G, Watson CR, Emson PC. 1980. AChE-stained horizontal sections of the rat brain in stereotaxic coordinates. J Neurosci Methods 3:129-149.
Pernia M, Estevez S, Poveda C, Plaza I, Carro J, Juiz JM, Merchan MA. 2017. c-Fos and Arc/Arg3.1 expression in auditory and visual cortices after hearing loss: Evidence of sensory crossmodal reorganization in adult rats. J Comp Neurol 525:2677-2689.

Petersen RS, Diamond ME. 2000. Spatial-temporal distribution of whisker-evoked activity in rat somatosensory cortex and the coding of stimulus location. J Neurosci 20:6135-6143.
Pezaris JS, Reid RC. 2007. Demonstration of artificial visual percepts generated through thalamic microstimulation. Proc Natl Acad Sci U S A 104:7670-7675.
Pfingst BE, O'Connor TA. 1981. Characteristics of neurons in auditory cortex of monkeys performing a simple auditory task. J Neurophysiol 45:16-34.
Piallat B, Chabardès S, Devergnas A, Torres N, Allain M, Barrat E, Benabid AL. 2009. Monophasic but not biphasic pulses induce brain tissue damage during monopolar high-frequency deep brain stimulation. Neurosurgery 64:156-162; discussion 162-153.
Pierce AL, Sommakia S, Rickus JL, Otto KJ. 2009. Thin-film silica sol-gel coatings for neural microelectrodes. J Neurosci Methods 180:106-110.
Polikov VS, Tresco PA, Reichert WM. 2005. Response of brain tissue to chronically implanted neural electrodes. J Neurosci Methods 148:1-18.
Polley DB, Steinberg EE, Merzenich MM. 2006. Perceptual learning directs auditory cortical map reorganization through top-down influences. J Neurosci 26:4970-4982.
Preuss A, Müller-Preuss P. 1990. Processing of amplitude modulated sounds in the medial geniculate body of squirrel monkeys. Exp Brain Res 79:207-211.
Quiroga RQ, Nadasdy Z, Ben-Shaul Y. 2004. Unsupervised spike detection and sorting with wavelets and superparamagnetic clustering. Neural Comput 16:1661-1687.
Raggio MW, Schreiner CE. 1994. Neuronal responses in cat primary auditory cortex to electrical cochlear stimulation. I. Intensity dependence of firing rate and response latency. J Neurophysiol 72:2334-2359.
Ranck J. 1975. Which Elements are Excited in Electrical Stimulation of Mammalian Central Nervous System: A Review. Brain Research 98:417-440.
Rao L, Zhou H, Li T, Li C, Duan YY. 2012. Polyethylene glycol-containing polyurethane hydrogel coatings for improving the biocompatibility of neural electrodes. Acta Biomater 8:2233-2242.
Raz A, Grady SM, Krause BM, Uhlrich DJ, Manning KA, Banks MI. 2014. Preferential effect of isoflurane on top-down vs. bottom-up pathways in sensory cortex. Front Syst Neurosci 8:191.
Read HL, Nauen DW, Escabí MA, Miller LM, Schreiner CE, Winer JA. 2011. Distinct core thalamocortical pathways to central and dorsal primary auditory cortex. Hear Res 274:95-104.
Regele O, Koivuniemi A, Otto Keditors. Year Published|. Title|, Conference Name|; Year of Conference Date|; Conference Location| Place Published|:Publisher|. Pages p|.
Richardson BD, Hancock KE, Caspary DM. 2013. Stimulus-specific adaptation in auditory thalamus of young and aged awake rats. J Neurophysiol 110:1892-1902.
Ries CR, Puil E. 1999. Mechanism of anesthesia revealed by shunting actions of isoflurane on thalamocortical neurons. J Neurophysiol 81:1795-1801.
Robblee L, Lefko J, Brummer S. 1983. Activated Ir: An electrode suitable for reversible charge injection in saline solution. Journal of the Electrochemical Society 130:731-733.
Romo R, Hernández A, Zainos A, Salinas E. 1998. Somatosensory Discrimination Based on Cortical Microstimulation. Nature 392:387-390.
Romo R, Salinas E. 2003. Flutter Discrimination: Neural Codes, Perception, Memory, and Decision Making. Nature Reviews 4:203-218.
Rouiller E, de Ribaupierre Y, Morel A, de Ribaupierre F. 1983. Intensity functions of single unit responses to tone in the medial geniculate body of cat. Hear Res 11:235-247.

Rouiller E, de Ribaupierre Y, Toros-Morel A, de Ribaupierre F. 1981. Neural coding of repetitive clicks in the medial geniculate body of cat. Hear Res 5:81-100.
Rouiller EM, Rodrigues-Dagaeff C, Simm G, De Ribaupierre Y, Villa A, De Ribaupierre F. 1989. Functional organization of the medial division of the medial geniculate body of the cat: tonotopic organization, spatial distribution of response properties and cortical connections. Hear Res 39:127-142.
Rouse A, Stanslaski S, Cong P, Jensen R, Afshar P, Ullestad D, Moran D, Denison T. 2011. A Chronic Generalized Bi-directional Brain-Machine Interface. Journal of Neural Engineering 8.
Rudolph U, Antkowiak B. 2004. Molecular and neuronal substrates for general anaesthetics. Nat Rev Neurosci 5:709-720.
Ryan TA, Smith SJ, Reuter H. 1996. The timing of synaptic vesicle endocytosis. Proc Natl Acad Sci U S A 93:5567-5571.
Saalmann YB. 2014. Intralaminar and medial thalamic influence on cortical synchrony, information transmission and cognition. Front Syst Neurosci 8:83.
Sadagopan S, Wang X. 2008. Level invariant representation of sounds by populations of neurons in primary auditory cortex. J Neurosci 28:3415-3426.
Sadagopan S, Wang X. 2009. Nonlinear spectrotemporal interactions underlying selectivity for complex sounds in auditory cortex. J Neurosci 29:11192-11202.
Sadagopan S, Wang X. 2010. Contribution of inhibition to stimulus selectivity in primary auditory cortex of awake primates. J Neurosci 30:7314-7325.
Sally S, Kelly J. 1988. Organization of Auditory Cortex in the Albino Rat: Sound Frequency. Journal of Neurophysiology 59:1627-1638.
Schlögl A, Neuper C, Pfurtscheller G. 2002. Estimating the mutual information of an EEG-based Brain-Computer Interface. Biomed Tech (Berl) 47:3-8.
Shannon R. 1992. A Model of Safe levels for Electrical Stimulation. IEEE Transactions on Biomedical Engineering 39:424-426.
Shannon RV, Zeng FG, Kamath V, Wygonski J, Ekelid M. 1995. Speech recognition with primarily temporal cues. Science 270:303-304.
Shelton KL, Nicholson KL. 2010. GABA(A) positive modulator and NMDA antagonist-like discriminative stimulus effects of isoflurane vapor in mice. Psychopharmacology (Berl) 212:559-569.
Sitdikova G, Zakharov A, Janackova S, Gerasimova E, Lebedeva J, Inacio AR, Zaynutdinova D, Minlebaev M, Holmes GL, Khazipov R. 2014. Isoflurane suppresses early cortical activity. Ann Clin Transl Neurol 1:15-26.
Skousen JL, Merriam SM, Srivannavit O, Perlin G, Wise KD, Tresco PA. 2011. Reducing surface area while maintaining implant penetrating profile lowers the brain foreign body response to chronically implanted planar silicon microelectrode arrays. Prog Brain Res 194:167-180.
Smith PH, Populin LC. 2001. Fundamental differences between the thalamocortical recipient layers of the cat auditory and visual cortices. J Comp Neurol 436:508-519.
Strong SP, de Ruyter van Steveninck RR, Bialek W, Koberle R. 1998. On the application of information theory to neural spike trains. Pac Symp Biocomput:621-632.
Subbaroyan J, Martin DC, Kipke DR. 2005. A finite-element model of the mechanical effects of implantable microelectrodes in the cerebral cortex. J Neural Eng 2:103-113.
Swadlow HA, Bezdudnaya T, Gusev AG. 2005. Spike timing and synaptic dynamics at the awake thalamocortical synapse. Prog Brain Res 149:91-105.

Swadlow HA, Gusev AG. 2001. The impact of 'bursting' thalamic impulses at a neocortical synapse. Nat Neurosci 4:402-408.
Swadlow HA, Gusev AG, Bezdudnaya T. 2002. Activation of a cortical column by a thalamocortical impulse. J Neurosci 22:7766-7773.
Syka J, Rybalko N, Brožek G, Jilek M. 1996. Auditory Frequency and Intensity Discrimination in Pigmented Rats. Hearing Research 100:107-113.
Takeuchi S, Ziegler D, Yoshida Y, Mabuchi K, Suzuki T. 2005. Parylene flexible neural probes integrated with microfluidic channels. Lab Chip 5:519-523.
Tehovnik EJ. 1996. Electrical stimulation of neural tissue to evoke behavioral responses. J Neurosci Methods 65:1-17.
Ter-Mikaelian M, Sanes DH, Semple MN. 2007. Transformation of temporal properties between auditory midbrain and cortex in the awake Mongolian gerbil. J Neurosci 27:6091-6102.
Thomson EE, Carra R, Nicolelis MA. 2013. Perceiving invisible light through a somatosensory cortical prosthesis. Nat Commun 4:1482.
Tononi G. 2004. An information integration theory of consciousness. BMC Neurosci 5:42.
Torab K, Davis TS, Warren DJ, House PA, Normann RA, Greger B. 2011. Multiple factors may influence the performance of a visual prosthesis based on intracortical microstimulation: nonhuman primate behavioural experimentation. J Neural Eng 8:035001.
Treves A, Panzeri S. 1995. The Upward Bias in Measures of Information Derived from Limited Data Samples. In. Neural Computation: Massachusetts Institute of Technology. p 399-407.
Troyk PR, Detlefsen DE, Cogan SF, Ehrlich J, Bak M, McCreery DB, Bullara L, Schmidt E. 2004. "Safe" charge-injection waveforms for iridium oxide (AIROF) microelectrodes. Conf Proc IEEE Eng Med Biol Soc 6:4141-4144.
Tsodyks M, Uziel A, Markram H. 2000. Synchrony generation in recurrent networks with frequency-dependent synapses. J Neurosci 20:RC50.
Tsodyks MV, Markram H. 1997. The neural code between neocortical pyramidal neurons depends on neurotransmitter release probability. Proc Natl Acad Sci U S A 94:719-723.
Turner JN, Shain W, Szarowski DH, Andersen M, Martins S, Isaacson M, Craighead H. 1999. Cerebral astrocyte response to micromachined silicon implants. Exp Neurol 156:33-49.
Ulanovsky N, Las L, Farkas D, Nelken I. 2004. Multiple time scales of adaptation in auditory cortex neurons. J Neurosci 24:10440-10453.
VanElzakker M, Fevurly RD, Breindel T, Spencer RL. 2008. Environmental novelty is associated with a selective increase in Fos expression in the output elements of the hippocampal formation and the perirhinal cortex. Learn Mem 15:899-908.
Venkatraman S, Hendricks J, King ZA, Sereno AJ, Richardson-Burns S, Martin D, Carmena JM. 2011. In vitro and in vivo evaluation of PEDOT microelectrodes for neural stimulation and recording. IEEE Trans Neural Syst Rehabil Eng 19:307-316.
Vetter RJ, Williams JC, Hetke JF, Nunamaker EA, Kipke DR. 2004. Chronic neural recording using silicon-substrate microelectrode arrays implanted in cerebral cortex. IEEE Trans Biomed Eng 51:896-904.
Villa AE, Abeles M. 1990. Evidence for spatiotemporal firing patterns within the auditory thalamus of the cat. Brain Res 509:325-327.
Villa AE, Rouiller EM, Simm GM, Zurita P, de Ribaupierre Y, de Ribaupierre F. 1991. Corticofugal modulation of the information processing in the auditory thalamus of the cat. Exp Brain Res 86:506-517.

Wang H, Isik M, Borst A, Hemmert W. 2011. Auditory information coding by modeled cochlear nucleus neurons. J Comput Neurosci 30:529-542.
Wang X, Lu T, Bendor D, Bartlett E. 2008. Neural coding of temporal information in auditory thalamus and cortex. Neuroscience 157:484-494.
Wehr M, Zador AM. 2005. Synaptic mechanisms of forward suppression in rat auditory cortex. Neuron 47:437-445.
Weiland JD, Anderson DJ. 2000. Chronic neural stimulation with thin-film, iridium oxide electrodes. IEEE Trans Biomed Eng 47:911-918.
Wilks SJ, Richardson-Burns SM, Hendricks JL, Martin DC, Otto KJ. 2009. Poly(3,4-ethylenedioxythiophene) as a Micro-Neural Interface Material for Electrostimulation. Front Neuroeng 2:7.
Wilks SJ, Woolley AJ, Ouyang L, Martin DC, Otto KJ. 2011. In vivo polymerization of poly(3,4-ethylenedioxythiophene) (PEDOT) in rodent cerebral cortex. Conf Proc IEEE Eng Med Biol Soc 2011:5412-5415.
Williams JC, Hippensteel JA, Dilgen J, Shain W, Kipke DR. 2007. Complex impedance spectroscopy for monitoring tissue responses to inserted neural implants. J Neural Eng 4:410-423.
Williams JC, Rennaker RL, Kipke DR. 1999. Long-term neural recording characteristics of wire microelectrode arrays implanted in cerebral cortex. Brain Res Brain Res Protoc 4:303-313.
Winer JA. 1984. Anatomy of layer IV in cat primary auditory cortex (AI). J Comp Neurol 224:535-567.
Winer JA, Sally SL, Larue DT, Kelly JB. 1999. Origins of medial geniculate body projections to physiologically defined zones of rat primary auditory cortex. Hear Res 130:42-61.
Wood N, Cowan N. 1995. The cocktail party phenomenon revisited: how frequent are attention shifts to one's name in an irrelevant auditory channel? J Exp Psychol Learn Mem Cogn 21:255-260.
Woodroofe MN, Sarna GS, Wadhwa M, Hayes GM, Loughlin AJ, Tinker A, Cuzner ML. 1991. Detection of interleukin-1 and interleukin-6 in adult rat brain, following mechanical injury, by in vivo microdialysis: evidence of a role for microglia in cytokine production. J Neuroimmunol 33:227-236.
Woolley AJ, Desai HA, Otto KJ. 2013. Chronic intracortical microelectrode arrays induce non-uniform, depth-related tissue responses. J Neural Eng 10:026007.
Woolley AJ, Desai HA, Steckbeck MA, Patel NK, Otto KJ. 2011. In situ characterization of the brain-microdevice interface using device-capture histology. J Neurosci Methods 201:67-77.
Wu CC, Luo X. 2014. Electrode Spanning with Partial Tripolar Stimulation Mode in Cochlear Implants. J Assoc Res Otolaryngol.
Yu YQ, Xiong Y, Chan YS, He J. 2004. In vivo intracellular responses of the medial geniculate neurones to acoustic stimuli in anaesthetized guinea pigs. J Physiol 560:191-205.
Zeng FG, Shannon RV. 1992. Loudness balance between electric and acoustic stimulation. Hear Res 60:231-235.
Zeng FG, Shannon RV. 1994. Loudness-coding mechanisms inferred from electric stimulation of the human auditory system. Science 264:564-566.
Zhong Y, Bellamkonda RV. 2007. Dexamethasone-coated neural probes elicit attenuated inflammatory response and neuronal loss compared to uncoated neural probes. Brain Res 1148:15-27.
Zhou Y, Wang X. 2010. Cortical processing of dynamic sound envelope transitions. J Neurosci 30:16741-16754.

VITA

RYAN S. VERNER

3401 Hopkins Drive, West Lafayette, IN 47906 | 3143243161 | vernerryan@gmail.com

EDUCATION

Purdue University, Department of Biomedical Engineering, West Lafayette, IN
Ph.D. in Biomedical Engineering **January 2013-December 2017**
Dissertation: Electrophysiological, Behavioral, and Histological Assessment of the Thalamocortical Network as a Stimulation Target for Central Auditory Neuroprostheses
Relevant Coursework: Measurement and Stimulation of Nervous Systems, Electromagnetic Field Theory, Biomedical Signal Processing, Bayesian Applied Decision Theory
GPA: 3.88

Washington University in St. Louis, School of Engineering and Applied Science, St. Louis, MO
B.S. in Biomedical Engineering **August 2009-December 2012**
GPA: 3.5

TEACHING EXPERIENCE

Purdue University, Department of Biomedical Engineering, West Lafayette, IN
Teaching Assistant: Machine Shop **August 2014 – May 2017**

- Advised teams of senior undergraduates on rapid prototyping using 3D printers, machine tools, and computer aided modeling software such as Solidworks, Autodesk Inventor, and ANSYS products.
- Manufactured sequential prototypes for students developing products ranging from low-cost lower limb prosthetics to bioreactors for muscle regeneration.

Purdue University, Department of Biomedical Engineering, West Lafayette, IN
Teaching Assistant: Biomolecules and Biomechanics Lab **August 2013 – May 2014**

- Lectured and coordinated undergraduate students in the execution of common biochemical and biomechanical assays including ELISA, Immunohistochemistry, cell culture, and tensile testing.

RESEARCH EXPERIENCE

Purdue University, Department of Biomedical Engineering – Central Auditory Processing Lab, West Lafayette, IN
PhD Candidate **August 2014 – December 2017**

- Developed a surgical protocol for aseptic surgeries which allowed for simultaneous placement of multielectrode arrays in the medial geniculate body and ipsilateral primary auditory cortex without post-operative neurologic or physical complications.
- Developed custom software in MATLAB, OpenEx (TDT), and RPvdsEx for Sharc DSPs on System3 hardware (TDT) for the collection and analysis of multielectrode performance and electrophysiologic data *in vitro* and *in vivo*.
- Analyzed neural responses to acoustic stimuli using custom and built-in MATLAB algorithms for information theoretic and spatiotemporal approaches including mutual information, spike-triggered averages, vector strength, and frequency response curves.

Purdue University, Department of Biomedical Engineering – Neuroprostheses Research Lab, West Lafayette, IN

PhD Student **January 2013 – August 2014**

- Performed chronic electrode implantation surgeries on rats in primary auditory and primary somatosensory cortices without fatal postoperative complications and an approximate 75% success rate.
- Assessed the behavioral perceptibility of intracortical microstimulation and acoustic stimulation using rats trained in a conditioned avoidance task and psychophysical metrics such as d' and adaptive determination of thresholds.
- Mentored an undergraduate student on an independent summer project related to somatosensation which resulted in a brief publication in an undergraduate research journal.

Washington University in St. Louis, Barnes Jewish Hospital – Moran Laboratory, St. Louis, MO

Undergraduate Researcher **May 2012 – December 2012**

- Analyzed local field potentials recorded from epidural electrodes in primary motor and premotor cortex using Kalman filtering in real time on DSPs to determine intended motor activity.

Washington University in St. Louis, Barnes Jewish Hospital – Electrical and Optical Imaging Laboratory, St. Louis, MO

Undergraduate Researcher **May 2011 – May 2012**

- Worked with a team to develop a custom MATLAB software package using Bayesian Decision Theory to automatically classify the sleep state of human subjects based on recorded electroencephalograms and electrocorticograms.

PUBLICATIONS

Zempel, J. M., Politte, D. G., Kelsey, M., **Verner, R.**, Nolan, T. S., Babajani-Feremi, A., ... & Larson-Prior, L. J. (2012). Characterization of scale-free properties of human electrocorticography in awake and slow wave sleep states. Frontiers in Neurology, 3.

Kelsey, M., Politte, D., **Verner, R.**, Zempel, J. M., Nolan, T., Babajani-Feremi, A., ... & Larson-Prior, L. J. (2012, August). Determination of neural state classification metrics from the power spectrum of human ECoG. In Engineering in Medicine and Biology Society (EMBC), 2012 Annual International Conference of the IEEE (pp. 4336-4340). IEEE.

Zempel, J., Politte, D., Kelsey, M., **Verner, R.**, Nolan, T. S., Babajani-Feremi, A., ... & Larson-Prior, L. (2012, January). DEFINING NEURAL STATE USING GLOBAL MEASURES OF BRAIN DYNAMICS. In SLEEP (Vol. 35, pp. A30-A30). ONE WESTBROOK CORPORATE CTR, STE 920, WESTCHESTER, IL 60154 USA: AMER ACAD SLEEP MEDICINE.

POSTERS AT NATIONAL AND INTERNATIONAL CONFERENCES

Verner, R., Banks, M. & Bartlett, E. Mutual Information in the Auditory Thalamocortical Circuit Diminishes with Loss of Consciousness. Poster presented at: International Conference on Auditory Cortex 2017, September 12th; Banff, Alberta, Canada.

Verner, R. & Bartlett, E. Behavioral Discrimination of Channel-Specific Microstimulation for Central Auditory Neuroprostheses. Poster presented at: Society for Neuroscience 2016, November 14th; San Diego, CA.

Koivuniemi, A., Regele, O., **Verner, R.**, Lycke, R., Youngs, M., & Otto, K. Development of Cortical Sensory Prostheses. Poster presented at: BMES 2013. 2013, September 25-28; Seattle, WA.

Politte, D., Zempel, J., Nolan, T., **Verner, R.**, Prior, F., & Larson-Prior, L. Measures of Global Brain Dynamics Define Differences in Neural State. Poster presented at: SLEEP 2012. The 26th Annual Meeting of the Associated Professional Sleep Societies (LLC); 2012, June 9-12; Boston, MA.

PRESENTATIONS

Verner, R. (2017, October). Effective Information in the Thalamocortical Circuit Diminishes with Loss of Consciousness. Biomedical Engineering Society Annual Conference 2017. Lecture conducted from the Phoenix Convention Center, Phoenix, AZ.

Verner, R. (2017, September). Mutual Information in the Auditory Thalamocortical Circuit Diminishes with Loss of Consciousness. Hearing Research Seminar Series. Lecture conducted from Purdue University, West Lafayette, IN.

Verner, R. (2016, December). Electrophysiological, Behavioral, and Histological Assessment of the Thalamocortical Network as a Stimulation Target for Central Auditory Neuroprostheses. Hearing Research Seminar Series. Lecture conducted from Purdue University, West Lafayette, IN.

Verner, R. (2013, October). Development of Discriminable Sensations for Auditory Cortical Prostheses. Hearing Research Seminar Series. Lecture conducted from Purdue University, West Lafayette, IN.

AWARDS

Eagle Scout **2005**

LANGUAGES

English (native), Spanish (basic competence), MATLAB (fluent), Python, and Java

PUBLICATIONS

Verner, R., Banks, M., and Bartlett, E. (2018). Global State Changes Induce Non-Reciprocal Reduction of Mutual Information in the Thalamocortical Network. *(In preparation)*

Verner, R., Nicolalde, B., Swanberg, C., and Bartlett, E. (2018). Threshold Stability in Chronically Implanted Central Nervous System Neuroprostheses. *(In preparation)*

Verner, R., Nicolalde, B., and Bartlett, E. (2018). An Auditory Thalamic Approach to Sensory Restoration: Discriminability of Microstimulation Percepts. *(In preparation)*

Zempel, J. M., Politte, D. G., Kelsey, M., **Verner, R.**, Nolan, T. S., Babajani-Feremi, A., ... & Larson-Prior, L. J. (2012). Characterization of scale-free properties of human electrocorticography in awake and slow wave sleep states. Frontiers in Neurology, 3.

Kelsey, M., Politte, D., **Verner, R.**, Zempel, J. M., Nolan, T., Babajani-Feremi, A., ... & Larson-Prior, L. J. (2012, August). Determination of neural state classification metrics from the power spectrum of human ECoG. In Engineering in Medicine and Biology Society (EMBC), 2012 Annual International Conference of the IEEE (pp. 4336-4340).

Zempel, J., Politte, D., Kelsey, M., **Verner, R.**, Nolan, T. S., Babajani-Feremi, A., ... & Larson-Prior, L. (2012, January). DEFINING NEURAL STATE USING GLOBAL MEASURES OF BRAIN DYNAMICS. In SLEEP (Vol. 35, pp. A30-A30).